Modeling and Optimization of a Semi-Interpenetrating Polymer Network Process

Submitted in partial fulfillment of the requirements for

the degree of

Doctor of Philosophy

in

Chemical Engineering

Weijie Lin

B.S., Chemical Engineering, Tsinghua University

Carnegie Mellon University
Pittsburgh, PA

May 2011

Acknowledgements

I would like to express my sincere thanks to Prof. Lorenz T. Biegler. It is my great fortune to have such an opportunity to work with him. I am grateful for benefiting from his wisdom, patience and encouragement. His unfading enthusiasm for new challenges and non-stop endeavor for improvements make him a great role model beyond the research. I thank him always for the invaluable fortune he shares with me.

I greatly appreciate the opportunity to be co-advised by Prof. Annette M. Jacobson. She encourages me to think from different points of view. Complex problems can often be visualized in a comprehensive way. She is always willing to help and encourage me under any difficult circumstances.

I owe great thanks to Mr. Paul Arch, Mr. Elliot Wolf and their research group for their strong support throughout my thesis work. This cooperation provided me a great opportunity to work on industrial-scale problems, and better understand the challenges in model-based optimization. Their valuable input and feedback contributed much to the research work.

I am indebted to my other thesis committee members, Prof. Ignacio Grossmann, Prof Myung S. Jhon and Prof. Shi-Chune Yao for their advices and suggestions during the course of the thesis work. I am grateful for the benefit of their enlightening discussions.

I am thankful for the financial support of my thesis work from Pennsylvania Infrastructure Technology Alliance (PITA) and Enterprise-wide Optimization Collaboration (EWO) in Carnegie Mellon University CAPD (Center for Advanced Process Decision-making) research center. I also enjoyed a lot of the stimulating discussions at project meetings.

I would like to thank Dr. John Hedengren, Dr. Carl. O. Schwanke and the process control applications group at ExxonMobil Chemicals for the wonderful experience during my summer internships. The challenging issues of multi-scenario dynamic optimization have been addressed and investigated since that time. Thanks also to Dr. Victor Zavala and my colleagues Rodrigo and Hans for the constructive discussions on the "sIPOPT" package to facilitate the application to the decomposition algorithm for the multi-scenario problem.

Thanks our PSE group and the faculty and staff of the Department of Chemical Engineering at Carnegie Mellon. They were generous and gracious with their time in helping me out for things big or small. I cherish their friendship and the great memories I have made.

Part of the thesis was written when I was back in China. I want to thank the full support from my whole family. After years of being away, I found my dear parents are growing old and gray. They love me more than anything, but I have nothing ever enough to repay. I hope they are happy for me because they have done so much for me to make this possible. I thank them for the warm family I enjoy, the life I have, and I respect and love them forever.

I thank my beloved husband, Qin Gao. He makes great efforts to accompany me during this journey. He stands beside me, with his love, courage and understanding. I thank him for coming into my life, and being a part of me.

Finally, I want to thank all my friends in the US, in China and other parts of the world. I am grateful to have you all in my life.

Abstract

The integration of modeling, simulation and optimization provides powerful tools for supporting advanced decision making in the competitive market. However, when applying the tools to polymerization processing, the challenging task is to accommodate the predictability of the mathematical model and the capability of model-based optimization due to its inherent complexities. In this thesis, novel strategies of modeling and optimization are developed and applied to a complex polymerization system, Semi-Interpenetrating Polymer Network (SIPN) process. By providing a comprehensive study on SIPNs, we show the great potential of advanced modeling and optimization in the polymer industry.

New mathematical modeling strategies are first presented in this work. In the SIPN process, improving the productivity while preserving the quality of final products are usually contradictory with each other because of a slow seeded polymerization mechanism. The presence and interaction between two polymers imposes complexity in the model. To simulate the complex interpenetration and networking process, the model needs to consider several key features, such as a particle growth mechanism, intra-particle heterogeneity and polymerization kinetics. Hence, the first highlight of the work is a multi-stage modeling framework which decouples the modeling complexity: a generalized reaction-diffusion model to describe the particle growth and the intra-particle dynamics; and a new multi-population-balance representation to integrate simultaneous crosslinking, grafting and degradation reactions into the kinetic model. The last component enables the prediction of gel content and molecular weight development simultaneously up to full conversion.

Advanced computational tools are developed to tackle the problem of computation. Acquisition of reliable parameters is the key to predict the process performance over a broad range of operation. However, we face the problem of large variation of polymerization parameters in the literature and limitations in obtaining analytical measurements for polymer composites. A hybrid approach is presented to reduce model distortion by selecting the most prominent parameters from a large parameter set. Parameters are ranked through successive orthogonalization of the sensitivity matrix, and then the selection is iteratively refined through statistical inference from simultaneous parameter estimation. Validated models obtained are therefore usable for process optimization. New operation policies are explored

through a new profile representation. In addition, Kriging surrogate modeling is introduced and combined with dynamic optimization. An efficient optimization algorithm is developed for the integrated multi-stage model based on surrogate sub-models. Furthermore, we develop a robust two-stage algorithm for large-scale multi-scenario dynamic optimization problems by taking advantage of NLP sensitivity analysis. This enables continuous developments in parameter estimation and process optimization applications.

The model derived shows consistent agreement with SIPN pilot plant experiments. Newly proposed operation policies significantly improve the productivity while maintaining the quality of the final product. The tools developed in this thesis are useful for other complex system analysis and optimization.

Table of Contents

List of Tables

List of Figures

Chapter 1

Introduction

1.1 Overview

The past decades have seen substantial growth of model-based optimization in many disciplines and application areas. A large number of mathematical models are developed to simulate processes in various domains. With the advance of mathematical foundation and improvement of computational implementation of optimization technologies, we can find optimal solutions of more complicated models that reflect the detail of the actual process, and learn from larger data sets that are collected from the observations in real processes. The integration of modeling, simulation and optimization provides powerful supporting tools for advanced decision making in the competitive market. This tide has since changed almost all industry domains, including the chemical industry. The most profound transformation in the chemical industry is observed on the approaches for the process design and operation. With process models and simulations, new processes can be developed in a much swifter manner and the optimization methods refine the process design for lower cost, better quality and higher productivity. Successful applications have been reported for many complex chemical systems, and the integration has become an active topic in both academia and industry.

Polymers are among the largest volume chemical products in the world at present, and the global market for polymer products keeps growing rapidly. Model-based optimization technologies are being expanded to meet the needs of the polymer industry. While innova-

tive modeling and optimization technologies have demonstrated vast opportunities in the area of polymer manufacturing, development of model-based applications for polymer processes face several challenges due to the inherent complexity of the polymerization process.

First of all, polymer systems are much more complex than other small molecule reaction systems. Since there is no uniform polymer species within a system, the macromolecules in the system cannot be described with a deterministic structure or measurement. Therefore, instead of single-valued parameters, we need distributions to model the characteristics of a polymer. For example, instead of using single-valued molecular weight, we use molecular weight distribution (MWD) to describe the property of the system. Furthermore, we need composition distribution for composite polymers, long chain branching distribution for branched polymers, etc. These distributional parameters introduce additional dimensions and complicate the modeling and parameter estimation.

Secondly, the complexity of polymer reaction models often results in overparameterized systems. In contrast, when finding parameters for the model, we often face limited information from experiments and large uncertainties in the system. These factors lead to large distortions in the resulting model. An important aspect of research on modeling polymer reactions is to develop systematic approaches to reduce the model distortion.

Finally, high dimensionality and nonlinearity of the model makes it difficult to optimize. Polymer process models usually consist of a large set of equations that are highly nonlinear. Standard optimization software packages are usually incapable of finding solutions for these problems. Moreover, the complexity of the models can easily become intractable with off-the-shelf tools. Novel effective and efficient solution algorithms are needed to solve these models.

In this thesis, comprehensive model-based optimization strategies are developed for a class of specialty polymers, Semi-Interpenetrating Polymer Networks (SIPNs). New tools and methodologies are developed to address the above challenges, allowing engineers to solve increasingly complex problems in polymer industry.

Interpenetrating polymer networks, IPNs, are a broad class of polymer composites defined as a combination of two polymers in a network form, with at least one of them synthesized and/or cross-linked in the immediate presence of the other (Sperling, 1981). Semi-IPN refers to a class of IPNs where only one of the polymers is crosslinked. Individual constituents in IPN are generically polymer resins and fibers, which serve as the matrix phase and the reinforcing phase, respectively (Advani, et al., 2002).

There are several motivations for studying the SIPN process. First, IPN products are valuable. It is an advanced polymer material with design flexibility and relative ease of processability. IPNs have been utilized in widespread commercial applications (Klempner, et al., 1994), and are considered promising in novel material development (Athawale, et al., 2002). Improvements in understanding and control of IPN processing will bring significant value to polymer composite development. Second, from a modeling point of view, the IPN process is representative, especially with regards to its kinetic model. Since kinetic studies of polymer mixtures are rare, the modeling approaches developed will not only be beneficial for IPNs, but also can help to facilitate the study of other multi-component polymer systems. Last but not least, the IPN process model provides a good example for investigating the computational challenges of model-based applications in the polymer industry. Development of the solution strategy will help the analysis of other complex systems, push the limit of computational power and drive the advancement of optimization. Overall, we believe this

study can bring new value to IPN manufacturing as well as generate new opportunities for broader interests.

1.2 Scope

As we have seen, applications of model-based optimization can lead to effective decision making, timely improvements and, consequently, enhanced process performance. However, crucial problems, which impede further expansion of model-based optimization to the polymer industry, lie in the increasing complexity of polymer process modeling and the resulting computational difficulty of associated optimization problems. To address these difficulties, the scope of this work includes the essential elements in the model-based process study, as shown in Figure 1.1. The synergy of new modeling and optimization tools is demonstrated for process improvement on a complex industrial SIPN product. The mathematical modeling part includes the development of a new multi-stage modeling framework for the SIPN process. The computational part includes novel strategies for parameter estimation and process optimization, such as parameter sub-set selection, optimal profile representation, surrogate-model-based optimization and multi-scenario dynamic optimization. Successful implementation of the model-based optimization solution is shown in plant trials.
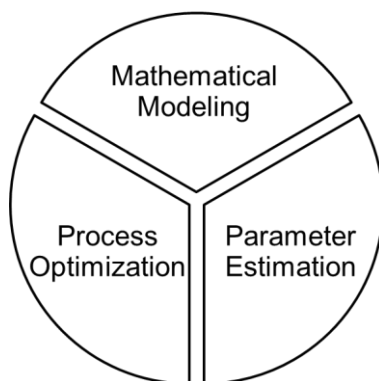
Figure 1.1 An integrated framework for model-based optimization

1.3 Objectives

The main objective of this thesis work is to achieve a close linkage of modeling and optimization tools to facilitate the application of model-based optimization to polymerization processes. In particular, a SIPN process is the application example of this work.
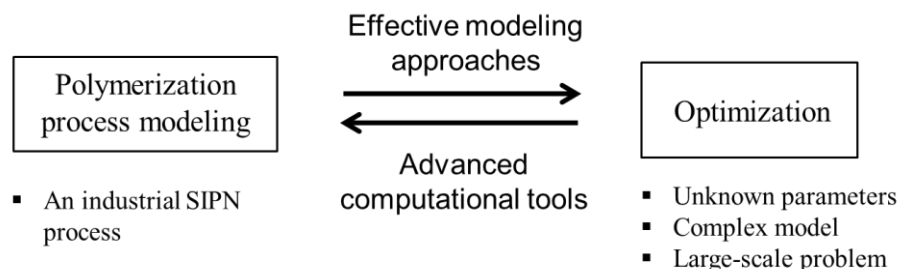
Figure 1.2 An outline of main research problems

Figure 1.2 outlines the main research problems in this study. On one hand, the challenges we face in "polymerization process modeling" are to obtain a mathematical representation for a complex industrial SIPN process. New modeling approaches are needed, which should be also effective for optimization. On the other hand, in "optimization", the resulting problem is difficult to be handled by off-the-shelf optimization tools. We want to develop advanced computational tools that are capable of finding novel solutions for the process,

In summary, this thesis addresses four primary research problems:

- SIPN process modeling. I aim to develop a comprehensive process model to understand the relationship between process conditions and SIPN product properties, while also computationally efficient for process optimization.

- Parameter estimation. I develop a systematic parameter estimation procedure for reducing model distortion in the presence of a large number of uncertain model parameters.

- Complex model optimization. I investigate various model reduction techniques to reduce the computational burden of the complex dynamic optimization problem. An improved algorithm of surrogate-model-based optimization is proposed.

- Multi-scenario optimization. A decomposition approach is developed to improve the solution robustness of large-scale multi-scenario optimization problems which arise from parameter estimation with multiple data sets.

1.4 Thesis Outline

This thesis is devoted to the development of a suitable SIPN process model and advanced computational techniques for large-scale complex process problems. Therefore, the thesis mainly consists of two parts accordingly, as "**Mathematical Modeling**" (**Chapters 3 ~ 5**) and "**Computational Strategies**" (**Chapters 6 ~ 8**).

Chapter 2 provides a brief overview of the research background, where unique challenges lie. State of the art modeling and optimization technologies in polymer reactor engineering are discussed.

In "**Mathematical Modeling**", the first highlight of the work is the comprehensive SIPN process model. It is featured as a multi-stage modeling framework which decouples the modeling complexity. Each sub-stage model reveals key effects during a particular time domain.

In **Chapter 3**, the SIPN product and process are introduced. An overview of model structure and modeling procedure is provided. A multi-stage modeling approach is proposed for the example SIPN process.

In **Chapter 4**, a particle growth model is developed for Stage I of the SIPN process, as one of the sub-models. Particle average properties and intra-particle properties are linked with its semi-batch operating conditions.

In **Chapter 5**, a SIPN kinetic model is developed for Stage II of the SIPN process, as another sub-model, which involves simultaneous polymerization, grafting, crosslinking and degradation. A component-wise decomposition strategy is proposed to simulate joint molecular weight distribution and gel content.

In the section part, "**Computational Strategies**", we discuss the computational strategies developed to tackle difficulties arising in the SIPN model-based application.

In **Chapter 6**, a new parameter selection and estimation approach is presented, which shows improved robustness and efficiency in reducing the model distortion under over-parameterized conditions. Successful applications are demonstrated for SIPN process model parameter estimation.

In **Chapter 7**, optimal operation policies are explored based on the two-stage SIPN model. A new profile representation is identified for the SIPN operation. Algorithms for surrogate-model-based optimization are studied. The stiff DAE sub-model is replaced by low order Kriging models. Optimization is carried out for the integrated model to achieve improved solution.

In **Chapter 8**, a two-stage decomposition algorithm is developed for multi-scenario dynamic optimization, which is particularly useful for parameter estimation from multiple data sets and optimization under parameter uncertainty. Improved robustness is achieved for the ill-conditioned SIPN problem.

Finally, a summary of the most important conclusions and key contributions are presented in **Chapter 9**. Suggestions and an outlook for potentially interesting future developments are presented.

Chapter 2

Polymerization Reactor Modeling and Optimization: State of the Art

This introductory chapter provides a brief overview of the state of the art technologies in polymerization reactor modeling and optimization. Modeling topics include mathematical representation of polymerization kinetics, transport phenomena and polymer reactors. Optimization topics involve parameter estimation and process optimization. Remaining challenges are the motivation of this work.

2.1 History of Polymer Reaction Engineering

Polymer products have advanced from synthetic rubbers and synthetic fibers to stereospecific polymers, functional polymers, biosynthetic polymers and hybrid polymer composites. In the meantime, polymerization research has improved from empiricism to a multidisciplinary integration of chemistry, mathematics and scientific computing (Meyer, et al., 2005). "Makromoleküle" (Macromolecule), a groundbreaking elucidation by Staudinger (1920), showed the chain structure of polymer molecule. This accounts for most special characteristics of polymers. Since then, polymer science and engineering has become a discipline and developed rapidly.

Polymers are an example of "products-by-process", where the final product properties are mostly determined during manufacture in the reactor. For example, polyethylene products,

though all polymerized from simple ethylene units, vary in a very broad range depending on what polymerization condition is taken. Therefore after Denbigh (1947) introduced the concept of Polymer Reaction Engineering (PRE), which considers polymerization reactions at both the chemical and at the process levels, the area developed quickly (Meyer, et al., 2005). PRE provides a link between the fundamentals of polymerization kinetics and polymer microstructure achieved in the reactor, which enables control over the final product through refinement of the process.

The needs of quantitative analysis and modeling of polymerization process were soon brought into attention in the field of PRE. Polymerization reactor modeling is recognized as an important tool for process study. The early work of Flory and other research groups in the 1930s (Staudinger, 1920; Kuhn, 1930; Chalmers, 1934; Flory, 1936) introduced models for chain length distribution in batch reactors resulting from different polymer chemistries. The methodology further developed in the 1940s led to more complex and comprehensive models, some of which are still being used today. In the early 1970s, PRE underwent another radical development due to the revolutionary advent of digital computers. As computer-aided modeling and optimization approaches were being introduced to all fields, commercial CAD (computer-aid design) packages for polymer processing were later used in the polymer industry (Sandland, et al., 1987). Since then, numerous commercial computer simulation packages have been developed and marketed. The scope of polymer reaction engineering is expanded and revolutionized. The power of computation brings polymer reaction engineering to a next new level, from capacity improvement, quality control towards advanced "macromolecular engineering" (Matyjaszewski, et al., 2007).

2.2 Polymerization Reactor Modeling

Due to the process-determined feature, an understanding of processes occurring in the polymerization reactor is therefore crucial to achieving efficient, consistent, safe and environmentally friendly production of polymeric materials (Asua, 2007). While Process Modeling technologies are developed as powerful tools for chemical plants, there are distinct challenges due to the intricacy of polymer processes.

A major objective of PRE is to understand how the reaction mechanism, the physical transport process (e.g. mass and heat transfer, mixing), reactor type and reactor operating conditions affect the "polymer quality" of the final product (Kiparissides, 1996). As Figure 2.1 illustrates, each polymerization process has specific features at three different scales, which makes the practice of process modeling for polymerization system more challenging. At the micro-scale, we need to consider polymer kinetics. There are two major polymerization mechanisms, addition polymerization and step-growth polymerization. Each of the mechanisms includes a family of polymerization types. General reaction steps may be similar for polymers produced in the same reaction class, but variations are not unusual for specific polymer products. At the meso-scale, the physical transport phenomena are most important. Polymerization systems can be classified into several reaction categories according to their phase composition, such as bulk polymerization, suspension polymerization, gas-phase polymerization, emulsion polymerization and slurry polymerization. Various transport phenomena must to be considered, especially in multi-phase systems. It is generally more complex to model mass transport in heterogeneous systems, such as emulsion polymerization, than in homogeneous systems, such as bulk polymerization. Even in a single phase reaction system, modeling of diffusion-limited reaction rates is still an important issue

to be addressed, as the polymer apparent reactivity changes because of changes of polymer chain mobility. At the macro-scale, i.e. the reactor scale, there are different kinds of reactors, such as continuous reactors, batch reactors and semi-batch reactors. The operation and control are different from each other, which require appropriate problem formulations to focus on different modeling objectives. Hence, there is no general model which is able to be applied for all polymerization systems. Instead, polymer reaction modeling technologies are systematized at different scales as modeling components. A general guideline for the development of a prototype polymerization process model is to start from a basic assembly of component models in these three scales. Then model modifications and developments will be further customized for the particular class of polymer products.
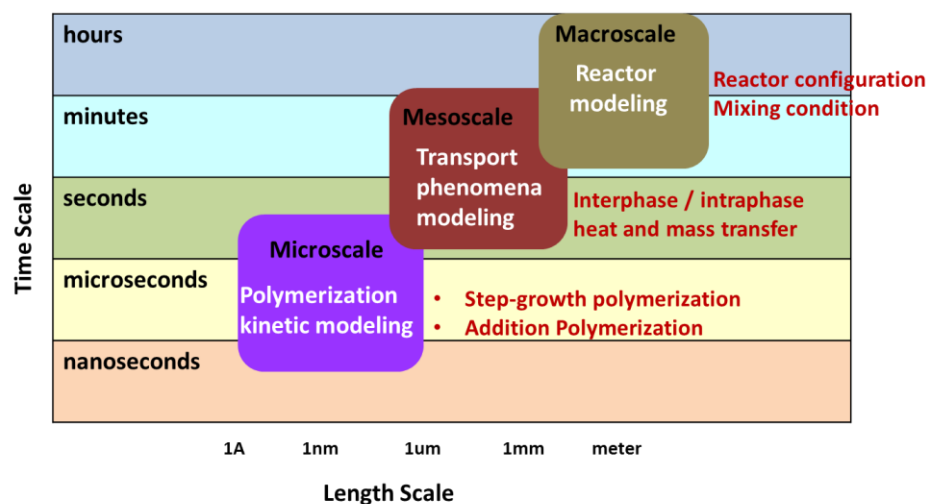
Figure 2.1 Different scales in polymerization reactor modeling

Several authors (Ray, 1971; Choi, 1993; Kiparissides, 1996; Dube, et al., 1997; Yoon, et al., 2004) have provided comprehensive reviews on polymer reaction modeling development. Villa (2007) also reviewed current tools and trends from the industrial point of view. Here, the development of polymer reaction modeling is reviewed, following the above three scales.

2.2.1 Polymerization Kinetic Modeling

It is a common observation that the end-use properties of polymeric materials are determined by the structure properties of the macromolecule. Research also reveals that the reaction kinetics determines the structure properties of the macromolecular polymer. Polymerization kinetic models aim to link the three factors mentioned above. I.e., how the polymer reaction kinetics affects the structure properties of the macromolecular species, and how it will ultimately affect the end-use properties. The models enable optimizing the end product quality by designing the molecular structure ("quality by design"), and more practically by manipulating the control of the process ("quality by control").

There are several molecular properties typically considered in the quality analysis. Since polymer materials are mixtures by nature, even processed at a strictly controlled condition, they have a chain length distribution. Hence, information about the distribution is needed for characterization of the macromolecules, for example, molecular weight distribution (MWD), copolymer composition distribution, short / long chain branching distribution and stereoregularity, etc. Average properties are also used to approximate the distribution, such as number average molecular weight ($\overline{Mn}$), weight average molecular weight ($\overline{Mw}$), and branching ratio etc.

As shown in Figure 2.2, polymerization systems can be classified into two main categories according to the reaction mechanism, as addition polymerization and step-growth polymerization. In the addition polymerization, monomers are successively added to the active center of the chain to form the macromolecule. The active reaction sites can be $R^{\bullet}$ (free radical polymerization), R^{+}, R^{-} (Ionic polymerization) and coordinate components (coordination polymerization). In the step-growth polymerization, polymer chains grow

gradually through reactions between monomers with multiple functional groups. Polycondensation and ring-open polymerization are examples of step-growth polymerization. Various polymerization mechanisms lead to different kinds of polymer structures with distinctive properties. A comprehensive introduction on polymerization chemistry can be found in Flory (1953), Odian (1981), Stevens (1998). The effort of building the kinetic model to systematically understand the relationship of polymer structure and reaction mechanism is of fundamental importance for model-based applications. In the family of polymerization products, addition polymerization composes about 70% of the polymer production, among which, free radical polymerization is the most common approach. Therefore, numerous endeavors are put into process modeling for the free radical polymerization system.
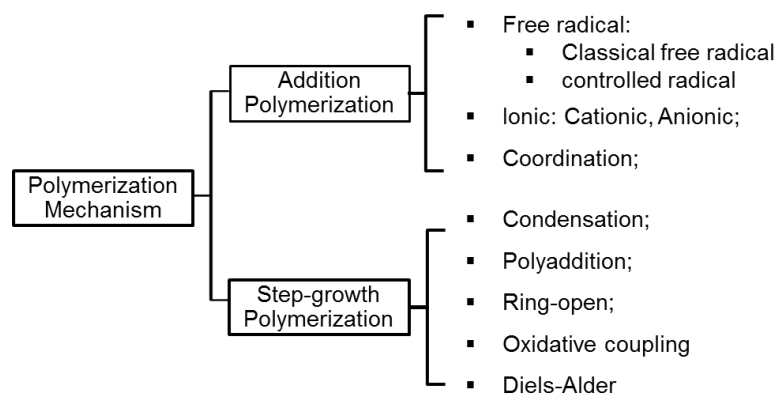
Figure 2.2 Classification of polymerization mechanisms

There are two main approaches to polymer mechanistic kinetic modeling, i.e. statistical approaches and population balance approaches. Statistical approaches are mostly used for step-growth polymerization, especially for random crosslinking and branching. The population balance approach is based on mass balance of reactive species involved in the reaction, and provides more detailed interpretation of reaction kinetics. Table 2.1 highlights some of

the kinetic modeling methods developed, with a focus on free radical polymerization systems.

As seen in Table 2.1, statistical approaches evolved from simple yet limited probability calculations to many powerful but expensive Monte Carlo simulations thanks to the development of the power of computing. Stochastic kinetic modeling starts to gain popularity for complex kinetic system analysis when population balance equations are difficult to derive. It is versatile in terms of kinetic simulation, but one of its important limitations is the difficulty to be used for optimization due to its stochastic nature. On the other hand, various numerical reduction techniques are developed for the population balance model in order to solve a large number of differential equations resulting from polymer species. For example, there are approximation approaches, generating function approaches, the method of moments and discrete weighted residuals etc. Interestingly, when the first study based on the direct numerical integration approach was published (Liu, et al., 1961), direct integration of the population balance model was soon abandoned for its obvious limitations in the early computing age. However, direct integration approaches are reconsidered to be a unified solution approach with the increasing computational power (Verros, et al., 2005). Computational cost appears to be overlooked in homo-polymerization systems. Nevertheless, it is important to point out that, when more complex polymer structures are formed, such as co-polymer, network polymer and branching polymer, more efficient numerical algorithms are necessary to provide a prediction within a realistic time. Depending on the application, models with different complexity may be selected. Meanwhile, development of comprehensive models with reduced complexity remains of great importance for advanced polymer kinetic modeling.

Table 2.1 Summary of kinetic modeling approaches

Modeling Approach	Property Prediction	Case study	Features & Limitations
Population Balance models			
Direct numerical integration	MWD	(Liu, et al., 1961) (Verros, et al., 2005)	Straightforward implementation, but up to a limited chain length
Instantaneous MWD method	MWD	(Hamielec, 1987; Xie, et al., 1993; Fiorentino, 1997)	Simulate instantaneous chain formation versus accumulative chains
Continuous variable approximation	$\overline{Mn}$, $\overline{Mw}$	(Bamford, et al., 1960; Bailagou, et al., 1985; Chaimberg, et al., 1990)	Require a large kinetic chain length; truncation error of Taylor expansion and boundary condition;
Generating functions (GF)			
• z-transforms	MWD	(Tirrell, et al., 1975; Mills, 1986)	Numerical inversion of discrete Poisson summation formula
• Fourier transforms	MWD	(Nordhus, et al., 1997)	Convolution integrals have to be calculated
• Laplace transforms	MWD, LCB	(Bamford, et al., 1960; Ray, 1971; Asteasuain, et al., 2002; Brandolin, et al., 2004)	Select possible generating function for various MWD
The method of moments	$\overline{Mn}$, $\overline{Mw}$ MWD	(Nagasubramanian, et al., 1970; Ray, 1972) (Crowley, et al., 1997)	Average properties of the distribution; extended to sectional average
Deconvolution techniques	MWD, LCB	(Soares, et al., 1995; Maschio, et al., 1999)	MWD as a weighted sum of most probable MWD

Discrete weighted residuals:
   • Galerkin finite element
   • Collocation
   • Gelerkin h-p
	MWD, LCB	(Budde, et al., 1991; Canu, et al., 1991)
		(Deuflhard, et al., 1989)
		(Wulkow, 1996)
			General usage for different reaction mechanism.

Discrete population balance approach	MWD, LCB	(Kumar, et al., 1997; Batte, et al., 1999)	Efficient for nonlinear polymer representation
Numerical fraction	Gel, MWD	(Teymour, et al., 1994; Arzamendi, et al., 1995; Papavasiliou, et al., 2002;)	Gel content predicted by higher polymer generations

Table 2.1 Summary of kinetic modeling approaches (Continue)

Modeling Approach	Property Prediction	Case study	Features & Limitations
Statistical models			
Probability calculation	$\overline{Mn}$, $\overline{Mw}$	Linear polycondensation (Orlova, et al., 1979) Random crosslinking (Flory, 1953; Tobita, 1995) Random branching (Miller, et al., 1998)	Relatively simple, but conclusions are generalized from a single chain probability
Monte Carlo Simulation	Gel, LCB, MWD	(Tobita, et al., 1989; Tobita, et al., 1995)	Flexible for various chain structure, but computationally expensive

In contrast to the mechanistic modeling approach, phenomenological models are also used in practice. Phenomenological models are semi-empirical, which are generally developed based on a relatively simple rate equation which does not consider reaction details for each species. Therefore, it only has a limited predictability.

2.2.2 Transport Phenomena Modeling

In this scale, interphase and intraphase transport phenomena would affect the polymer structure properties through controlling the concentration of a species and altering different elementary reaction rates. Modeling of phase equilibria and apparent kinetic rates in polymerization systems are important as well as challenging.

Table 2.2 lists some major polymerization types according to their phase composition. The challenges which are confronted are highlighted. Main concerns for bulk system modeling would be the intraphase transport limitations, while other polymerization systems face different interphase transport problems in addition to the bulk phase. A typical example of the multiphase system involving intricate mass transport is emulsion polymerization. Even though the underlying polymer kinetics follow the same free radical polymerization mechanisms, compartmentalized effects of the free radicals lead to different final products than bulk polymerization. As seen in Table 2.2, a multi-phase system raises challenges in transport phenomena modeling. For systems considered at equilibrium, an equation of state is generally used. However, for dynamic systems, more investigation is often needed.

Variation in polymer chain mobility is another important fact to be considered by the model. In free radical polymerization, apparent reaction rate constants change during the reaction due to the well-known gel effect, glass effect and cage effect. The gel effect refers

to the decrease of apparent termination rate (k_t) between macro-radicals, also known as Trommsdorff-Norrish Effect. Since the viscosity of the system increases with the increase of the monomer conversion, the mobility of the macro-radical is confined. Gel effect usually results in "auto acceleration" of the polymerization. The glass effect is related to the decrease in the propagation rate constant caused by a decrease in the mobility of monomer molecules at the glass transition temperature. The cage effect is associated with the decrease of initiator efficiency, since decomposed initiator only has a limited range of diffusivity before reaching monomer. Discussion of the reaction rate coefficient model is often combined with the kinetic modeling. For different polymerization systems, incorporation of these three effects has different considerations. For example, gel effect is considered to take place at high monomer conversion ratio in bulk polymerization, while it occurs at low conversion in emulsion polymerization (van der Hoff, 1958). Some representative models are listed in Table 2.2, classified based on their theoretical background. As seen in Table 2.3, many theories and correlations are developed for modeling gel effect. Good agreement in reaction rate and molecular weight predictions has been reported by different groups. Glass effect and cage effect are later unified in the same modeling framework by some of the groups. In general, models which claim universal applicability based on fundamental principles require a large number of input parameters. Some of the empirical models introducing breaking points and critical values are also difficult to justify. Some benchmark studies were done to evaluate the rate coefficients experimentally. Propagation rate coefficients for bulk free-radical polymerizations derived from Pulsed-laser Polymerization (PLP) and Size-Exclusion Chromatography (SEC) experiments have been critically evaluated (Beuermann, et al., 1997; Asua, et al., 2004).

Table 2.2 Summary of polymerization types according to the phase composition

Polymeriza-tion system	Reaction site	Advantage	Limitations	Examples	Mesoscale Model-ing Challenges
Bulk	bulk	high purity; contin-uous production	reaction heat removal	LDPE, GPPS, HIPS, SAN, SMA	diffusion limited reaction rate; reac-tion heat transfer
Suspension	suspension particle	reaction heat re-moval; lower viscosity of the re-action medium; large spherical par-ticle.	post-reaction process; diffi-cult for continuous operation	PS, PVC, PVDC	phase equilibria for water soluble initia-tor/ monomer system
Emulsion	micelles	high molecular weight and high reaction rate; low temperature reac-tion; reaction heat removal	post-reaction process; con-trol of de-emulsification	SBR, PVA, PMMA, PVC, VAE	phase equilibria; free radical entry mechanism
Solution	solution	temperature con-trol; low viscosity; direct usage	chain transfer to solvent;	block copol-ymers, functional particles: PDMAEMA-b-PBMA, PS-b-PB	dispersion system distribution
Slurry	catalyst site	mild operating con-dition; easy heat removal; high monomer conver-sion; high solids content; broad range of Mw	low reaction rate; purifica-tion; solvent pollution	HDPE	gas-liquid mass transfer limitations
Interfacial	interface	high molecular weight, low tem-perature	high reaction surface, sur-factant usage	Nylons	interfacial concen-tration

However, it is important to note that most of the model predictions were compared with the results from batch isothermal experiments; they may fail in special situations of semi-batch and/or non-isothermal operations, as pointed out by Ghosh et al. (1998) and Srinivas et al. (1996), due to the dependence on initial values of molecular weight and/or initiator

concentration. Though significant effort has been made on the study of the coefficient modeling, few successful applications are reported in industrial practice besides empirical formulations. Solving an inverse problem is considered to be a promising and practical alternative to accurately represent polymerization dynamics.

Table 2.3 Summary of polymerization reaction rate modeling approaches

	Modeling approach	**Background**	**Representative study**
Gel effect (k_t)	Empirical approach	Viscosity Monomer conversion / polymer weight fraction Stage-wise function Chain length dependent	(Duerksen, et al., 1968) (Friis, et al., 1976; Ballard, et al., 1984) (Qin, et al., 2002) (Zhu, et al., 1989; Russell, et al., 1992)
	Free volume theory	Mobility changes with polymer free volume	(Marten, et al., 1979; Chiu, et al., 1983)
	Reptation theory	Time- dependent rate constant for different reaction regimes	(Ito, 1980; de Gennes, 1982a; de Gennes, 1982b)
	Entanglement theory	Onset depends on polymer average size	(Tulig, et al., 1982)
Glass effect (k_p, k_{tr})	Collision theory	Translation diffusion- sectional diffusion-reaction	(Chiu, et al., 1983; Ray, et al., 1995)
	Encounter-pair model	Two stage process assumption	(Casey, et al., 1992)
	Generalized free volume theory	Extension of gel effect model	(Keramopoulos, et al., 2002)
Cage effect (f)	Generalized free volume theory	Extension of gel effect model	(Arai, et al., 1976; Keramopoulos, et al., 2002)

2.2.3 Polymer Reactor Modeling

All the above models are eventually related to the polymer reactor where the polymer is being produced and for which the operation is controlled. Although there are various types of polymer reactors, in terms of mixing conditions, they can mainly be divided into four categories: batch reactor, semi-batch reactor, continuous-flow reactors without back-mixing and

continuous-flow reactors with back-mixing. Reactor configuration examples include continuous/semi-continuous CSTR, tubular reactor, fluidized bed, reaction columns and reactors in series. Different mixing conditions have important impacts on polymer properties. In addition, the formed structure of the polymer affects the flow of the complex fluid. The quality distribution within the reactor should be taken into account at this macro-scale level.

Commodity polymer products are usually produced through continuous operation. Typical examples are low density polyethylene (LDPE), which is produced in a high pressure tubular reactor. Steady-state is often assumed for continuous processes. Therefore, the dynamics of the reactions may be simplified.

Batch/semi-batch processes are common for engineering and specialty polymers. Though the capacity of batch and semi-batch processes is much lower than continuous operation, it allows additional controls to achieve fine product properties.

For the particulate process, particle size distribution is another important issue of the product quality. A particulate population balance equation is considered in the model. Vivaldo-Lima, et al. (1997) provided a review on modeling of particle size distribution (PSD) in suspension system. A unified population balance approach was reviewed in Kiparissides (2006) following the time evolution of molecular and morphological polymer properties in batch and continuous polymerization reactors.

Table 2.4 lists some reactor modeling studies from the literature. The resulting reactor models incorporate the micro-scale and meso-scale models with different foci. Special features of the reactor configuration are taken into account.

Table 2.4 Polymer reactor modeling

Reactor Configuration	Representative Study	Representative Study
Continuous Process	Tubular reactor	HDPE (Bokis, et al., 2002; Buchelli, et al., 2005)
	Fluidized bed reactors	LLDPE (Xie, et al., 1994; Alizadeh, et al., 2004)
	Reactors in series	PP (Zheng, et al., 2011)
	Reactive distillation columns	Polycondensation (Grosser, et al., 1987)
Batch Process	Autoclave reactor	Nylon 6,6 (Robertson, et al., 1995)
	Stirred tank reactor	PS (Cherbanski, et al., 2007)
Semi-batch Process	Stirred tank reactor	Emulsion polymer (Chylla, et al., 1993; Doyle, et al., 2003)
		PS (Crowley, et al., 2000)
		PVC (Xie, et al., 1991)

2.3 Polymerization Process Control and Optimization

Advanced process simulators provide powerful tools for modern engineering. Reliable process models can be used to control, design and optimize a complex process in an accurate, prompt and comprehensive way. Successful applications that lead to improved productivity and quality have been widely reported among the chemical industry. The needs for advanced control and optimization in polymer industry have also been recognized. Here, there are two key challenges when applying the process control and optimization for the polymer process model. First, how can we obtain an accurate model? Second, how can we solve the specific optimization problem in an effective and efficient way? Distinguished from the topics discussed in the previous section on process model development and problem formulation, which are mostly from the polymer engineering point of view, the focus of this section is on computational issues in the model-based application, especially for the complex polymeriza-

tion process model. In this respect, these two challenges are related with the problem of parameter estimation and process optimization, which will be reviewed in the following section.

2.3.1 Parameter Estimation

Modeling is never complete until all relevant model parameters are determined or estimated. In fact, determining the parameters of a kinetic model by using laboratory, pilot plant, or plant data is perhaps the most critical step for the successful development of a process model and at the same time it might be the most time-consuming, costly, and difficult process (Yoon, et al., 2004). Parameter estimation is a discipline that provides tools for the efficient use of data for aiding in mathematical model of phenomena and the estimation of constants appearing in these models (Beck, et al., 1977). There are three main topics involved in the study of parameter estimation.

- Data fitting: estimation of optimal parameters which best fit the current data;

- Design of experiments (DOE): maximize the information obtained from the experiment to obtain the best parameter estimates;

- Model discrimination: the determination of the mathematical model with fitted parameters which best describes the system from which data are measured, including a model of error processes (Zhang, 1997).

In this content, the parameter estimation problem refers to the first topic, data fitting, specifically. Estimation problem formulation and analysis, and efficient solution algorithms are two main issues in the parameter estimation problem. Here, general background information is briefly reviewed, and the specific issues for the polymerization process are highlighted.

2.3.1.1 Parameter Estimation in General

- **Parameter estimation problem statement**

A general functional relationship can be written as

$$y \approx f(x, \theta) \tag{2.1}$$

where y is the response (dependent) variable, x is the independent variable, θ is the unknown parameter vector, $\theta = (\theta_1, \theta_2, \cdots, \theta_p)$. Table 2.5 outlines three main formulations of the parameter estimation problem.

Table 2.5 Parameter estimation problem formulations

Least Squares	$\min \phi(\theta) = \displaystyle\sum_{\mu=1}^{n} b_\mu e_\mu^T B^{-1} e_\mu$ weighted by experiment (weight b_μ) and variable (covariance B)
Maximum Likelihood	Maximize likelihood function: $L(\theta, \Psi) \equiv p(E(\theta)|\Psi) = p(Y - F(X, \theta)|\Psi)$
Bayesian	$p(\theta|D) = \dfrac{p(D|\theta) \cdot p(\theta)}{\int p(D|\theta) \cdot p(\theta) d\theta}$

where θ represents the unknown parameter vector of the deterministic model; n is the dimension of θ; n is the number of experiments; M is the moment matrix of the residuals, defined by $M_{ab} \equiv \sum_{\mu=1}^{n} e_{\mu a} e_{\mu b}$; D is the sample data.

Zhang (1997) provided a review on parameter estimation techniques. Computational implementations of linear-in-parameter estimation problems are well studied. Montgomery et al. (2001) and Weisberg (2005) provided comprehensive introductions to linear regression analysis and applications. Commercial and open source packages are widely used. Nonetheless, in chemical engineering problems, systems are often nonlinear and dynamic. Many of

the conclusions for linear systems could not be extended for nonlinear systems directly. Some of the approaches are modified to consider the nonlinearity. However, the analysis is only approximately valid under certain conditions. Special care is required when the system is nonlinear. Nonlinear parameter estimation theory and algorithms are developed for more general engineering applications (Aster, et al., 2005). In the polymerization system, the non-linearity becomes so important that specific approaches are necessary. Some of the typical problems are discussed in the next section.

2.3.1.2 Special Issues for Polymerization Process Model

There are several factors making the parameter estimation problem especially challenging for the polymerization process model.

- **Limited measurement data**

Many of the kinetic and transport parameters are strongly system-dependent in polymerization processes, and accurate predictions from first principles are often impossible. Applying estimated values based on output measurements is a typical approach in polymerization process model construction. However, although analytical approaches for characterization of polymer material become more and more powerful, many polymer structure properties are still not able to be measured directly. For example, simulation models are capable of calculating the 2D molecular weight distribution of LDPE, i.e. backbone chain distribution and its long chain distribution, while experiments could not provide such information for comparison. Accurate sampling during reaction is not an easy task either. Richards, et al. (2006) surveyed the polymerization instrumentation technologies with emphasis on, for example, measurement of viscosity, composition, molecular weight, and particle size. Even for those offline measureable properties, many analytical experiments are

time and resource consuming, and are not always implemented. Lack of measurements is not an uncommon case in many parameter estimation problems.

In terms of mathematical computation, study of parameter estimability and parameter selection is often neglected but critical to reduce the distortion of the obtained model in the case of limited data. Sensitivity study is an area closely related with parameter estimation. Weakly and linear dependently parameters are aimed to be identified, and removed from the parameter estimation problem. Parameter selection approaches based on local sensitivity (Brun, et al., 2001; Velez-Reyes, et al., 1995; Sandink, et al., 2001; Yao, et al., 2003) were generalized from the methods for linear-in-parameter systems, assuming initial parameter values are close to the optimal. However, the robustness of the selection is often questionable due to the near-optimal assumption in nonlinear problem. Hence, global sensitivity (Chu, et al., 2007; Burgos, et al., 2007) approaches are developed, aiming to overcome the limitation of localized selection. Nevertheless, a large number of simulations are often required, and it becomes prohibitively expensive for large-scale problems. Regularized parameter estimation (Eriksson, 1996; Renaut, et al., 2008) is another alternate. Nonetheless, how to find suitable regularization parameters is also nontrivial.

- **Complex process model**

As seen in the previous discussion, polymerization process models usually consist of highly nonlinear and stiff differential-algebraic equations (DAEs). The obtainment of an optimal solution is computationally challenging for this class of problems. DAE / PDAE constrained optimization problems drive the need of advanced algorithms to achieve better convergence properties and handle higher dimensional optimization problems.

There are three main solution approaches for dynamic optimization. First, the variational method, which calculates the first order necessary conditions for optimality without reformulating model equations, is usually prohibitively expensive to solve. Second, the partial discretization approach, considers a discretization of the control problem $u(t)$, and then applies dynamic programming or sequential methods. However, these approaches cannot treat bounds on state variables or path constraints directly, which will result in difficulties to consider polymer quality as additional constraints, for example. Third, full discretization methods, which explicitly discretize all the variables of the DAE system following a simultaneous approach, have advantages with state variable constraints and path constraints. Though it generates a large-scale nonlinear programming problem, efficient NLP algorithms can be applied with special decomposition strategies, such as the NLP solver, IPOPT (Wächter, 2002) which can solve large-scale NLP problems efficiently. A more detailed description of the simultaneous method is given by Biegler (2002).

2.3.2 Process Optimization

One of the ultimate goals of process modeling is to obtain an optimized solution which is not obvious by a traditional trial-and-error approach. Model utilization for process optimization is of great importance in the modeling practice. In general, there are offline and online process optimizations designed for different purposes.

Offline process optimization problems are typically involved in the process design, operation policy development, etc. Optimization is carried out based on steady-state or dynamic polymerization process models. When a deterministic model is used, the resulting (dynamic) optimization problem can be solved through similar solution strategies like the parameter estimation problems discussed above. If process uncertainty must be considered,

special treatments are required in the problem formulation and solution computation. Multi-scenario formulation is a convenient way to formulate optimization under the uncertainty problem (Laird, et al., 2008). However, its application is limited in polymer process analysis due to the high computational cost resulting from the large-scale nonlinear problem.

Recently, research has been active in the area of online process optimization that takes advantages of state-estimation technology and growing computation power. However, many important variables, which are related to end-use polymer properties, cannot be measured on-line or can only be measured at low sampling frequencies. State-estimation technologies provide "soft sensors" for model predictive control. In each decision step, the process model is updated with real-time data, and the optimization solution is determined through online calculators based on the online validated model. The online optimization framework overcomes the uncertainty of the offline model, enabling on-line monitoring of polymer quality and improved existing optimization solution. Since some of these topics are beyond the scope of our discussion, the interested reader is referred to recent books on state estimation (Simon, 2006), and introductory review articles for nonlinear model predictive control (Camacho, et al., 2007) for more details.

In case the simulation model is too expensive to be used for optimization directly, various model reduction techniques are developed to obtain an optimum.

2.4 Commercial Software for Polymerization Reactor Modeling

Due to the time and effort-consuming procedure for developing polymerization process model-based application, significant efforts are devoted to develop a general purpose solu-

tion for polymerization process modeling and optimization that includes above features. As a result, commercial software has been heavily investigated. It is reported to achieve notable successes for some important commercial polymer processes in industry, and plays an important role in modern polymer reaction engineering. Some of the competitive commercial packages are briefly discussed here. Interested readers can refer to vendors' websites for more details.

"Aspen Polymers", formerly "Aspen Polymers Plus^{TM}", is one of the core elements of AspenTech's aspenONE^{TM} Engineering applications. It aims to employ first-principles polymer modeling technology for conceptual design of polymerization processes. It features extensive databases for polymer system physical properties calculation, where polymer activity coefficients and equations of state are incorporated. General classes of polymerization kinetics are provided, and user-defined reactions may be added. The simulation model is solved through an equation-oriented solution strategy. Dynamic optimization with embedded DAE problem is solved with sequential approach. Chen (2002) listed several industrial modeling practices through Aspen Polymers, including PBT, PET, Nylon 6, Silicone, LDPE, HDPE, PP, PS etc. Users may take advantage of combining other analysis packages in Aspen for process study.

Other general purpose modular modelers, such as gPROMS, Pro II (Polymer II Tm) also support polymerization modeling in addition to small molecule chemical processes.

"PREDICI" is a relatively new simulation package for polymerization processes. It evolved from a solver for population balances describing molecular weight distribution in polymer reaction kinetics to a comprehensive tool for variety of polymer processes (Wulkow, 2008). The main feature of PREDICI lies in its mathematical concepts for model-

ing and computation. Polymerization reaction is defined through "reaction step patterns". It enables additional flexibility for polymer kinetic modeling. More importantly, Galerkin h-p-method is used as its core algorithm. It claims to be capable of simulating complete molecular weight distributions of any form up to any degree of polymerization. A recent overview of PREDICI and a detailed description of the mathematical techniques and algorithms behind PREDICI can be found in Wulkow (2008), as well as in the literature, where advanced kinetic models are constructed on PREDICI with customized features.

Commercial software packages provide a convenient way for construction and demonstration of polymer process models. However, a closer integration between modeling and optimization tools is needed to facilitate model-based applications for a boarder family of polymer products. Continuous efforts are also needed to improve the underlining modeling and computational strategies to tackle increasingly complex problems arising in the polymer industry.

2.5 Summary

In summary, polymer reaction engineering embraces tremendous developments benefiting from advanced polymerization reactor modeling and optimization technologies. First-principle models are being developed at different scales for understanding the relationship between process conditions and product properties. Parameter estimation and process optimization are carried out based on polymer reactor models through advanced computational strategies. Commercial packages continuously incorporate new advancements in modeling and optimization for model-based applications in polymer engineering. While remarkable successes have been achieved in the past, there are unique challenges in polymerization pro-

cess which remain to be addressed. Therefore, there are broad potential and opportunities for further development to handle complex modeling and optimization problems. The investment in developing polymer process models yields returns in many different ways.

Chapter 3

Interpenetrating Polymer Network Process and Modeling Framework

The Semi-Interpenetrating Polymer Network (SIPN) process is the focus in this work for studying model-based application. This chapter introduces the family of Interpenetrating Polymer Network products and their process features. Associated modeling and optimization problems are identified. An industrial SIPN process is presented as an example, and a multi-stage modeling framework for SIPN is outlined.

3.1 Introduction of IPN

Interpenetrating polymer networks, IPNs, are a broad class of polymer composites defined as a combination of two polymers in a network form, with at least one of them synthesized and/or cross-linked in the immediate presence of the other (Sperling, 1981). The first known IPN material was reported in the patent by Alysworth (1994) (Sperling, 2004). Yet, the term of "interpenetrating polymer network" was not used until 1960, where it was first introduced by Millar (1960). During that period, cross-linked and grafted polymer products were widely developed. Studies on IPN started to attract growing interests. Kahovec et al. (1997) systematically defined the nomenclature of IPN materials. IPNs were formally added to the polymer dictionary.

Individual constituents in IPN are generically polymer resin and fibers, which serve as the matrix phase and the reinforcing phase, respectively (Advani, et al., 2002). IPNs possess several interesting characteristics in comparison to normal polyblends, in particular, its valuable synergistic effect. The distinctive properties of IPNs have attracted considerable attention, and continue to be of interest in both fundamental and applied R&D investigations. IPNs have been utilized in widespread commercial applications (Klempner, et al., 1994), and are considered promising in novel material development (Athawale, et al., 2002). IPN's capability of forming tough but flexible materials enables its utilization for sound and vibration damping, biomedical applications, natural products and renewable resources, tough and impact-resistant materials, etc. Several comprehensive reviews of IPNs can be found in Klempner and Frisch (1994), Gupta and Srivastava (1994), Sperling (2004) and Myung et al. (2008), where the nomenclature, synthesis and properties of IPN are discussed.

3.1.1 IPN Molecular Structure

As its name suggests, two key features of IPN products are "interpenetrating" and "Network", which lead to the characteristics of IPN chemical and mechanism properties. Figure 3.1 presents schematic representations of IPN structures. Different lines symbolize polymer chains which consist of different monomer units. Dots are crosslinking or grafting sites between two polymers.

(a) Full IPN   (b) Semi-IPN
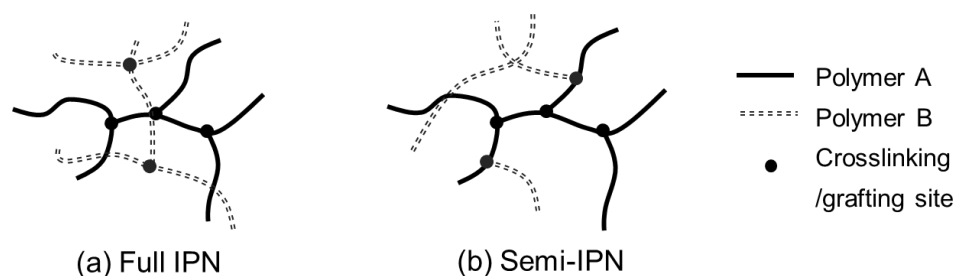
Figure 3.1 Schematic representations of IPN structure

Figure 3.1(a) illustrates the structure of the full IPN, which has both polymers homo-crosslinked. The intimately combining crosslinked macromolecular network has advantages in controlling the phase separation. Even for polymers which are thermodynamically incompatible, permanent entanglements between the different crosslinked networks prevent complete phase separation in such system. Consequently, various types of crosslinking formation have important impact on its product morphology. Besides the full IPNs, there are semi-IPNs (SIPN). Figure 3.1(b) shows an example of SIPN, which only contains one polymer network. The other polymer presented in Semi-IPN is linear or branched. There are semi-I and semi-II SIPN, which refer to having the first or second polymers cross-linked, respectively. In fact, the formulation of the non-crosslinked polymer plays an important role in SIPN phase behavior. Without permanent entanglements between the two polymers, it is possible to separate the non-crosslinked polymer from the composite.   Therefore, in order to reinforce the apparent compatibility, some degree of branched-structure is preferred in the system. The well-interpenetrated structure is thermodynamically more stable. Hence, the relationship between IPN crosslinking kinetics and IPN structure is of great interests for product development.

3.1.2 IPN Material Morphology

Different ways and degrees of interpenetration lead to various IPN morphologies. IPNs represent a special example of topological isomerism in macromolecules (Frisch, 1985). The growing quantity of one polymer will transform from a separate phase, co-continuous phase to become continuous phase, called phase inversion. For example, if one polymer is glassy and the other is elastomeric at room temperature, one obtains either a reinforced rubber or a high impact plastic depending on which phase is continuous (Frisch, et al., 1974). When the

interpenetrating process is well-controlled, gradient composites are possible to be produced. Successful applications are widely reported. Understanding and control of IPN interpenetration dynamics is important for IPN production.

3.1.3 IPN Polymerization Process

The procedure to synthesize IPNs can be generally classified into two categories, i.e., simultaneous and sequential approaches. Simultaneous synthetic methods start with a mixture of both monomers to form two polymer networks simultaneously through different reaction routes. Sequential synthetic methods control different network reactions by sequentially adding different monomers. Currently, many commercial materials are produced as sequential IPNs, due to their flexibility and relatively ease of processability. The sequential approach also enables post-processing modification of mass-produced commodity polymers into value-added specialties for a broader range of applications, such as polyethylene based products. Molecular properties of SIPNs are strongly affected by their processing conditions.

(a) Simultaneous synthesis method

(b) Sequential synthesis method
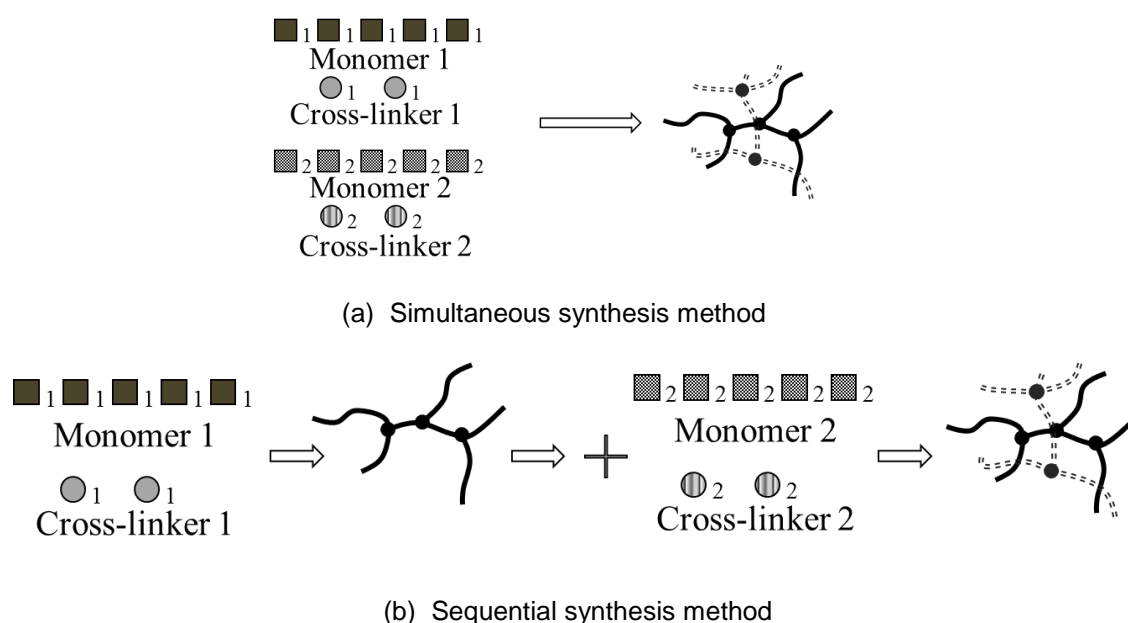
Figure 3.2 Schematic representations of IPN synthesis methods

In particular, SIPNs synthesized through post-process modification are generally produced in a particulate form. Pre-polymerized seed is used for in-situ polymerization. A typical process technology is seeded suspension polymerization.
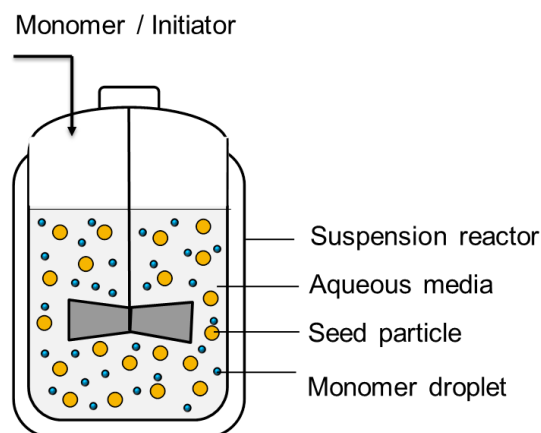
Figure 3.3 A schematic representation of PES semi-batch process

As shown in Figure 3.3, seeded suspension polymerization begins with a pretreated polymer seed swollen with monomer. Then, monomer solution is fed under strong agitation into the suspension reactor containing water, seed particles, and suspending agents. In-situ polymerization is carried out with a controlled feeding of initiator and monomer. Depending on the formulary and polymerization conditions, various penetrations can be achieved in the seed for different applications. This technology provides unique advantages in controlling of particle size distribution and polymerization rate, which is particularly suitable for specialty polymer production.

3.1.4 Examples of IPN Products

The capability of formulating synergistic polymer composite paves a way for new material design. Numerous IPN materials are developed and investigated. Table 3.2 updated from (Sperling, 2004) shows some examples of commercial IPN materials.

Table 3.1 Examples of commercial IPNs

Manufacturer	Trade Name	Composition	Application
Shell Chemical Co.	Kraton IPN	SEBS-polyester	Automotive parts
LNP Plastics	Rimplast	Silicon rubber-nylon or PU	Gears or medical
DSM N.V.	Kelburon	PP-EP or rubber-PE	
Uniroyal (Reichhold Chemical Co)	TPR	EPDM-PP	Auto bumper parts
Rohm & Haas		Anionic-cationic	Ion-exchange resins
Monsanto	Santoprene	EPDM-PP	Tires, hoses, belts and gaskets
BF Goodrich	Telcar	EPDM-PP or PE	Tubing, liners and
Exxon	Vistalon	EPDM-PP	Paintable automotive parts
Cook Composites	Acpol	Acrylic-urethane-polystyrene	Sheet molding compounds
Dentsply International	Trubyte, Bioform	Acrylic-based	Artificial teeth
NOVANA Inc	Macro-IPN		Healthcare, drug delivery
Bio Med Sciences	Silon	PDMS-PTFE	Burn dressing, scar abatement

3.2 Related Modeling Studies

Although SIPN products have been being widely commercialized, mathematical models for SIPN process are not yet available. The process complexity leads to particular challenges for applying modeling and optimization technology. In this section, related modeling studies are reviewed. Their applicability and restrictions for the SIPN modeling system are highlighted.

3.2.1 SIPN Kinetic Modeling

Important characteristics of SIPN products include gel content for the insoluble part (network), joint molecular weight for the soluble part (linear), as well as branch content in both parts (nonlinear). Therefore, the reactions of grafting, crosslinking, possible degradation and polymer interactions should all contribute to the SIPN kinetics. Though numerous models

are developed for free radical polymerization system, no kinetic models are available for SIPN binary systems.

The kinetic modeling approaches summarized in Table 2.1 are generally suitable for linear polymer systems. However, modeling the process beyond the gel point and considering polymer, and polymer-polymer reactions are main difficulties for SIPN kinetic modeling. Various modifications of linear polymer models are developed for gel and grafting systems.

The gel point refers to the starting time of the network formation. Type-I SIPN (the first synthesized polymer is crosslinked) preparation is different from the crosslinking formation during polymerization. As saturated polymer is crosslinked in the presence of peroxides, gelation does not only indicate the decrease of macro-radical mobility as in the linear polymer system, but also leads to polymer networks. Some of the main concerns in modeling peroxide induced polymer networking have been gel prediction with a *MWD* simulation. The well-known Saito-Kimura-Tobita scheme (Saito, 1958) was first developed as a simple integral-differential equation to predict gel content and MWD in a random crosslinking process. This was further developed by (Kimura, 1962) and (Tobita, 1995), where a series of solutions for various types of initial polymer distributions were derived. A further class of models follows this framework (Zhu, 1996; Cheung, et al., 1997; Tai, 1999), but they suffer from several limitations. First, the gelation point is always a point of discontinuity for kinetic analyses (modeling) (Hamielec, et al., 1991). The gel point is determined by the widely known Charlesby-Pinner equation which is valid only when the initial molecular weight distribution (MWD) is the most probable one. However, the Charlesby-Pinner equation is frequently used for distributions where it is not applicable (Shyichuk, 1996). Furthermore, the general solution of MWD starting from an arbitrary initial polymer distribution is not

available. When the decomposed initiator participates in reactions other than initiation with polymer backbones, calculation of crosslinking density is also not straightforward. Consequently, the model becomes incapable of predicting the polymer composite product.

A class of models which focuses on gel prediction is developed (Kim, et al., 1984; Sen, et al., 1991; Ghosh, et al., 1998a), where exothermic change due to polymerization of the monomer is studied by DSC. These kinetic models achieve good agreement of conversion rate despite their simplicity. However, the molecular weight development is not taken into account. As a result, the underlying chemical mechanisms are still hidden. The kinetic study of Suwanda, et al. (1993) is considered to be the first kinetic study of this kind. Here, the effect of degree of unsaturation and branch points in the polyethylene chain is studied at a very low initiator concentration, and crosslinking and chain scission are neglected in the work. Pedernera, et al. (1999) developed a double moment technique, which uses a particular combination of chain length and vinyl number as moment indices, so that number, weight and z-average molecular weight can be calculated. Asteasuain et al. (2002) applied the approach of probability generating functions (PGF) to describe complete molecular weight distributions for peroxide modification of polyethylene. Three different PGFs are defined to describe number, weight and chromatographic distribution. However, the general shortcoming of this class of models is the inability to describe the simulation beyond the gel point, as the highest moment or chain length approaches infinity.

To overcome this barrier, a Monte Carlo (MC) simulation method is introduced for this complex system, and becomes a powerful method for investigating the whole molecular constitution. The Monte Carlo sampling technique (Tobita, 1994; Zhu, et al., 2003) is applied to simulate molecular weight distribution and crosslinking density involving

crosslinking, branching as well as degradation reactions for the modification of polymers. Wen, et al. (2003a, 2003b) developed kinetic gelation models to simulate kinetics of cross-linking polymerization on fixed lattices, where propagation and termination reactions are restricted to occur only between nearest neighbors. Probability density function and stochastic approaches were applied to simulate network formation and inhomogeneous reaction rate. With the MC simulation method, one can obtain and directly observe detailed structural information for each polymer molecule formed in a straightforward manner (Verros, 2003). Despite this capability for property simulation, the MC approach is generally computationally expensive, and its stochastic nature leads to difficulties in process control, design and optimization.

Another fundamental kinetic modeling approach was developed by Likozar, et al. (2002), where a detailed model is constructed for simulation of chemical kinetics of an elastomer crosslinking by organic peroxides. A population balance equation is used for the collection of elastomer backbone sites and segment reactivity is taken into account. The concentration of total crosslinks, elastomer-elastomer bonds, and peroxide-elastomer bonds are predicted by the kinetic model. While this approach has roots in fundamental crosslinking chemistry, it is not able to predict molecular weight distribution and gel content properties. Hence, no direct comparison to the process data can be made through this kinetic model. As MWD and gel content prediction are both desirable properties for quality indication, more work is needed in developing a comprehensive model which is capable of considering detailed kinetics while maintaining satisfactory simplicity.

Finally, although polymer degradation is not intended for the SIPN process, it is worth noting that peroxide-induced degradation could take place in such systems. Modeling of

peroxide enhanced degradation was studied (Kim, et al., 2000). When both polymers in the composite undergo degradation, a similar approach can be applied (Sivalingam, et al., 2004). Inclusion of possible degradation mechanisms are important for SIPN product quality control, and therefore require further investigation.

3.2.2 SIPN Particle Modeling and Semi-batch Operation

Seeded suspension polymerization is an important class of heterogeneous polymerization technology. The in-situ polymerization stage is different from conventional suspension polymerization in several aspects. The heterogeneous nature complicates the study of this process. Gon çalves, et al. (2008) showed that different average molecular weights were obtained through seeded suspension polymerization. This could result from the high viscosity of the monomer swollen particle, which limits mobility of the growing chains and decreases their termination rate. Understanding and exploiting the relationship between process operation conditions and polymer particle properties are crucial for product quality control and process improvement.

However, while numerous models have been developed for suspension polymerization, models for seeded suspension polymerization are scarce. Conventional styrene batch/semi-batch reactor models, which are similar to the bulk system model, would encounter difficulties in describing heterogeneous seeded particles. Also, the single particle model developed for batch reactors by Zhang, et al. (1997), which assumes equilibrium mass partition and constant particle density, becomes inappropriate for semi-batch dynamics. A more detailed meso-scale particle model for an emulsion modified semi-batch styrene suspension polymerization process is developed by Lenzi, et al. (2005), where mass transfer and various kinetic mechanisms are taken into account. However, intra-particle composition and swelling are

not considered for their single polymer system; this limits model applicability for the SIPN seeded particulate process.

Determination of SIPN particle size distribution in semi-batch process is complicated by several factors, such as initial seed PSD, monomer-polymer interaction, second particle formation, semi-batch feeding rate and mixing conditions. A uniform PSD of SIPN product is typically desired for better end-use properties. Therefore, process conditions are required to meet several constraints in the operation.

3.3 Modeling and Optimization Framework

Due to the complexity of IPN products, experimental studies are often time and resource consuming. Reduction in production cost and more stringent product quality requirements become major challenges for polymer manufacturers in the increasingly competitive polymer market. While specific polymer structures are desired for various applications, poor control of process conditions can prevent the formation of the preferred structure, and consequently affects ultimate properties. Advanced mathematical models and optimization approaches are pursued to provide insights for process operation and material design. In this section, an example of a commercial SIPN process is described. An overview of SIPN modeling and optimization framework is sketched. Confronting modeling and optimization problems are discussed.

3.3.1 An Example SIPN Process

Since polyethylene is currently the largest commodity polymer product, SIPN modification of polyethylene is of particular interest. On the other hand, styrenic resin is one of the main commercial resins produced by suspension polymerization processes. A sequential SIPN

process from polyethylene seed with styrenic monomer modification, {net-polyethylene}-ipn-{polystyrene} Semi-I IPN, is considered as an application example for our study. The product produced serves as an advanced impact-resistant packaging material, with rigidity, impact strength and good dimensional stability. Here "PES" is used as an abbreviation of its full name. A description of PES is provided here.

- **PES process**

Polymerization of PES begins with polyethylene seeds that are swollen with styrene monomer. Fine structured PES particles are formed and grown by semi-batch feeding of monomer and initiator solution.

Figure 3.4 illustrates the development of a PES particle. The particle undergoes pretreatment, polymerization and crosslinking. At the beginning of the process, polyethylene seed is suspended in the suspension reactor; a portion of styrene monomer solution is slowly added at a non-reacting condition; and the reactor is held until initial swelling is completed. Then, initiator and monomer are slowly added to the suspension reactor to initiate in-situ polymerization process following a free radical polymerization mechanism. When the styrene polymerization approaches completion, polyethylene is crosslinked into networks at a high temperature.

This SIPN modification technology significantly improves conventional polymer particle properties. Many successful results have been reported and patented (eg. Kitamori, 1976; Kitamori, 1979; Kajimura, et al., 1981; Kobayashi, et al., 1985; Adolph, et al., 1987; Adolph, et al., 1987). Thus, it is desirable to develop model-based optimization strategies based on this example.

3.3.2 Proposed Modeling Framework

A modeling framework is sketched for an SIPN process based on the example of the PES process. The SIPN modeling procedure is featured as a multi-stage modeling approach. Sub-models are developed for each stage of the SIPN process accordingly, in order to decouple the modeling complexity. The main assumptions include that crosslinking and monomer diffusion are negligible in each stage correspondingly.

Figure 3.4 and Table 3.2 outline the modeling and optimization framework for the SIPN process, and provides an organized reference for the following chapters. The polymerization stage is considered as the first stage in the modeling which starts from the condition after pretreatment. A single particle model is developed to link the polymerization kinetics and semi-batch operation at the particle level. Since polyethylene is assumed to be inert during this stage, the evaluation of the "interpenetrating" feature is the main focus in the particle growth model. The second part of the model focuses on SIPN kinetics. The full kinetic mechanism is considered to simulate the final product properties. Then the two sub-models are connected to represent a complete SIPN process. Optimization is carried out individually and jointly to obtain an optimal semi-batch feeding rate. Dynamic optimization and surrogate-model-based optimization strategies are developed accordingly.

Pretreatment   **Stage I**   **Stage II**

- monomer
- monomer + initiator
- seed polymer
- polymerized polymer
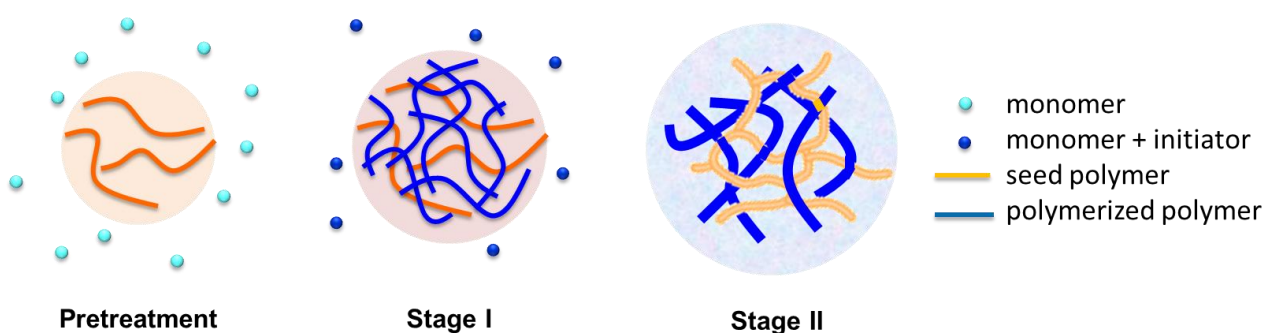
Figure 3.4 A two-stage SIPN process

Table 3.2 Modeling and optimization framework for the SIPN process

	Stage I	**Stage II**
Features	Complex diffusion; Single component reaction.	Complex composite networking reaction
Modeling	**Particle Growth model**	**SIPN Kinetic model**
Optimization variables	• Monomer feeding rate • Initiator feeding rate	• Initial polymer • Monomer concentration • Initiator mixture concentration • Holding temperature • Holding duration
Optimization approaches	**Dynamic optimization**	**Surrogate modeling**
	Integrated optimization; multi-scenario optimization	

The process models intend to answer the following questions:

- How process conditions affect SIPN structure properties.

- How to produce the SIPN product in an optimal way.

Prototype process modeling, parameter estimation and dynamic optimization are foci in the following sections.

3.4 Summary

SIPN is a class of advanced polymer composites, which has been used for a broad range of applications. It is typically synthesized through a sequential approach, where two key features of IPN, "interpenetration" and "network", are able to be produced and controlled relatively conveniently. An example of commercial SIPN product, PES, is examined in more detail. Main research questions are brought forward during the model-based optimization practice. A modeling and optimization framework is outlined as a road map of this thesis work.

Chapter 4

Stage I Model: Single Particle Modeling

In this chapter, we focus on the SIPN system at the polymerization stage, which is a seeded suspension polymerization process. A single particle growth model is developed, with consideration of three key features of the seeded suspension polymerization — particle growth mechanism, intra-particle heterogeneity and polymerization kinetics. The moving boundary integral-differential-algebraic equation is solved by dimensionless coordinate discretization. Intra-particle dynamics are able to be revealed through model simulation.

4.1 Model Development

As shown in Figure 3.4, Stage I of SIPN process is a semi-batch seeded suspension polymerization process. Here, a sub-model is built for this stage, assuming crosslinking reaction is negligible.

Semi-batch seeded suspension polymerization systems present unique characteristics that greatly differ from classical suspension polymerization, such as the monomer feeding rate and the mass transfer mechanisms of monomer to the polymer particles (Gonçalves, et al., 2008). To the best of our knowledge, this study is the first to use a single particle model to develop composite particles in suspension polymerization systems.

4.1.1 Single Particle Model Representation

The mathematical model for the seeded suspension styrene polymerization process was created using the following assumptions on process conditions, which mirror observations in the pilot plant.

1) The polymerization reactor is perfectly mixed.

2) Reactions occur under isothermal conditions.

3) The solubility of the monomer and initiator in the aqueous phase is negligible.

4) Swollen seed particles maintain spherical geometry.

5) Coalescence and breakage of seed particles do not occur at the polymer particle level.

6) Secondary particle formation is avoided in the studied system, when homogeneous nucleation and monomer droplet nucleation are restricted.

7) Phase separation is restricted by pretreatment of seed particles.

8) Pre-polymerized seed polymer is monodisperse and inert during second stage polymerization.

9) Imbibition of styrene and initiator are diffusion limited, following a Fickian diffusion mechanism in the radial direction. Also, polymer diffusion is negligible.

10) Kinetic parameters are independent of polymer chain length.

The reaction mechanism is presented in Table 1, following the well-known steps of free radical polymerization: initiation, propagation, termination and chain transfer.

Assumptions (5) ~ (7) are desirable conditions for seeded suspension polymerization manufacturing. Particle coalescence and breakage phenomenon are affected by a combination of different factors, such as the suspension agent, the degree of agitation, the design of stirrer/reactor system etc. (Vivaldo-Lima, et al., 1997). Seeded suspension polymerization is

Table 4.1 Free Radical Polymerization of Styrene

Initiation Reactions	$X_2 \xrightarrow{k_I} 2X^\bullet$	Initiator scission
	$X^\bullet + M \xrightarrow{k_{IM}} R^\bullet(1)$	Radical initiation
	$3M \xrightarrow{k_{th}} 2R^\bullet(1)$	Thermal initiation
Propagation Reactions	$R^\bullet(n) + M \xrightarrow{k_p} R^\bullet(n+1)$	
Termination Reactions	$R^\bullet(n) + R^\bullet(n') \xrightarrow{k_t} P(n+n')$	Combination
Chain Transfer Reactions	$R^\bullet(n) + M \xrightarrow{k_{fs}} P(n) + R^\bullet(1)$	Transfer to monomer

different from conventional suspension polymerization, because seed particle integrity is mainly controlled by the property of the monomer swollen seed. In addition, to control the reactor mixing conditions, the seed particle is chosen so that it cannot be dissolved by the monomer after pretreatment. The monomer to seed polymer composition ratio is usually limited to avoid particle breakage (Gon çalves, et al., 2008). In addition, it is observed that the type of monomer strongly influences the formation of secondary particles. The fraction of secondary particles decreases when monomers with lower water solubility are used. Styrene, which is essentially water insoluble (water solubility is 0.0271% at 25°C) (Bovey, et al., 1950) is observed to be almost totally incorporated in the seeds with negligible secondary particles formed (Gon çalves, et al., 2009). A series of styrenic monomers, such as alpha-methylstyrene, para-t-butylstyrene, monochlorostyrene, dichlorostyrene, also fall into this category. Hence, from a modeling point of view, a single particle model is an appropriate representation for the seeded suspension process. Assumption (8) is a valid simplification. For the application of suspension polymerized polymers, an important task in the process is to obtain polymer particles of a narrow size distribution (Kichatov, et al., 2003). The major aim in suspension polymerization is the formation of a dispersion of monomer droplets in

the aqueous phase that is as uniform as possible by controlled coalescence of these droplets during the polymerization process (Vivaldo-Lima, et al., 1997). Monodisperse seed is usually adopted for particle size control in seeded polymerization, since it is considered to be suitable to achieve a very narrow particle size distribution with such a technique (Salamone, 1996). From industrial practice, the particles produced have a similar narrow size distribution as the initial added seeds. The inert seed assumption can be applied for seed polymer with only a few functional groups. For functional seed polymers, the model can be further modified with different reaction mechanisms, while the presented modeling procedure will remain valid. Finally, as justified in Stubbs, et al. (1999), we consider the assumption of Fickian diffusion sufficient for the purpose of these calculations, although we recognize that more complex diffusion phenomena can occur in these systems (e.g., we may require case II diffusion).

Based on the above conditions, we define spherical coordinates at the center of the seed particle and write the mass conservation equation for the monomer and initiator in a single particle as:

$$\frac{\partial C_l(r,t)}{\partial t} = \nabla(D_l \nabla C_l) - v_l = \frac{1}{r^2}\frac{\partial}{\partial r}\left(D_l r^2 \frac{\partial C_l}{\partial r}\right) - v_l, \qquad l = M, I \qquad (4.1)$$

where l represents monomer M and initiator I, (r,t) specifies the state at radius r at time t, C_l is the molar concentration, v_l is molar consumption rate, and D_l is the effective diffusion coefficient of l. Though various models are developed to model diffusion behavior in polymers, no general formulation of diffusion rate could be obtained over a wide concentration range of the monomer in polymer solution. In the case that styrene monomer can be easily

and rapidly absorbed in the polyolefin resin beads (Kobayashi, et al., 1985), a constant average D_l is used in our model. Equation (4.1) is then reduced to

$$\frac{\partial C_l(r,t)}{\partial t} = \frac{D_l}{r^2}\frac{\partial}{\partial r}\left(r^2\frac{\partial C_l}{\partial r}\right) - v_l, \qquad l = M, I \tag{4.2}$$

For the polymer species, swelling is considered to be the main effect on the concentration change. The rate equation for polymer is derived as equation (4.3), where we consider polymer diffusion to be negligible.

$$\frac{\partial C_{\mathcal{P}_i}(r,t)}{\partial t} = v_{P(i)} \tag{4.3}$$

Here $C_{\mathcal{P}_i}$ is the molar concentration of $P(i)$, live or dead polymer of chain length i, and v_{P_i} is the production rate of $P(i)$. Equations (4.2) and (4.3) are the basis for the single particle model, discussed in more detail in the following sections.

4.1.2 Particle Growth Mechanism

Solving the mass conservation equation (4.2) and (4.3) is complicated by a moving boundary condition, since the particle growth mechanism includes both monomer absorption and heterogeneous diffusion-reaction. For distinguishing properties of seeded suspension polymerization, mass transfer as well as varying particle density must be taken into account for rigorous particle size modeling, and a collision-absorption mechanism and particle volume approximation are introduced to determine the boundary condition.

4.1.2.1 Collision-absorption Mechanism

Monomer absorption is the initial step in particle growth. Whereas the semi-batch polymerization is usually not operated at equilibrium, the collision-absorption mechanism can be

applied to make a valid modeling simplification. This mechanism assumes that once the dispersed monomer droplets collide with the seed polymer particles, they swell the seed boundary instantaneously to reduce the chemical potential of the system. Also, the aqueous phase boundary layer resistance and surfactant layer resistance of the seed are negligible compared to the intra-particle diffusion resistance.

Finally, in seeded suspension systems, monomer droplets are smaller, providing a large relative surface area, and are much less stable than the seed particle. As also observed in emulsion modified semi-batch suspension processes, irreversible mass transfer is favored under these conditions. Emulsified monomer droplets tend to aggregate onto the larger suspension beads to form an outer shell of the particle (Lenzi, et al., 2005), Unlike mass transfer models for partially water soluble monomer, mass-transfer resistance of the aqueous phase and surfactant layer is not considered to be important in our single particle model (Zhang, 1997). Thus, the resistance of the aqueous phase boundary for water insoluble monomer is expected to be even smaller and the boundary layer resistance can be ignored, provided that monomer feeding is controlled and the agitation speed is high.

Under ideal mixing conditions, the chance of collision with a monomer droplet is identical for every seed from all directions, and the boundary condition at the surface of the seed can be represented as equation (4.4).

$$at \ r = R(t), \quad 4\pi R(t)^2 \cdot D_l \frac{\partial C_l}{\partial r} = F_l(t), \quad l = M, I \qquad (4.4)$$

where $R(t)$ is the particle radius at time t, $F_l(t)$ is the molar absorption rate of reactants M and I by each particle. Based on the mono-disperse assumption, equation (4.5) is considered for the single particle model.

$$F_l(t) = \frac{\mathbb{F}_l(t)}{\mathbb{N}_{seed}} \tag{4.5}$$

where $\mathbb{F}_l(t)$ the molar feeding is rate of reactant M and I into the reactor, and $\mathbb{N}_{seed}$ is the total number of seed particles in the reactor, calculated based on average particle size. If a distributed seed particle is used, a population balance equation will need to be introduced to compute $F_l(t)$.

At the center of the seed, there is no diffusional driving force, so the boundary condition is set as:

$$at \ \ r = 0, \quad \frac{\partial C_l}{\partial r} = 0 \tag{4.6}$$

Also, the initial condition is defined as the initial state of the polymerization stage.

$$at \ \ t = 0, \quad C_l = C_l(0) \tag{4.7}$$

4.1.2.2 Particle Volume Approximation

Intra-particle heterogeneity is an important feature of seeded suspension polymerization which is not considered in other single component particle systems. The absorbed monomer swells the seed, while diffusing and polymerizing inside the particle. The changes in particle density are calculated from partial volume properties. The partial molar volume of species l, $\bar{V}_l$, is defined as equation (4.8).

$$\bar{V}_l = \frac{\partial V}{\partial n_l}|_{T,P,n_{l' \neq l}} \tag{4.8}$$

where polymer species are represented by their composite segments. Hence, the particle volume can be represented as a sum of the volume for each component through equation (4.9) :

$$V = \sum_l V_i = \sum_l \int_{particle} \bar{V}_l dn_l \qquad (4.9)$$

In spherical coordinates, this is written as:

$$dn_l = C_l dV = 4\pi \cdot C_l \cdot r^2 dr. \qquad (4.10)$$

Since only a small amount of initiator is used in the process, the contribution of initiator volume is neglected. By substituting (4.10) into (4.9), the overall volume of the particle can be written as:

$$
\begin{aligned}
V(t) &= \frac{4}{3}\pi R(t)^3 = V_{P_1}(t) + V_{P_2}(t) + V_M(t) \\
&= 4\pi \cdot \left(\int_0^{R(t)} C_{P_1} \cdot \bar{V}_{P_1} \cdot r^2 dr + \int_0^{R(t)} C_{P_2} \cdot \bar{V}_{P_2} \cdot r^2 dr \right. \\
&\quad \left. + \int_0^{R(t)} C_M \cdot \bar{V}_M \cdot r^2 dr \right)
\end{aligned}
\qquad (4.11)
$$

where $\bar{V}_{P_1}$, $\bar{V}_{P_2}$, $\bar{V}_M$ are the partial molar volumes for seed polymer, second stage polymer and styrene monomer respectively, and they are functions of states.

As the absorption does not reach equilibrium, an empirical relationship is proposed, as equation (4.12). The particle molar volume is assumed to be a function of monomer concentration and the coefficients a_0^l and a_1^l represent the contributions from the bulk volume and the monomer swelling effect for species l, as the monomer is a solvent for both polymers:

$$\bar{V}_l = a_0^l + a_1^l \cdot C_M \qquad (4.12)$$

Here $\bar{V}_l$ is the partial molar volume for l. Substituting equation (4.12) into equation (4.11) we obtain

$$
\begin{aligned}
V(t) \ &= \ \tfrac{4}{3}\pi R(t)^3 = 4\pi \cdot (\int_0^{R(t)} C_{P_1} \, (a_0^{P_1} + a_1^{P_1} \cdot C_M) \cdot r^2 dr \\
&= \ \int_0^{R(t)} C_{P_2} \, (a_0^{P_2} + a_1^{P_2} \cdot C_M) \cdot r^2 dr \\
&\quad \int_0^{R(t)} C_M \left(a_0^{M} + a_1^{M} \cdot C_M\right) \cdot r^2 dr)
\end{aligned}
\tag{4.13}
$$

Equations (4.4), (4.6) and (4.13) are then used to describe the moving boundary of the seed particle.

4.1.3 Particle Property Simulation

Mechanical properties of the polymer are usually reflected through polymer molecular characteristics, which are developed during the polymerization stage. In addition, for composite polymer particles, the formation of intra-particle morphology is of particular significance on the end-use properties. This morphology development can be affected by several factors. One of the important factors is the mechanism of diffusion controlled kinetics for the polymerization system, i.e., the apparent reaction rate is affected by the mobility of the reacting chain. Hence, the single particle modeling framework, which incorporates intra-particle dynamics, shows advantages for particulate properties simulation.

Also, in free radical polymerization, one of the main reaction steps, chain termination by macro-radical combination, is significantly influenced by the macro-radical diffusion ability, which is reflected by changes in intra-particle viscosity. The decrease of the termination rate at high monomer conversion ratio, known as the gel effect, becomes position dependent inside the particle. Hence, change of apparent termination rate needs to be incorporated in the reaction rate and molecular weight simulation.

There are several mechanistic models that describe the gel effect in the bulk system. A comprehensive review can be found in (Tefera, et al., 1997). For industrial modeling applications, the empirical formula from (Hui, et al., 1972) is typically considered.

$$k_t = k_{t0} \cdot \exp[-2(A_1 x_s + A_2 x_s^2 + A_3 x_s^3)] \tag{4.14}$$

where K_{t0} is a termination constant in an ideal system without gel effect, A_1, A_2, A_3 are temperature dependent coefficients, and x_s is the monomer conversion ratio. Adapting equation (4.14) to the single particle model, we define a local monomer conversion ratio, $x_s(r, t)$ as:

$$x_s(r, t) = \frac{C_{P_2}(r, t)}{C_{P_2}(r, t) + C_M(r, t)} \tag{4.15}$$

Where $C_{P_2}(r, t)$ and $C_M(r, t)$ are polymerized polymer and added monomer concentration at radius r at time t, respectively.

Finally, there are several approaches used to compute the polymerization rate and polymer molecular weight. Here we choose the method of moments, as it permits solution of the leading chain length distribution moments with considerably less computational effort (McKenna, et al., 2001). Let Y_i denote molar concentration of the ith moment of living polymer, Q_i denote molar concentration of the ith moment of dead polymer, and $r(j)$ and $p(j)$ are concentrations of living and dead polymer with j monomer units. The moments can be written as

$$Y_i = \sum_{j=1}^{\infty} j^i r(j), \quad Q_i = \sum_{j=1}^{\infty} j^i p(j) \tag{4.16}$$

Applying the quasi-steady-state approximation (QSSA) for the primal free radical, we obtain the following equations:

$$
\begin{aligned}
v_M &= (k_p + k_{fs})C_M Y_0 \\
v_I &= k_I C_I \\
\frac{\partial Y_0(r,t)}{\partial t} &= 2fk_d C_I + 2k_{th}C_M^3 - k_t Y_0^2 \\
\frac{\partial Y_1(r,t)}{\partial t} &= 2fk_d C_I + 2k_{th}C_M^3 + k_p C_M Y_0 \\
&\quad -(k_{fs}C_M + k_t Y_0)Y_1 \\
\frac{\partial Y_2(r,t)}{\partial t} &= 2k_I C_I + 2k_{th}C_M^3 + k_p C_M(2Y_1 + Y_0) \\
\\
\frac{\partial Q_0(r,t)}{\partial t} &= 0.5k_t Y_0^2 + k_{fs}C_M Y_0 \\
\frac{\partial Q_1(r,t)}{\partial t} &= k_t Y_0 Y_1 + k_{fs}C_M Y_1 \\
\frac{\partial Q_2(r,t)}{\partial t} &= k_t(Y_1^2 + Y_0 Y_2) + k_{fs}C_M Y_2.
\end{aligned}
\tag{4.17}
$$

The local monomer conversion ratio can be written as:

$$
x_s(r,t) = \frac{Q_1(r,t)}{Q_1(r,t) + C_M(r,t)}
\tag{4.18}
$$

and the overall monomer conversion ratio is calculated as

$$
\bar{x}_s(t) = \frac{\int_0^{R(t)} Q_1 r^2 dr}{\int_0^{R(t)} C_M r^2 dr + \int_0^{R(t)} Q_1 r^2 dr} = \frac{\int_0^{R(t)} Q_1 r^2 dr}{\int_0^{R(t)} C_M(t_0) r^2 dr + \int_0^t F_{feed} dt}
\tag{4.19}
$$

The number average and weight average molecular weight at radius r can be computed by the leading polymer moments as:

$$
\begin{aligned}
\overline{Mn}_r(t) &= \frac{(Q_1 + Y_1)}{(Q_0 + Y_0)} \cdot M_0, \\
\overline{Mw}_r(t) &= \frac{(Q_2 + Y_2)}{(Q_1 + Y_1)} \cdot M_0
\end{aligned}
\tag{4.20}
$$

where M_0 is the average molecular weight of polymer segments. Similarly, particle average molecular weight can be evaluated through equation (4.21):

$$
\begin{aligned}
\overline{Mn}(t) &= \frac{\int_0^{R(t)}(Q_1 + Y_1)r^2 dr}{\int_0^{R(t)}(Q_0 + Y_0)r^2 dr} \cdot M_0 \\
\overline{Mw}(t) &= \frac{\int_0^{R(t)}(Q_2 + Y_2)r^2 dr}{\int_0^{R(t)}(Q_1 + Y_1)r^2 dr} \cdot M_0
\end{aligned}
\tag{4.21}
$$

Therefore, while only the properties of particle composition and polymer average molecular weight are measured, it is important to point out that applying a lumped model to predict average properties will not capture the effect of diffusion controlled kinetics.

4.1.4 Solution Strategy

As equations (4.1)-(4.21) show, the derived model features coupled differential-integral-algebraic equations. Differential equations describe the inside of the particle, an integral equation describes the moving boundary and algebraic equations describe the output properties. To reduce the computational complexity, a shell-type spatial discretization approach is proposed to solve the coupled equations efficiently.
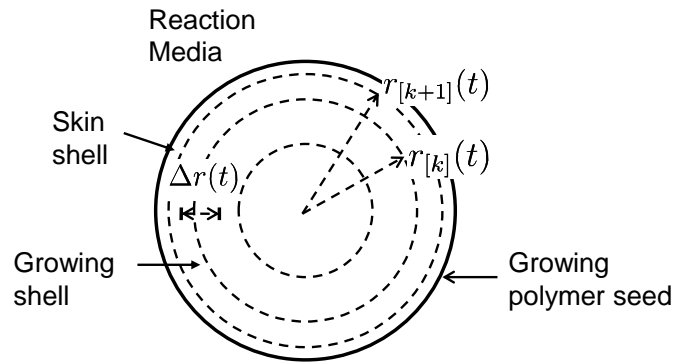
Figure 4.1 Representation of shell-type spatial discretization

As shown in Figure 4.1, the single particle is discretized into a number of hypothetical shells, which can be equally spaced in radius or in volume size. Each shell is regarded as an individual reaction zone, as in pseudo-homogeneous micro-bulk systems. Diffusion is con-

sidered for monomer and initiator from shell to shell. These shells are labeled from the core to the skin,[1] for the center, which is a full sphere, and $[ns]$ for the surface. The $[k]^{th}$ $(k = 1, \cdots, ns)$ shell has an inner radius $r^{[k-1]}$, outer radius $r^{[k]}$, and volume $V^{[k]}$, where $r^{[0]} = 0$.

While there are other discretization approaches for spatial discretization, e.g. based on method of weighted residuals, the finite difference scheme presents a particularly easy form in the case of growing shells. The discretized representation of the model can be obtained in a finite difference scheme. From equation (4.1), we define diffusion flux between the shells as (4.22), and represent monomer and initiator diffusion reaction dynamics in each shell as (4.23) - (4.25).

$$J_l^{[k]} = D_l \nabla C_l^{[k]} = D_l \frac{\partial C_l}{\partial r}\Big|_{r=r^{[k]}} \approx D_l \frac{\Delta C_l}{\Delta r}\Big|_{r=r^{[k]}} = \begin{cases} 2D_l \dfrac{C_l^{[2]} - C_l^{[1]}}{r^{[2]}}, k = 1 \\ 2D_l \dfrac{C_l^{[k+1]} - C_l^{[k]}}{r^{[k+1]} - r^{[k-1]}}, k = 2, \cdots, ns - 1 \end{cases} \tag{4.22}$$

At the surface layer, $k = ns$:

$$\begin{aligned} \frac{dn_M^{[ns]}}{dt} &= F_M(t) - 4\pi(r^{[ns-1]})^2 J_M^{[ns-1]} - V^{[ns]}(k_p + k_{fs})C_M^{[ns]}Y_0^{[ns]} \\ \frac{dn_I^{[ns]}}{dt} &= F_I(t) - 4\pi(r^{[ns-1]})^2 J_I^{[ns-1]} - V^{[ns]}k_I C_I^{[ns]} \end{aligned} \tag{4.23}$$

At the kth layer, $2 \leq k \leq ns - 1$:

$$\begin{aligned} \frac{dn_M^{[k]}}{dt} &= 4\pi((r^{[k]})^2 J_M^{[k]} - (r^{[k-1]})^2 J_M^{[k-1]}) - V^{[k]}(k_p + k_{fs})C_M^{[k]}Y_0^{[k]} \\ \frac{dn_I^{[k]}}{dt} &= 4\pi((r^{[k]})^2 J_I^{[k]} - (r^{[k-1]})^2 J_I^{[k-1]}) - V^{[k]}k_I C_I^{[k]} \end{aligned} \tag{4.24}$$

At the central layer $k = 1$:

$$\frac{dn_M^{[1]}}{dt} = 4\pi(r^{[1]})^2 J_M^{[1]} - V^{[1]}(k_p + k_{fs})C_M^{[1]}Y_0^{[1]}$$

$$\frac{dn_I^{[1]}}{dt} = 4\pi(r^{[1]})^2 J_I^{[1]} - V^{[1]}k_I C_I^{[1]}$$

(4.25)

For the polymer species, no diffusion term is included and we write (4.26) as the discretized versions of equation (4.3).

For the kth layer, $1 \leq k \leq ns$

$$\frac{dn_{Y_0}^{[k]}}{dt} = V^{[k]}(2fk_I C_I^{[k]} + 2k_{th}C_M^{[k]^3} - k_t^{[k]}Y_0^{[k]^2})$$

$$\frac{dn_{Y_1}^{[k]}}{dt} = V^{[k]}(2k_I C_I^{[k]} + 2k_{th}C_M^{[k]^3} + k_p C_M^{[k]}Y_0^{[k]}$$
$$- (k_{fs}C_M^{[k]} + k_t^{[k]}Y_0^{[k]})Y_1^{[k]})$$

$$\frac{dn_{Y_2}^{[k]}}{dt} = V^{[k]}(2kC_I^{[k]} + 2k_{th}C_M^{[k]^3} + k_p C_M^{[k]}(2Y_1^{[k]} + Y_0^{[k]})$$
$$- (k_{fs}C_M^{[k]} + k_t^{[k]}Y_0^{[k]})Y_2^{[k]})$$

$$\frac{dn_{Q_0}^{[k]}}{dt} = V^{[k]}(0.5k_t^{[k]}Y_0^{[k]^2} + k_{fs}C_M^{[k]}Y_0^{[k]})$$

$$\frac{dn_{Q_1}^{[k]}}{dt} = V^{[k]}(k_t^{[k]}Y_0^{[k]}Y_1^{[k]} + k_{fs}C_M^{[k]}Y_1^{[k]})$$

$$\frac{dn_{Q_2}^{[k]}}{dt} = V^{[k]}(k_t^{[k]}(Y_1^{[k]^2} + Y_0^{[k]}Y_2^{[k]}) + k_{fs}C_M^{[k]}Y_2^{[k]})$$

(4.26)

As a result, the partial differential equations are reduced to ordinary differential equations in time and the integral equation (4.13) is transformed to a set of algebraic equations, (4.27)-(4.28), based on the shell structure.

$$\frac{4}{3}\pi r^{[k]}(t)^3 = \sum_1^k V^{[k]}(t) \quad k = 1, \cdots, ns$$

(4.27)

$$V^{[k]} = n_M^{[k]}\bar{V}_M + n_{P_1}^{[k]}\bar{V}_{P_1} + n_{P_2}^{[k]}\bar{V}_{P_2}$$
$$= n_M^{[k]}(a_0^M + a_1^M C_M^{[k]}) + n_{P_1}^{[k]}(a_0^{P_1} + a_1^{P_1}C_M^{[k]}) + n_{P_2}^{[k]}(a_0^{P_2} + a_1^{P_2}C_M^{[k]})$$

(4.28)

The shell average molecular weights remain as algebraic equations, (4.20):

$$\overline{Mn}^{[k]} = \frac{(Q_1^{[k]} + Y_1^{[k]})}{(Q_0^{[k]} + Y_0^{[k]})} \cdot M_0, \quad \overline{Mw}^{[k]} = \frac{(Q_2^{[k]} + Y_2^{[k]})}{(Q_1^{[k]} + Y_1^{[k]})} \cdot M_0, k = 1, \cdots, ns \qquad (4.29)$$

and the overall average molecular weights from (4.21) are:

$$\overline{Mn} = \frac{\sum_1^{ns}(Q_1^{[k]} + Y_1^{[k]})}{\sum_1^{ns}(Q_0^{[k]} + Y_0^{[k]})} \cdot M_0, \qquad \overline{Mw} = \frac{\sum_1^{ns}(Q_2^{[k]} + Y_2^{[k]})}{\sum_1^{ns}(Q_1^{[k]} + Y_1^{[k]})} \cdot M_0 \qquad (4.30)$$

With this spatial discretization, the algebraic and ordinary differential equations (DAEs) (4.22) to (4.30) represent the dynamics of the original moving boundary reaction-diffusion model. In practice, the number of discretized shells is chosen to be sufficiently large to obtain the desired accuracy of the predicted parameters. For the PES particle simulation, 20 shells are adequate. With the kinetic parameters and process condition provided, this model can be solved by a DAE solver to predict particle growth, monomer conversion ratio, average molecular weight and the spatial composition distribution.

4.2 Results and Discussion

4.2.1 Intra-particle Dynamics

Given process parameters, SIPN intra-particle dynamics can be revealed by the single particle model. Here, model parameters are obtained through a parameter estimation approach based on sample measurements of $\overline{Mw}$, $\overline{xs}$ and $R(t)$, which will be discussed in chapter 6. Simulations of particle development which could not be directly measured are interesting topics discussed here.

The intra-particle composition distribution and average molecular weight are properties of interest. Therefore, simulations are carried out to provide some insight of particle property distribution and development. Figure 4.2 shows an example of styrene and polystyrene distribution evolution across the particle from an initial radius of 0.485mm for the monomer swollen seed. Monomer concentration, as shown in Figure 4.2 (a), increases with time due to external monomer feeding. Polystyrene concentration, shown in Figure 4.2 (b), also increases with time, while the concentration gradient is influenced by the external monomer feed. The simulation also indicates small radial concentration gradients for polystyrene within the particle. Moreover, as monomer conversion ratio increases above a certain level, an intraparticle gel effect develops, the termination rate decreases significantly and we can observe changes in the shape of the polystyrene concentration gradient. Finally, Figure 4.3 shows the molecular weight development across the radius. Due to fast diffusion of styrene monomer, the molecular weight gradient inside the particle is relatively small.

(a) Styrene monomer concentration   (b) Polystyrene concentration
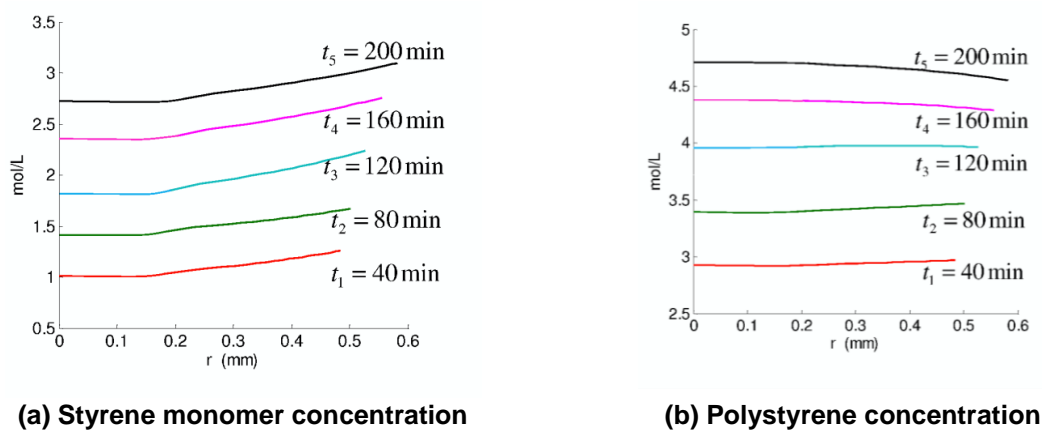
Figure 4.2 Simulation of Intra-particle concentration development
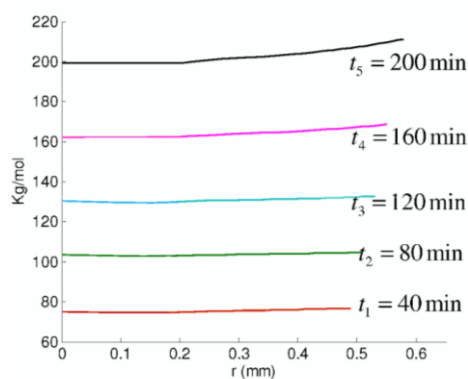
Figure 4.3 Simulation of Intra-particle polystyrene Mw development

In this example, the SIPN particle presents a near uniform distribution at given feeding rate in terms of polymer concentration and molecular weights. However, it is important to notice that, intra-particle dynamics are affected by a combination of factors from diffusion and polymerization, which are different from a batch process in a bulk system. Changing either the seed polymer, monomer, initiator or feeding rate, can lead to different dynamics from these depicted shown above.

4.3 Summary

This chapter developed a generalized reaction-diffusion single particle model for seeded suspension polymerization, as Stage I of the SIPN process. Key product properties, such as molecular weight, particle size and composition are modeled. An effective mass transport mechanism is proposed, which builds a relationship between the semi-batch operation and product properties. Rigorous particle size modeling includes polymer swelling, intra-particle heterogeneity, and position dependent kinetic rates. This leads to a shell model which de-couples the integral-differential-algebraic moving boundary formulation. Intra-particle dynamics and effects of process conditions can be simulated. The model provides an important component for the SIPN model-based study.

Chapter 5

Stage II Model: SIPN Kinetic Modeling

In this chapter, we focus on the SIPN systems at the crosslinking stage. A comprehensive kinetic model is developed, which involves simultaneous crosslinking, grafting and degradation, to predict SIPN gel content and molecular weight development simultaneously up to full conversion. Computational expense has been reduced considerably through a new component-decomposition strategy. Continuous variable approximation is applied for monomer polymerization and grafting reactions. Discrete population balance approach is introduced for simulation of crosslinking reaction as well as simultaneous chain transfer and chain scission. The inter-polymer formulation is reconstructed through a statistical approach.

5.1 Model Development

5.1.1 Reaction Mechanism

We propose a component-wise modeling strategy which provides a straightforward description for the reaction mechanism, and enables efficient computational methods to be applied similarly to linear polymer systems. The following assumptions are made in the model:

1) The SIPN system is maintained in co-continuous morphology during the reaction.

2) Single phase properties are assumed for concentration calculations.

3) Indifferent backbone reactivity is maintained in the same polymer chain.

4) The macromolecular free radical contains a single radical center.

Co-continuous morphology is a typical property for the IPN material. If two polymers are processed under proper conditions of composition and viscosity, it may be possible for the two components to form continuous interlocking phases regardless of the miscibility (Sperling, 1976; Renfree, et al., 1999). In this type of dual phase co-continuous structure, the two phases intertwine in such a way that both phases remain continuous throughout the material. Co-continuous morphology usually leads to a desirable synergistic effect, and is generally a required condition for IPN processing (Sperling, 1994). Therefore, the system is treated as a single phase system for the concentration calculation of this apparent compatibility. The second assumption, indifferent backbone reactivity, can be relaxed for different polymers, but is shown to be sufficient for low density polyethylene (LDPE) in our system. Finally, the single radical center assumption might be violated as the size of polymer network grows. A maximum network size is introduced in the simulation to avoid such possible deviation.
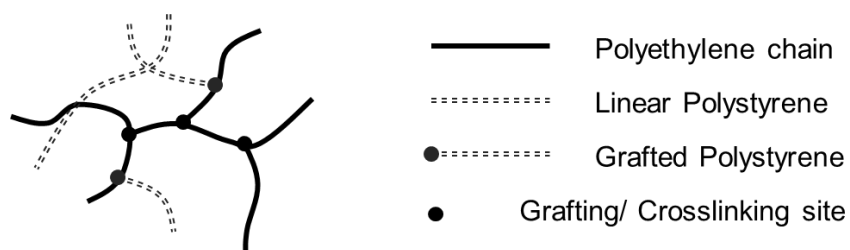
Figure 5.1 Schematic representation of the PES structure

As shown in Figure 5.1 several types of polymers are formed in the PES process, such as linear polystyrene, polystyrene-grafted-polyethylene, and crosslinked polyethylene networks. It is challenging to describe this topology directly. Instead, a component-wise decomposition strategy is proposed to address this problem as shown in Figure 5.1. The polymer mixture is divided into three classes of structure components, which are polyethylene chain (A), linear

polystyrene chain (B) and grafted-polystyrene chain (gB). Each of them is treated as a single species.
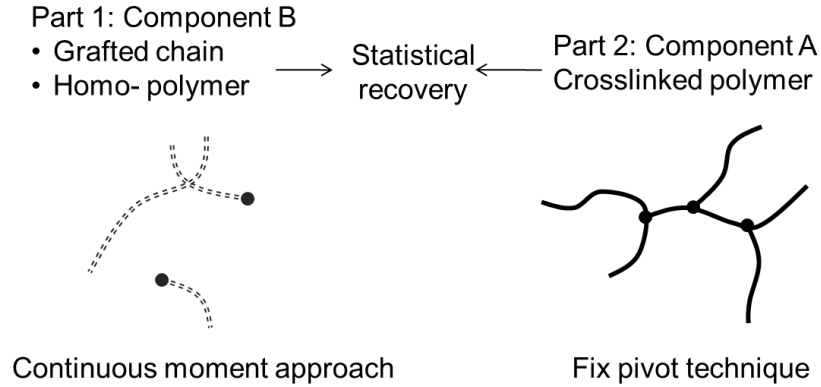
Figure 5.2 A component decomposition modeling strategy

We denote M as monomer, P as polymer and R as the radicals. $P_A(m)$, $P_B(n)$, $P_{gB}(n)$ and $R_A^{\bullet}(m)$, $R_B^{\bullet}(n)$, $R_{gB}^{\bullet}(n)$ represent the polymers and their radicals, respectively. m, n are the numbers of repeated units in the polymer A and B. m refers to ethylene units, and n refers to styrene units. Thus, the kinetic mechanism of IPN can be described by these components in a straightforward manner. Since certain reaction rates are expected to increase with the number of available reaction sites with molecular weight (MW), a proportional MW dependent reaction rate assumption (Kim, et al., 2000; Sterling, et al., 2001), is adopted. This linear dependence is expressed in the form of Equation (5.1),

$$k_Q(s) = s\kappa_Q \tag{5.1}$$

where k_Q represents MW dependent kinetic rate, κ_Q denotes the reaction rate of chain length 1, and s is the size of the particular chain, either m or n. The following reaction mechanisms (steps A-G) are considered in the model.

(A) Initiation.

The primal free radicals are mainly generated by peroxide dissociation, where peroxide decomposes into two identical radicals as Reaction (5.2).

$$X_2 \xrightarrow{k_I} 2X^{\bullet} \tag{5.2}$$

X and $X^{\bullet}$ represent the peroxide and its primary radicals.

Peroxide radicals initiate monomer (M) or abstract hydrogen from the polymer backbone through the following Reaction (5.3).

$$
\begin{aligned}
X^{\bullet} + M & \xrightarrow{k_{IM}} R_B^{\bullet}(1) \\
X^{\bullet} + P_A(m) & \xrightarrow{k_{HA}} R_A^{\bullet}(m) \\
X^{\bullet} + P_B(n) & \xrightarrow{k_{HB}} R_B^{\bullet}(n) \\
X^{\bullet} + P_{gB}(n) & \xrightarrow{k_{HB}} R_{gB}^{\bullet}(n)
\end{aligned}
\tag{5.3}
$$
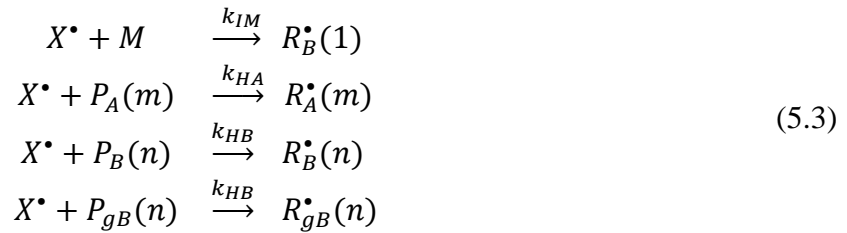
where k_{IM} is the rate constant for initiation of monomer double bond, k_{HA} and k_{HB} are the rate constants for hydrogen abstraction from polymer A, B/gB accordingly, and are considered proportional to polymer chain length. $k_{HA} = m\kappa_{HA}$ and $k_{HB} = n\kappa_{HB}$. k_{IM} is expected to be much higher than k_{HA} and k_{HB}. Thus, Reaction (5.2) is the rate controlling step over the polymer modification in the presence of monomer. Styrene monomer can also undergo thermal initiation, as Reaction (5.4).

$$3M \xrightarrow{k_{th}} 2R_B^{\bullet}(1) \tag{5.4}$$

where k_{th} is styrene thermal initiation rate.

(B) Propagation.

In the presence of monomer B, live polymer chains quickly propagate to form linear polymer B and grafted polymer B as Reaction (5.5).

$$R_B^\bullet(n) + M \xrightarrow{k_p} \quad R_B^\bullet(n+1)$$
$$R_A^\bullet(m) + M \xrightarrow{k_p} \quad P_A(m) + R_{gB}^\bullet(1) \tag{5.5}$$
$$R_{gB}^\bullet(n) + M \xrightarrow{k_p} \quad R_{gB}^\bullet(n+1)$$
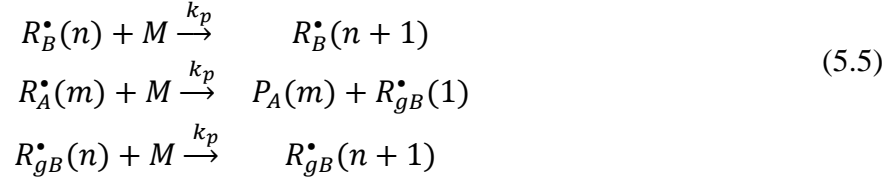
Notice that the growth of polymer B branch from polymer A backbone is modelled as the last two reactions in (5.5). Because polymer A backbone and polymer B side chain are modelled separately, the size of $P_A(m)$ remains the same after grafting of monomer B. Therefore, the grafting reaction is described as moving the backbone free radical from polymer A to the beginning of the side chain B as in the second reaction in Reaction (5.5). This representation significantly reduces the modeling complexity.

(C) Chain transfer to monomer.

For styrene free radical polymerization, chain transfer to monomer is considered. B and gB are modelled similarly in Reaction (5.6).

$$R_B^\bullet(n) + M \xrightarrow{k_{fs}} \quad P_B(n) + R_B^\bullet(1)$$
$$R_{gB}^\bullet(n) + M \xrightarrow{k_{fs}} \quad P_{gB}(n) + R_B^\bullet(1) \tag{5.6}$$
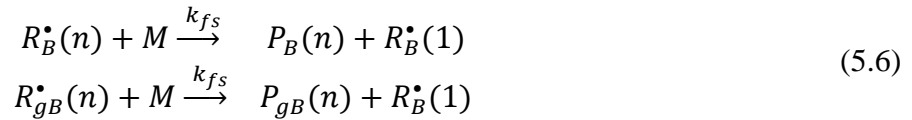
(D) Reversible hydrogen abstraction.

Polymer radicals can abstract hydrogen from another chain. When the hydrogen abstraction takes place between the same polymer components, reversible interchange of a polymer to a radical (eg. Kim, et al., 2000; Sivalingam, et al., 2004) is often assumed as a simplified representation of the reaction. Here, we adopt this expression for all the components. The ratio of the reversible reaction rate approximately follows the Arrhenius relationship. While this reaction rate could be modified or even removed due to the confinement of grafted chain, we have not considered this in the model. As a result, the same reaction rates for free polymer and grafted polymer are used in the current model. Nevertheless, the low concentration

of the grafted polymer and its radical leads to a very small reaction rate. Hence, Reaction (5.7) is considered.

$$
\begin{aligned}
P_A(m) &\underset{k_{ha2}}{\overset{k_{ha1}}{\rightleftharpoons}} R_A^\bullet(m) \\
P_B(n) &\underset{k_{hb2}}{\overset{k_{hb1}}{\rightleftharpoons}} R_B^\bullet(n) \\
P_{gB}(n) &\underset{k_{hb2}}{\overset{k_{hb1}}{\rightleftharpoons}} R_{gB}^\bullet(n)
\end{aligned}
\tag{5.7}
$$
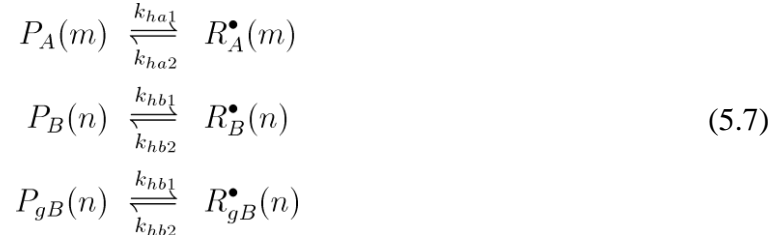
where $k_{ha1} = m\kappa_{ha1}$, $k_{hb1} = m\kappa_{hb1}$. Notice that, the reversed hydrogen abstraction reaction rates k_{ha2}, k_{hb2} are not dependent on the chain length because of the single radical center assumption. Reversible hydrogen abstraction essentially leads to a radical center redistribution and long chain polymers are affected more by the redistribution.

(E) Interaction between polymers.

Similar to mechanism (D), hydrogen abstraction can occur between different types of polymers. In the case of polymer mixtures, the interaction between the polymers can lead to an alteration in the reaction rate of individual polymers (Sivalingam, et al., 2004). In the study of thermal degradation, a mixture of polyethylene and polystyrene shows strong interaction through hydrogen abstraction (Lee, et al., 2002). An analogous mechanism is considered here. Since polystyrene radical is a strong hydrogen-acceptor and polyethylene is a strong hydrogen-donor polymer, hydrogen is considered to be abstracted from polyethylene chain by polystyrene radical, as Mccaffery, et al. (1996) also proposed and observed in the thermolysis experiment.

$$
\begin{aligned}
R_B^\bullet(n) + P_A(m) &\overset{k_{fb}}{\rightarrow} P_B(n) + R_A^\bullet(m) \\
R_{gB}^\bullet(n) + P_A(m) &\overset{k_{fb}}{\rightarrow} P_{gB}(n) + R_A^\bullet(m)
\end{aligned}
\tag{5.8}
$$
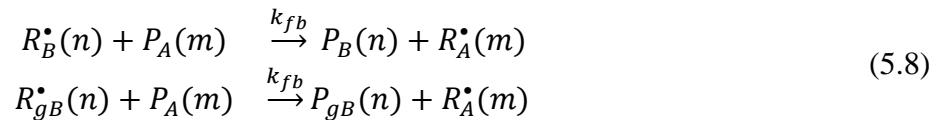
where $k_{fb} = m\kappa_{fb}$.

(F) Chain scission.

Chain scission reactions can take place on both polymer radicals. However, the detailed kinetic mechanism of random scission of branched polymer chains is a complex problem, and the role of random scission is not fully understood (Krallis, et al., 2007). Following the polystyrene degradation model (Sivalingam, et al., 2004) and polyethylene modification model (Pedernera, et al., 1999), the mid-chain radical and the end-chain radical are not discriminated. Instead, a compact representation of chain scission can be written as Reaction (5.9).

$$R_A^\bullet(m) \xrightarrow{k_{bA}} R_A^\bullet(m') + P_A(m - m') \tag{5.9}$$
$$R_B^\bullet(n) \xrightarrow{k_{bB}} R_B^\bullet(n') + P_B(n - n') \tag{5.10}$$
$$R_{gB}^\bullet(n) \xrightarrow{k_{bB}} R_{gB}^\bullet(n') + P_B(n - n') \tag{5.11}$$
$$R_{gB}^\bullet(n) \xrightarrow{k_{bB}} R_B^\bullet(n') + P_{gB}(n - n') \tag{5.12}$$
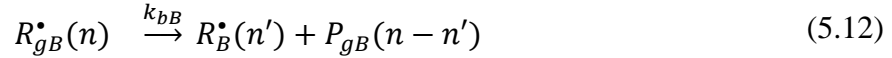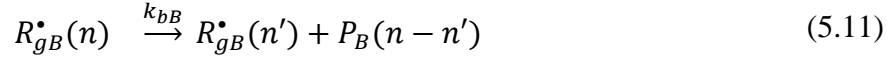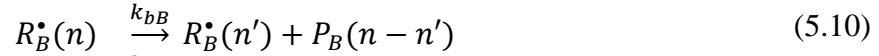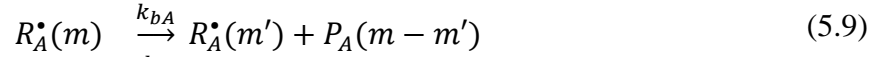
where k_{bA} and k_{bB} are β-scission rate for radical A and B.

Notice that there are two possible pathways for radical $R_{gB}^\bullet$ β-scission, either to generate a live linear chain $R_B^\bullet$ and a dead grafted chain P_{gB} or to form a live grafted chain $R_{gB}^\bullet$ and a dead linear chain P_B. Both reactions are included as Reaction (5.11) and (5.12). Chain scission reactions lead to decrease of MW, and can become noticeable side reactions.

(G) Termination.

Based on the properties of each polymer, polystyrene radicals undergo combination termination, while polyethylene radicals are terminated either by combination or disproportion. The reactions can be written as follows.

Termination by combination

$$R_A^{\bullet}(m) + R_A^{\bullet}(m') \xrightarrow{k_{tca}} \quad P_A(m+m') \qquad (5.13)$$

$$R_B^{\bullet}(n) + R_B^{\bullet}(n') \xrightarrow{k_{tcb}} \quad P_B(n+n') \qquad (5.14)$$

$$R_B^{\bullet}(n) + R_{gB}^{\bullet}(n') \xrightarrow{k_{tcb}} \quad P_{gB}(n+n') \qquad (5.15)$$
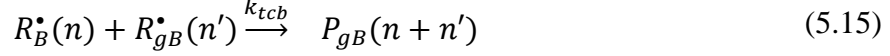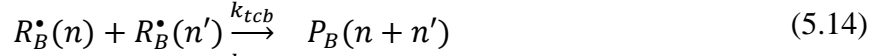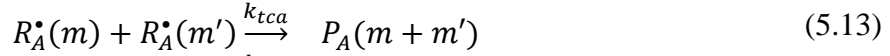
Termination by disproportion

$$R_A^{\bullet}(m) + R_A^{\bullet}(m') \xrightarrow{k_{tda}} \quad P_A(m) + P_A(m') \qquad (5.16)$$
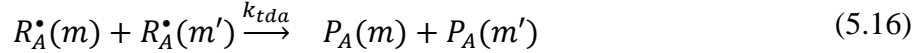
In principle, grafted-polystyrene radicals ($R_{gB}^{\bullet}(n)$) can terminate with another ($R_{gB}^{\bullet}(n)$) radical. Nevertheless, these reactions are less frequent compared to other termination steps due to low radical concentration. Thus, this type of termination is not modelled. In comparison to homo-polymer termination, the rate of termination between two polymer species is also negligible due to relative difficulties of the reaction-diffusion process. Whether the polymer mixture becomes a semi-I or semi-II SIPN is mainly determined by the relative rate of radical combination and β-scission. In this case, the predominant reaction for polyethylene (A) is chain combination, while the degradation reaction is enhanced for polystyrene (B) in the presence of peroxide. Thus, Reaction (5.13) contributes mostly to the final network formation. As the reaction proceeds, polymer chain length increases exponentially and the formed network becomes the insoluble fraction in the gel measurement. Since some of polymer B is grafted on polymer A, the obtained gel consists of a polymer A network with a fraction of the grafted B chain.

5.1.2 Population Balance Approach

In this section, population balance equations for each component are derived based on the Reactions (5.2)-(5.16). Different solution strategies are employed for each component ac-

cording to its structural characteristics. As shown in Figure 5.2, MWD of component B is solved by continuous variable approximation, and MWD of component A is solved by the fixed pivot technique. Then a statistical approach is applied to recover the structure of the mixture. Details are discussed in this section.

5.1.2.1 Population Balance for Polystyrene Components and their Radicals

Here, the chain length of polymer B is treated as a continuous variable. This assumption then combined with the method of moments to provide an effective way to consider the side reaction of polymer degradation. The molecular weight moments are defined by

$$p^{(i)}(t) = \int_0^\infty p(n,t) \ n^i dn, \quad i = 0,1,2 \tag{5.17}$$

where the superscript (i) represents the ith moment of the distribution, so that $p^{(0)}$ is the molar concentration of polymer, $p^{(1)}$ is the mass concentration, and $p^{(2)}$ determines the spread of the distribution. The number- and weight- average chain length are defined as

$$\overline{Cn} = \frac{p^{(1)}}{p^{(0)}}, \qquad \overline{Cw} = \frac{p^{(2)}}{p^{(1)}} \tag{5.18}$$

The population balances for polystyrene component are written as Equation (5.19)-(5.22).

$$
\begin{aligned}
\frac{\partial r_B(n)}{\partial t} &= \delta(n-1)(2k_{th}(C_M)^3 + k_{IM}C_{x\bullet}C_M) + \kappa_{HB}nC_{x\bullet}p_B(n) - k_pC_M\frac{\partial r_B(n)}{\partial n} \\
&\quad +\delta(n-1)k_{fs}C_M\int_0^\infty (r_B(n') + r_{gB}(n'))dn' - k_{fs}C_Mr_B(n) + \kappa_{hb1}np_B(n) - k_{hb2}r_B(n) \\
&\quad -\kappa_{fb}r_B(n)\int_0^\infty m'p_A(m')dm' - k_{bB}r_B(n) \\
&\quad +k_{bB}\int_n^\infty r_B(n')\Omega(n,n')dn' + k_{bB}\int_n^\infty r_{gB}(n')\Gamma(n,n')dn' \\
&\quad -k_{tcb}r_B(n)\int_0^\infty r_B(n')dn' - k_{tcb}r_B(n)\int_0^\infty r_{gB}(n')dn'
\end{aligned}
\tag{5.19}
$$

$$\frac{\partial r_{gB}(n)}{\partial t} = \kappa_{HB}nC_{x\cdot}p_{gB}(n) - k_pC_M\frac{\partial r_{gB}(n)}{\partial n} + \delta(n-1)k_pC_M\int_0^\infty r_A(m')dm'$$
$$-k_{fs}C_Mr_{gB}(n) + \kappa_{hb1}np_{gB}(n) - k_{hb2}r_{gB}(n)$$
$$-\kappa_{fb}r_{gB}(n)\int_0^\infty m'p_A(m')dm' - k_{bB}r_{gB}(n) + k_{bB}\int_n^\infty r_{gB}(n')\Gamma(n,n')dn' \tag{5.20}$$
$$-k_{tcb}r_{gB}(n)\int_0^\infty r\_B(n')dn'$$

$$\frac{\partial p_B(n)}{\partial t} = -\kappa_{HB}nC_{x\cdot}p_B(n) + k_{fs}r_B(n)C_M - \kappa_{hb1}np_B(n) + k_{hb2}r_B(n)$$
$$+\kappa_{fb}r_B(n)\int_0^\infty m'p_A(m')dm'$$
$$+k_{bB}\int_n^\infty r_B(n')\Omega(n,n')dn' + k_{bB}\int_n^\infty r_{gB}(n')\Gamma(n,n')dn' \tag{5.21}$$
$$+k_{tcb}\int_0^{\frac{n}{2}} r_B(n')r_B(n-n')dn'$$

$$\frac{\partial p_{gB}(n)}{\partial t} = -\kappa_{HB}nC_{x\cdot}p_{gB}(n) + k_{fs}r_{gB}(n)C_M - \kappa_{hb1}np_{gB}(n) + k_{hb2}r_{gB}(n)$$
$$+\kappa_{fb}r_{gB}(n)\int_0^\infty m'p_A(m')dm'$$
$$+k_{bB}\int_n^\infty r_{gB}(n')\Gamma(n,n')dn' \tag{5.22}$$
$$+k_{tcb}\int_0^n r_B(n')r_{gB}(n-n')dn'$$

where $\Omega(n,n')$ and $\Gamma(n,n')$ are the kernel functions of chain scission for R_B and R_{gB} respectively, which represent the probability of producing a fragment of chain length n radical from a chain length n' radical. Based on the indifferent reactivity assumption, the possibility of R_B random scission is considered to be $\frac{1}{n'}$ in the continuous variable approximation approach, i.e. for the asymmetric scission of R_{gB}, $\Gamma(n,n') = \frac{1}{2}\Omega(n,n') = \frac{1}{2n'}$. The continuous variable approximation thus shows advantage in obtaining the moment equations, because the moments of the integrals apply the continuous kernel function, they have analytical ex-

pressions. For example, denoting an expression as: $\Phi = k_{bB} \int_n^\infty r_B(n')\Omega(n,n')dn$, the following relationship holds:

$$\Phi^{(i)} = k_{bB} \frac{r_B^{(i)}}{(i+1)} \tag{5.23}$$

where $\Phi^{(i)}$ is the ith moment of the expression Φ, and i $= 0,1,2$ corresponds to the zeroth, first, and second moments, respectively. Similarly, the integrals for the rate of p_{gB} and r_{gB} can be evaluated. Thus, applying the moment operation to the above equations yields the ordinary differential Equation (5.24) - (5.27),

$$\begin{aligned}
\frac{dr_B^{(i)}}{dt} &= 2k_{th}(C_M)^3 + k_{IM}C_x \cdot C_M + k_p C_M \phi_i + \kappa_{HB}C_x \cdot p_B^{(i+1)} + k_{fs}C_M r_{gB}^{(0)} \\
&+ k_{fs}C_M(r_B^{(0)} - r_B^{(i)}) + \kappa_{hb1}p_B^{(i+1)} - k_{hb2}r_B^{(i)} - \kappa_{fb}r_B^{(i)}p_A^{(1)} \\
&+ \frac{1}{2(i+1)}k_{bB}r_{gB}^{(i)} - \frac{i}{i+1}k_{bB}r_B^{(i)} - k_{tcb}r_B^{(i)}(r_B^{(0)} + r_{gB}^{(0)})
\end{aligned} \tag{5.24}$$

where $\phi_0 = 0, \phi_1 = r_B^{(0)}, \phi_2 = (2r_B^{(1)} + r_B^{(0)})$.

$$\begin{aligned}
\frac{dr_{gB}^{(i)}}{dt} &= \kappa_{HB}C_x \cdot p_{gB}^{(i+1)} + k_p C_M r_A^{(0)} + k_p C_M \omega_i + \kappa_{hb1}p_{gB}^{(i+1)} - k_{hb2}r_{gB}^{(i)} \\
&- \frac{2i+1}{2(i+1)}k_{bB}r_{gB}^{(i)} - (k_{tcb}r_B^{(0)} + k_{fs}C_M + \kappa_{fb}p_A^{(1)})r_{gB}^{(i)}
\end{aligned} \tag{5.25}$$

where $\omega_0 = 0, \omega_1 = r_{gB}^{(0)}, \omega_2 = (2r_{gB}^{(1)} + r_{gB}^{(0)})$,

$$\begin{aligned}
\frac{dp_B^{(i)}}{dt} &= -\kappa_{HB}C_x \cdot p_B^{(i+1)} + k_{tcb}\theta_i + (k_{fs}C_M + \kappa_{fb}p_A^{(1)})r_B^{(i)} \\
&- \kappa_{hb1}p_B^{(i+1)} + k_{hb2}r_B^{(i)} + \frac{1}{i+1}k_{bB}r_B^{(i)} + \frac{1}{2(i+1)}k_{bB}r_{gB}^{(i)}
\end{aligned} \tag{5.26}$$

where $\theta_0 = \frac{1}{2}(r_B^{(0)})^2, \theta_1 = r_B^{(1)}r_B^{(0)}, \theta_2 = ((r_B^{(1)})^2 + r_B^{(0)}r_B^{(2)})$.

$$
\begin{aligned}
\frac{dp_{gB}^{(i)}}{dt} &= -\kappa_{HB}C_x \cdot p_{gB}^{(i+1)} + k_{tcb}\psi_i + (k_{fs}C_M + \kappa_{fb}p_A^{(1)})r_{gB}^{(i)} \\
&\quad -\kappa_{hb1}p_{gB}^{(i+1)} + k_{hb2}r_{gB}^{(i)} + \frac{1}{2(i+1)}k_{bB}r_{gB}^{(i)}
\end{aligned}
\tag{5.27}
$$

where $\psi_0 = r_B^{(0)}r_{gB}^{(0)}, \psi_0 = \left(r_B^{(1)}r_{gB}^{(0)} + r_B^{(0)}r_{gB}^{(1)}\right), \psi_2 = \left(r_{gB}^{(0)}r_B^{(2)} + 2r_{gB}^{(1)}r_B^{(1)} + r_{gB}^{(2)}r_B^{(0)}\right).$

A closure form is required to compute the third moment involved. In this study, a log-normal distribution was assumed. The third moment of the distribution can be expressed as Equation (5.28)

$$
\mu_3 = (\frac{\mu_2}{\mu_1})^3 \mu_0
\tag{5.28}
$$

where μ_i is the ith moment of the log-normal distribution. The above closure method is applied to the dead polymer B chains.

5.1.2.2 Population Balance for Polyethylene Components and their Radicals

The population balance equations for polymer A are derived. Net formation rate of **live polymer** A of chain length m is written as:

$$
\begin{aligned}
\frac{dr_A(m)}{dt} &= k_{HA}mC_x \cdot p_A(m) - k_p r_A(m)C_M + \kappa_{ha1}mp_A(m) - k_{ha2}r_A(m) \\
&\quad +\kappa_{fb}mp_A(m)\int_0^\infty (r_B(n') + r_{gB}(n'))dn' \\
&\quad -(k_{tca} + k_{tda})r_A(m)\int_0^\infty r_A(m')dm' \\
&\quad -k_{bA}r_A(m) + k_{bA}\int_m^\infty r_A(m')\Omega(m,m')dm'
\end{aligned}
\tag{5.29}
$$

Net formation rate of **dead polymer** A of chain length m:

$$\begin{aligned}
\frac{dp_A(m)}{dt} &= -\kappa_{HA}mC_{x^\bullet}p_A(m) + k_p r_A(m)C_M - \kappa_{ha1}mp_A(m) + k_{ha2}r_A(m) \\
&\quad -\kappa_{fb}mp_A(m)\int_0^\infty (r_B(n') + r_{gB}(n'))dn' \\
&\quad +k_{tca}\int_0^{\frac{m}{2}} r_A(m')r_A(m-m')dm' + k_{tda}r_A(m)\int_0^\infty r_A(m')dm' \\
&\quad +k_{bA}\int_m^\infty r_A(m')\Omega(m,m')dm'
\end{aligned}$$
(5.30)

where $\Omega(m,m')$ is the random scission kernel function as stated before. It is important to point out that due to the network formation, the continuous variable approximation approach no longer applies, as the higher order moments of polyethylene approach infinity, and the moment closure approximation no longer holds. To overcome this difficulty, we combine the fixed pivot technique, also known as the sectional grid method, with the method of moments. The zero-th moment is obtained through moment operation of the population, while discrete-continuous equations are derived for each sectional grid to avoid the involvement of higher order terms. The zero-th moment equations are derived as Equation (5.31) and (5.32):

$$\begin{aligned}
\frac{dr_A^{(0)}}{dt} &= \kappa_{HA}C_{x^\bullet}p_A^{(1)} - k_p C_M r_A^{(0)} + \kappa_{ha1}p_A^{(1)} - k_{ha2}r_A^{(0)} + \kappa_{fb}p_A^{(1)}(r_B^{(0)} + r_{gB}^{(0)}) \\
&\quad -(k_{tca} + k_{tda})(r_A^{(0)})^2
\end{aligned}$$
(5.31)

$$\begin{aligned}
\frac{dp_A^{(0)}}{dt} &= -\kappa_{HA}C_{x^\bullet}p_A^{(1)} + k_p C_M r_A^{(0)} - \kappa_{ha1}p_A^{(1)} + k_{ha2}r_A^{(0)} - \kappa_{fb}p_A^{(1)}(r_B^{(0)} + r_{gB}^{(0)}) \\
&\quad +\frac{1}{2}k_{tca}(r_A^{(0)})^2 + k_{tda}r_A^{(0)}r_A^{(1)} + k_{bA}r_A^{(1)}
\end{aligned}$$
(5.32)

The fixed pivot technique is discussed in the following section.

5.1.2.3 Fixed Pivot Technique

The fixed pivot technique was first proposed by Kumar, et al. (1996) to solve the continuous population balance equations (PBEs) for a population of particles which undergo break-up

as well as aggregation. The discrete equations are internally consistent with regard to the selected moments of the distribution. This technique was recently introduced by Krallis, et al. (2007) to simulate of MWD of several polymerization systems involving branching. In our study, the fixed pivot technique is adapted for modeling reactions of crosslinking and chain scission, and shown to be an effective solution strategy to solve the PBEs of polyethylene component. A detailed description of the fixed pivot technique can be found in Kumar, et al. (1996). A brief introduction is summarized here.
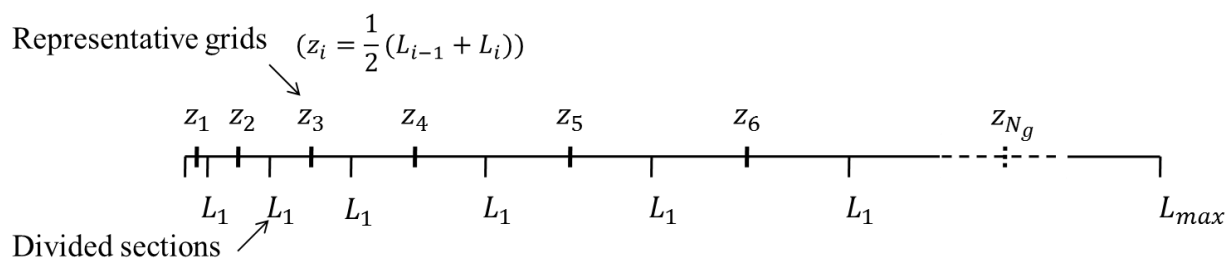
Figure 5.3 A general grid representation of the fixed pivot technique

A population of polymer with chain length distributed from 1 to L_{max} is discretized into N_g sections, as shown in Figure 5.3. A representative chain length z_i is chosen for each grid. Combination or breakage reactions of the entire population are described only through the discrete distribution at the particular chain length. Notice that discrete representation is an exact match only when the reactions generate polymers at the representative chain length from chains also at representative sizes; this is generally not exact for arbitrary chain lengths. The fixed pivot technique is such an approach that preserves selected properties for arbitrary sizes after discretization. For example, to preserve two properties, f_1 and f_2, for any size of v in the distribution, interpolation Equations (5.33) should be satisfied:

$$a(v, z_i)f_1(z_i) + b(v, z_{i+1})f_1(z_{i+1}) = f_1(v)$$
$$a(v, z_i)f_2(z_i) + b(v, z_{i+1})f_2(z_{i+1}) = f_2(v), \quad z_i \leq v \leq z_{i+1}$$

(5.33)

where z_i and z_{i+1} are two closest neighbour grids of v. The exact properties $f_1(v), f_2(v)$ are then represented through a linear combination of their neighbourhoods. Here, a and b are coefficients of the combination, which depend on the relationship between v and z_{i+1}. For MWD simulation, the number- (the zero-th moment) and weight (the first moment) distribution are of particular importance. Therefore, f_1 and f_2 are chosen to be 0th and 1th moments of the distribution, and the coefficients are calculated accordingly.
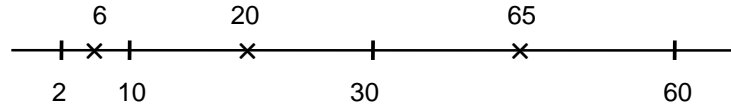
Figure 5.4 An illustrative example of the fixed pivot technique

Figure 5.4 shows a simple example of the procedure. Continuous chain lengths are divided into sections with $L_i = 2, 10, 30, 60$, etc. The representative grids z_i in each section are 6, 20, 45, etc. For instance, assume a radical of chain length 6 combines with a radical of chain length 20 to form a dead polymer of chain length 26. The produced polymer is no longer at the fixed grid size. To conserve the number and mass change of the population, the reaction is re-described by the given grids as:

$$1R(6) + 1R(20) \rightarrow \frac{19}{25}P(20) + \frac{6}{25}P(45)$$

(5.34)
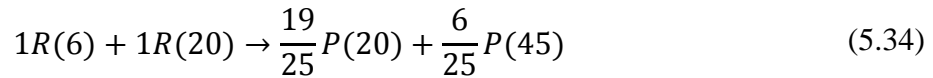
After reassignment, there is still "1" polymer chain ($\frac{19}{25} + \frac{6}{25} = 1$) with total weight of 26 ($\frac{19}{25} \times 20 + \frac{6}{25} \times 45 = 26$). Prediction of the number and weight properties of the population remains exact. Based on this idea, higher order moments can be expressed in the same way

by adding more grid balance equations. Nevertheless, prediction up to the first moment is sufficient for the gel content calculation and only the zero-th and first moments are needed. The derived continuous-discrete equations can be written as follows, where the index (i) denotes the ith representative grid. Continuous-discrete rate for **live polymer** A:

$$
\begin{aligned}
\frac{dr_A(i)}{dt} = {} & \kappa_{HA}C_x \cdot z_i p_A(i) - k_p r_A(i)C_M + \kappa_{ha1}z_i p_A(i) - k_{ha2}r_A(i) \\
& + \kappa_{fb}z_i p_A(i)\int_0^\infty (p_B(n') + p_{gB}(n'))dn' \\
& - (k_{tca} + k_{tda})r_A(i)\sum_{k=1}^{N_g} r_A(k) \\
& - k_{bA}r_A(i) + k_{bA}\sum_{k=i}^{N_g}(T_{01} + T_{02})r_A(k)
\end{aligned}
\tag{5.35}
$$

Continuous-discrete rate for **dead polymer A**:

$$
\begin{aligned}
\frac{dp_A(i)}{dt} = {} & -\kappa_{HA}C_x \cdot z_i p_A(i) + k_p r_A(i)C_M - \kappa_{ha1}z_i p_A(i) + k_{ha2}r_A(i) \\
& - \kappa_{fb}z_i p_A(i)\int_0^\infty (r_B(n') + r_{gB}(n'))dn' \\
& + k_{tda}r_A(i)\sum_{y=1}^{N_g} r_A(k) \\
& + k_{tca}\sum_{j,k}^{j \geq k}\left(1 - \frac{1}{2}\delta_{(j-k)}\right)B(i,k,j)r_A(k)r_A(j) \\
& + k_{bA}\sum_{k=i}^{N_g}(T_{01} + T_{02})r_A(k)
\end{aligned}
\tag{5.36}
$$

where

$$
\begin{aligned}
T_{01} &= \int_{z_{i-1}}^{z_i}\frac{n - z_{i-1}}{z_i - z_{i-1}}\Omega(n,n')dn \\
T_{02} &= \int_{z_i}^{z_{i+1}}\frac{z_{i+1} - n}{z_{i+1} - z_i}\Omega(n,n')dn
\end{aligned}
\tag{5.37}
$$

$$B(i,k,m) = \begin{cases} \dfrac{z_{i+1} - (z_k + z_m)}{z_{i+1} - z_i} & \text{when } z_i \leq (z_k + z_m) \leq z_{i+1} \\[2ex] \dfrac{(z_k + z_m) - z_{i-1}}{z_i - z_{i-1}} & \text{when } z_{i-1} \leq (z_k + z_m) \leq z_i \end{cases} \tag{5.38}$$

The first moments of the population are conserved as Equation (5.39)

$$\begin{aligned} p_A^{(1)} &= \sum_{k=1}^{N_g} z_k \, p_A(k) \\ r_A^{(1)} &= \sum_{k=1}^{N_g} z_k \, r_A(k) \end{aligned} \tag{5.39}$$

5.1.2.4 Population Balance for Monomer and Initiator

Concentration of monomer (C_M), initiator (C_{X_2}) and primary free radicals ($C_{x\cdot}$) are derived as Equation (5.40). Based on the long chain approximation (LCA), monomer consumed by thermal initiation is ignored and f denotes the initiator efficiency.

$$\begin{aligned} \frac{dC_M}{dt} &= -k_{IM} C_{x\cdot} C_M - k_p (r_B^{(0)} + r_{gB}^{(0)} + r_A^{(0)}) C_M - k_{fs} C_M (r_B^{(0)} + r_{gB}^{(0)}) \\ \frac{dC_{X_2}}{dt} &= -k_I C_{X_2} \\ \frac{dC_{x\cdot}}{dt} &= f k_I C_{X_2} - C_{x\cdot} (k_{IM} C_M + \kappa_{HB} (p_B^{(1)} + p_{gB}^{(1)} + \kappa_{HA} p_A^{(1)})) \end{aligned} \tag{5.40}$$

With Equation (5.24)-(5.28), (5.31)-(5.32) and (5.35)-(5.40), the population balance equations are complete for the reactions considered in the model.

5.1.3 Property Calculation

The final molecular properties can be rebuilt in several ways. Statistical assumptions are introduced to attain an expected formulation from the information of each component.

5.1.3.1 Homo-Polystyrene Average Molecular Weight

For polystyrene remaining in the linear form, the average molecular weight is computed from its leading moments.

$$
\begin{aligned}
\bar{M}_{n_B} &= p_B^{(1)}/p_B^{(0)} \cdot \bar{M}_B \\
\bar{M}_{w_B} &= p_B^{(2)}/p_B^{(1)} \cdot \bar{M}_B
\end{aligned}
\tag{5.41}
$$

where $\bar{M}_B$ is the molecular weight of styrene unit.

5.1.3.2 Polystyrene-g-Polyethylene Molecular Weight Distribution

The MWD of polystyrene-g-polyethylene is a bivariate distribution. The original formation of polymer chains should be recovered. With an approximated polystyrene grafting ratio, a statistical approach is applied to evaluate the expected MWD of polystyrene-g-polyethylene. The grafting ratio is defined as the ratio of grafted polystyrene versus overall polyethylene by weight.

$$
\gamma_g = \frac{w_{gB}}{w_A} = \frac{p_{gB}^{(1)} \ \bar{M}_B}{p_A^{(1)} \ \bar{M}_A}
\tag{5.42}
$$

Considering the most probable chain formation, equation (5.43) represents the expected molecular weight for original polyethylene of molecular weight $\overline{Mw}_A$ after grafting.

$$
\overline{Mw}_{\text{AgB}} = (1 + \gamma_g)
\tag{5.43}
$$

Thus, the expected MW for polyethylene-g-polystyrene from original polyethylene in grid i is represented as equation (5.44).

$$
\overline{Mw}_{\text{AgB}}(i) = \overline{Mw}_{\text{A}}(i)(1 + \gamma_g)
\tag{5.44}
$$

5.1.3.3 Gel Content

As justified from an experimental point of view (Plessis, et al., 2001), gel is defined as polymer which cannot be dissolved in the solvent, rather than one whose molecular weight approaches infinity. An indication of the maximum molecular weight of soluble polymer is obtained from gel permeation chromatography (GPC). Therefore, the gel content can be defined as the polymer size that exceeds the maximum soluble chain length. In our study, a critical gel size is obtained from GPC measurements, as approximately 3×10^6 g/mol for polyethylene ($\log_{10} M \approx 6.5$). Since the gel of this IPN contains crosslinked A with grafted B, both components are taken into account.

$$f_{gel}^A = \frac{\sum_{i \geq g^C} z_i \left(r_A(i) + p_A(i) \right) \bar{M}_A}{w_A} \times 100\% \tag{5.45}$$

$$w_{gel} = w_A \cdot f_{gel}^A \cdot (1 + \gamma_g) \tag{5.46}$$

where f_{gel}^A denotes the insoluble fraction of polymer A in all polymer A; g^C is the lowest grid defining a gel. The representative chain length in g^C grid refers to the critical gel size, which is set to be 1×10^5. w_{gel} is the overall gel content. In addition, we define the gel content of the final product as:

$$f_{gel} = \frac{w_{gel}}{w_{total}} \times 100\% \tag{5.47}$$

Hence, Equation (5.41)-(5.46) are used to simulate molecular weights of polystyrene, polystyrene-g-polyethylene and gel content of the product.

5.1.4 Specification of Rate Constants

Before the model solution can be obtained, expressions for the rate parameters must be specified. Assuming the validity of the Arrhenius relationship for the elementary reaction steps, chain length independent reaction rate and unit reaction rate for chain length dependent reaction can be stated as $k_i(\kappa_i) = A_i \exp(-E_i/RT)$. It is well known that the termination reaction in a free radical reaction is a diffusion-controlled process.

Here, a separate treatment is used for each termination reaction. A classical empirical form (Hui, et al., 1972) is adopted for styrene polymerization as shown in Equation (5.48):

$$k_{tcb} = k_{tcb0} \cdot \exp[-2(A_1 x_s + A_2 x_s{}^2 + A_3 x_s{}^3)], (0 \leq x_s \leq 1) \qquad (5.48)$$

where k_{tcb0} is a termination constant in an ideal polymerization system without gel effect, A_1, A_2, A_3 are temperature-dependent coefficients, and x_s is the styrene monomer conversion ratio, defined as $x_s = C_{\text{Polystyrene}}/(C_{\text{Polystyrene}} + C_M)$, where $C_{\text{Polystyrene}}$ and C_M are the concentration of polystyrene and styrene, respectively. When styrene reaches full conversion, i.e. $x_s = 1$, k_{tcb} approaches a constant value. For crosslinking/degradation reactions, a molecular weight independent rate constant was assumed (Pedernera, et al., 1999; McCoy, et al., 2001; Sivalingam, et al., 2004). A satisfactory fit to the experimental data was achieved for the studied cases, and this assumption is considered to be valid for a certain range of MWs. On the other hand, a chain length dependent termination rate was also considered in previous studies (Berchtold, et al., 2001; Andrzejewska, et al., 2005; Kruse, et al., 2002). Also, the simplified Smoluchowski equation was adapted (Kruse, et al., 2002), where the termination rate was assumed to be proportional to the average of the inverse chain

length. In our study, to maintain the simplicity and validity of the model, a lumped rate is used in the form of Equation (5.49):

$$k_{ta} = \alpha k_{ta}^0 \tag{5.49}$$

where k_{ta} denotes k_{tca} and k_{tda} . k_{ta}^0 represents the termination rate constant following Arrhenius relationship, and the α constant is an adjustable parameter which depends on the polymer properties and processing conditions. For example, polymer with the same initial MWD above its melting point is regarded to have the same α value. The α value is estimated experimentally. Finally, although an inversely proportional relationship between polymer chain transfer rate and size of the abstracting radical for branched polystyrene is suggested, (Kruse, et al., 2002) we do not consider the difference of chain transfer mobility for the polystyrene radical in this model, due to the (mostly) linear structure of the polystyrene chain. Instead an average reaction rate which follows Arrhenius relationship is applied on k_{fs} .

5.2 Results and Discussion

The model in the previous section is now examined and validated through comparison with experimental studies. In order to understand the interaction of styrene, polyethylene and polystyrene in the polyethylene/polystyrene inter-polymer process, and to demonstrate the validity of the model, data from two single polymer systems as well the as polymer mixture system are collected and compared. The cases are listed as follows:

a) Polyethylene modification by dicumyl peroxide (DiCup). Gel content was compared.

b) Peroxide enhanced degradation of polystyrene. Number and weight average MW were compared.

c) Polyethylene/polystyrene SIPN product was analyzed. Gel content, grafting ratio, polystyrene molecular weight, and joint MWD were compared.

Finally, the sensitivity of product properties to the process operation conditions was investigated.

5.2.1 Single Polyethylene Crosslinking

We first consider the crosslinking of polyethylene through modification using DiCup. Here we consider the behaviour of the model using the equations for polymer A.

5.2.1.1 Experimental Data

The study of LDPE modification by DiCup is taken from (Kim, et al., 1984). Four grades of LDPE samples were shown in Table 5.2. The concentration of DiCup was varied from 0.5 to 3.5 w/w%. The samples were crosslinked at $160°C$ for 1hr, at less than 50 psig. Soluble fractions were measured by the extraction test according to ASTM D2765 standard test method. The data are converted to gel contents presented in Figure 5.5.

5.2.1.2 Model Validation

In the absence of polystyrene and styrene, the model is reduced to peroxide-induced polyethylene modification. Since the MWDs of the test samples are not available, a log-normal distribution is assumed for the initial MWD. It is found that inclusion of reversible hydrogen abstraction has little effluence on gel prediction. As also justified in (Pedernera, et al., 1999) a reasonable prediction of the molecular weight could be accomplished with or without polymer transfer mechanism for polyethylene modification. Because only PE is present, a reduced form of the model is used. The representative crosslinking parameters are presented in Table 5.1. k_{tda} is estimated based on the relationship of k_{tca}/k_{tda} for secondary free

radical. (Huskic, et al., 1993). Because it provides a reasonable fit to data, initiator efficiency is set to be 0.65 for all the runs, and the α values for the sample A, B, C, D are 0.1, 0.17, 0.18, 0.23 respectively. The increase of α reflects the effect of MWD from different samples. Figure 5.5 is a plot of gel content vs. C_{X_2} . It summarizes the comparison between simulation and experimental data provided, and a consistent trend is observed for all the samples. Considering the variation of initiator efficiency due to the difference in sample impurity and initiator concentration, gel contents can be fitted exactly when allowing the initiator efficiency (f in (5.40)) to vary from 0.6 ~ 0.8. Figure 5.5 shows the simulation results with initiator efficiency set to 0.65.

Table 5.1 Representative kinetic constants for the single polyethylene crosslinking system

Reaction	Constant	k_0	E
		s^{-1} or $\mathrm{l \cdot mol^{-1} s^{-1}}$	$\mathrm{kcal \cdot mol^{-1}}$
peroxide decomposition	k_I	7.47×10^{15}	36.5 [a)]
hydrogen abstraction from polyethylene	κ_{HA}	5.00×10^{7}	15.0 [b)]
β-scission (polyethylene)	k_{bA}	4.47×10^{14}	38.5 [c)]
radical recombination (polyethylene)	k_{tca}^0	2.60×10^{9}	15 [b)]
radical disproportionation (polyethylene)	k_{tda}^0	3.65×10^{8}	15 [d)]

a) Arkema, INC; b) (Pedernera, et al., 1999); c) (Likozar, et al., 2009); d) k_{tda}^0 is estimated based on the relationship of $\mathrm{k_{tca}/k_{tda}}$ for secondary free radical (Huskic, et al., 1993).

5.2.2 Single Polystyrene Degradation

We now consider the degradation of polystyrene with DiCup and demonstrate how the kinetic model predicts this behaviour using the equations for polymer B.
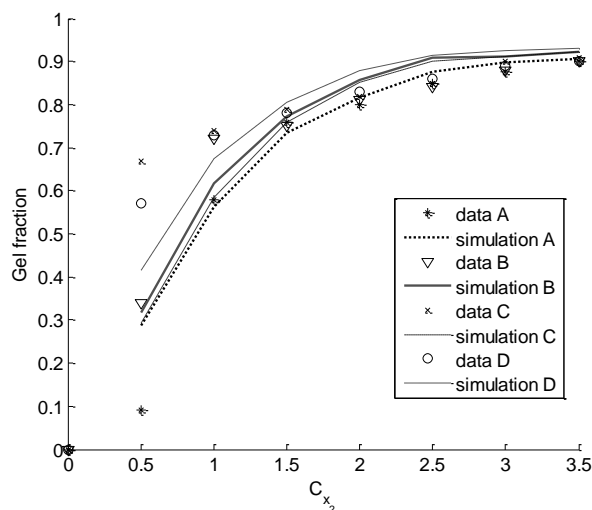
Figure 5.5 Predicted and experimentally measured gel content for the polyethylene

Table 5.2 Experiment data from Kim, et al. (1984)

Designation	$\bar{M}_n$	PDI	Melt	Density
	$g \cdot mol^{-1}$	$= \bar{M}_w/\bar{M}_n$	Index	$g \cdot cm^{-3}$
LDPE-A	11,300	7.60	1.0	0.920
LDPE-B	10,600	7.34	1.5	0.920
LDPE-C	9,300	7.19	3.0	0.919
LDPE-D	9,000	9.74	2.0	0.919

5.2.2.1 Experimental Data

Peroxide enhanced polystyrene degradation experiments were carried out in an industrial lab with and without styrene monomer. A set of polystyrene samples was prepared from standard commercial grade products with $Mw \approx$ 200,000 and 300,000 g/mol, polydispersity 2.7 ~ 3.1. In one group of experiments, dicumyl peroxide (DiCup) (Akzo Nobel Perkadox BC-FF, 99%) was mixed with 75g polystyrene powder samples in a batch mixer at room temperature to obtain different peroxide concentrations: 0, 0.025 and 0.045 wt/wt%. In another group of experiments, the ratio of polystyrene/DiCup was kept the same, while 7.5g

styrene monomer (Lyondell Chemical Co, 99.95%) is used to mix with DiCup at the begin-

ning. Once DiCup is well dispersed in the polymer, the mixture is sealed into glass ampoules

under nitrogen and reacted by heating the glass ampoule reactor at $130°C$ for 12 hours to

ensure complete reaction. MWDs of obtained samples were determined by GPC. A calibra-

tion curve of retention time versus Mw was based on polystyrene standards. Figure 5.6

shows the experimental results obtained from polystyrene degradation study as markers.

5.2.2.2 Model Validation

In the absence of the polyethylene component, the reduced model is similar to the single

polystyrene degradation model. Notice that, styrene monomer is present in the system at the

beginning and both polymerization and degradation occur for polystyrene macro-radicals.

Here the polymerization reaction is dominant, because the radical termination rate is much

higher than the chain scission rate when the concentration of polystyrene radicals is high. In

this study, polystyrene $\overline{Mw}$ increases until the monomer is consumed. Then, polystyrene

$\overline{Mw}$ decreases as the reaction of hydrogen abstraction from polystyrene starts to take effect.

Since additional styrene monomer changed the initial MWD before PS degradation, differ-

ent final $\overline{Mw}$ and $\overline{Mn}$ in two groups were observed. The parameters used for simulation are

summarized in Table 5.3.

Figure 5.6 shows the comparison between simulation and experimental results. Con-

sistent agreement on number and weight average molecular weight was observed for

different levels of peroxide within 10% experimental error. This model shows several dis-

tinctions with the polystyrene degradation model developed in the literature (eg. Kim, et al.,

2000; Sterling, et al., 2001; Sivalingam, et al., 2004). First, an important assumption, quasi-

steady state radical concentration (QSSA), used in the previous models to obtain a solution,

is not required here. Also, the assumption of self-similar distributions can be relaxed to compute both $\overline{Mw}$ and $\overline{Mn}$, since the model includes up to the second moment equation. Different closure forms can be chosen depending on the actual distribution; this introduces more flexibility for modeling different raw materials.

Table 5.3 Representative kinetic constants for the polystyrene degradation system

Reaction	Constant	k_0	E
		s^{-1} or $\text{l} \cdot \text{mol}^{-1}\text{s}^{-1}$	$\text{kcal} \cdot \text{mol}^{-1}$
peroxide decomposition	k_I	7.47×10^{15}	36.5 [a)]
thermal initiation	k_{th}	2.19×10^{5}	27.4 [b)]
hydrogen abstraction from styrene	k_{IM}	1.00×10^{7}	7.1 [b)]
hydrogen abstraction from polystyrene	κ_{HB}	5.00×10^{7}	15.5
polystyrene chain propagation	k_p	1.00×10^{7}	7.1 [b)]
chain transfer to monomer	k_{fs}	2.31×10^{7}	12.6 [b)]
reversible hyrogen abstraction (polystyrene)	κ_{hb1}	1.00×10^{0}	10.5
reversible hyrogen abstraction (polystyrene)	k_{hb2}	2.10×10^{6}	10.5 [c)]
β-scission (polystyrene)	k_{bB}	4.10×10^{12}	26.0 [c)]
radical recombination (polystyrene)	k_{tcb}	3.16×10^{6}	1.7 [b)]

a) Arkema, INC; b) (Curteanu, 2003); c) (Kruse, et al., 2002).
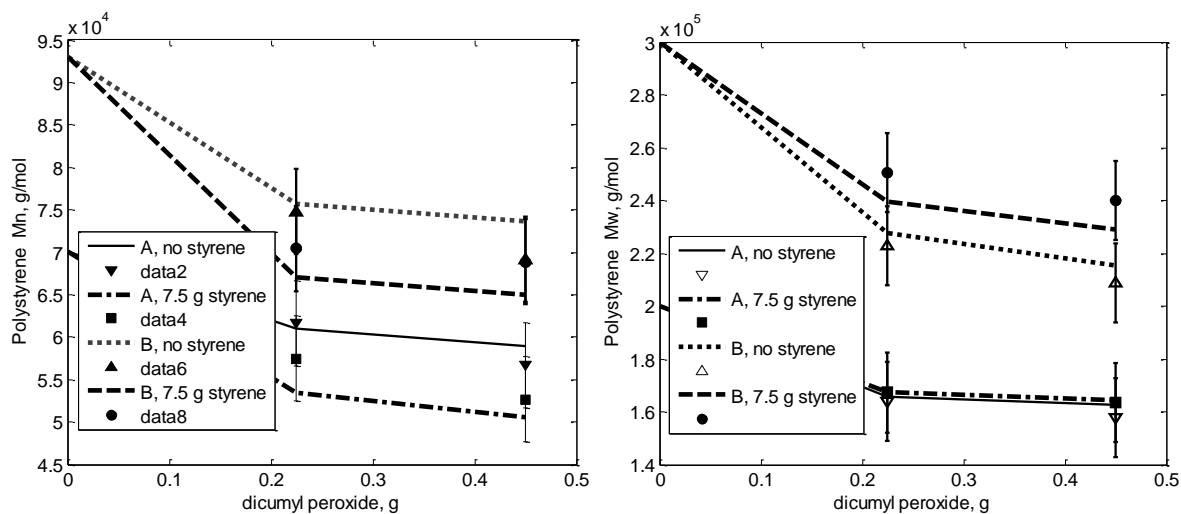
Figure 5.6 Predicted and experimentally measured polystyrene average molecular weight for the polystyrene degradation system

5.2.3 Simultaneous Reaction of Polyethylene/Polystyrene Semi-IPN

We now consider the crosslinking of both polystyrene and polyethylene and demonstrate the behaviour of our model for both polymers A and B.

5.2.3.1 Experimental Data

Process data from PES Stage II were collected in the industrial lab. Manufacturing details can refer to the patent (Matsumura, et al., 2007). Low density polyethylene ($MI \leq 2$) was prepared as nucleus particles, suspended in an aqueous medium. Crosslinking agent, dicumyl peroxide (Akzo Nobel,99%) was dissolved in styrene (Lyondell Chemcial,99.95%) solution and fed dropwise to the aqueous medium to cause absorption by the polyethylene resin particles. After styrene was partially polymerized in polyethylene particle at a lower temperature ($\leq 90℃$) with the addition of peroxide, a ramped temperature was applied until the reactor was heated up to 143℃. The reaction is held at constant temperature ($140 \sim 143℃$) for $2 \sim 4$ hours, then was gradually cooled down to room temperature. The final gel content was measured based on the standard test method ASTM D2765. A SEC−FTIR−viscometry method (Zhang, et al., 2007) was applied for the determination of molar mass averages, molar mass distribution, and composition distributions of the soluble fraction of the synthesized SIPN. Size-exclusion chromatography (SEC) provides a rapid method for determining polymer molar mass distributions. The combination of online FT-IR and viscometry enables universal calibration of copolymer composition. Samples of experimental resins were prepared and measured as described in (Zhang, et al., 2007). Figure 7(d) and 7(e) show the measurement of the initial distribution of the inter-polymers as dashed lines. On-

line FT-IR detection by Temperature Rising Elution Fractionation (TREF) technique (Zhang, 2009) was used to study the grafting ratio of polystyrene. The initial condition for the process model is considered to be the beginning of the temperature ramp, and was determined through sample measurement. Two product grades, $G1$ and $G2$, which contain different polystyrene compositions, are examined.

5.2.3.2 Model Validation

The polyethylene/polystyrene Semi-I IPN model includes all reactions above and the polymer interactions. Assuming the volume change during the process is negligible, reactant concentrations are computed based on ideal mixing rules. The molar volume of each species is set to be the average value in the process. Since initiator efficiency varies widely in different conditions, the value of initiator efficiency is re-estimated to be 0.5 in this system. Polystyrene gel pre-factor is set to 0.085. Representative kinetic values are summarized in Table 5.4.

Figure 5.7 summarizes the model simulation results for the two grades, $G1$ and $G2$. Figure 5.7 (a) shows the development of gel content over time. At the beginning of the process, DiCup mainly participates in styrene polymerization, hence, no gel is observed. After a certain point, when styrene monomer has been consumed, the polyethylene gel content starts to increase as DiCup continues to decompose. This result suggests that it is possible to polymerize styrene monomer in situ without generating crosslinked polyethylene even though a crosslinking agent is present. Consistent results have been found in recently patented inventions (Matsumura, et al., 2006), where linear low density polyethylene (LLDPE) is used for lower crosslinking capability, and crosslinking agent promotes the grafting reaction during polymerization. As a result, a non-crosslinked polyethylene-based modified polystyrene res-

in is obtained, where the gel consists of a grafting polymer. On the other hand, when cross-linking structure is intended, polymer with higher crosslinking capability, such as branched low-density polyethylene and its copolymer are preferred. (Matsumura, et al., 2007).

Table 5.4 Representative kinetic constants for the PES system

Reaction	Constant	k_0	E
		$\mathrm{s^{-1}}$ or $\mathrm{l \cdot mol^{-1} s^{-1}}$	$\mathrm{kcal \cdot mol^{-1}}$
peroxide decomposition	k_I	7.47×10^{15}	36.5 [a]
thermal initiation	k_{th}	2.19×10^{5}	27.4 [e]
hydrogen abstraction from styrene	k_{IM}	1.00×10^{7}	7.1 [e]
hydrogen abstraction from polyethylene	κ_{HA}	5.00×10^{7}	15.0 [b]
hydrogen abstraction from polystyrene	κ_{HB}	5.00×10^{7}	15.5
polystyrene chain propagation	k_p	1.00×10^{7}	7.1 [e]
chain transfer to monomer	k_{fs}	2.31×10^{6}	12.6 [e]
reversible hydrogen abstraction (polystyrene)	κ_{hb1}	1×10^{0}	10.5
reversible hyrogen abstraction (polystyrene)	k_{hb2}	2.10×10^{6}	10.5 [f]
chain transfer to polyethylene	k_{fb}	2.50×10^{5}	13.0
β-scission (polyethylene)	k_{bA}	4.47×10^{14}	38.5 [c]
β-scission (polystyrene)	k_{bB}	4.1×10^{12}	26.0 [f]
radical recombination (polyethylene)	k_{tca}	2.6×10^{9}	15.0 [b]
radical disproportionation (polyethylene)	k_{tda}	3.65×10^{8}	15.0 [d]
radical recombination (polystyrene)	k_{tcb}	3.16×10^{6}	1.7 [e]

a) Arkema, INC; b) (Pedernera, et al., 1999); c) (Likozar, et al., 2009); d) k_{tda}^{0} is estimated based on the relationship of $\mathrm{k_{tca}/k_{tda}}$ for secondary free radical. (Huskic, et al., 1993); e) (Curteanu, 2003); f) (Kruse, et al., 2002).

Figure 5.7 (c) shows the simulation of grafting ratio development. The styrene grafting ratio first increases during the styrene polymerization, then it starts to decrease due to degradation by the remaining peroxide after polymerization. The trend of the grafting polymer growth during polymerization is also consistent with the results in recent patents (Matsumura, et al., 2006). The development of polystyrene average molecular weight is shown in Figure 5.7 (b). Degradation of polystyrene is shown during polyethylene crosslinking. Samples were taken at the end of the reaction. The endpoints of the simulation values lie within the 10% error

bar of experimental measurements. Also, the MWD of polystyrene-only fraction could be well represented through the log-normal distribution. To investigate the development of the inter-polymer joint MWD, polymer composition distributions of the soluble fraction before and after modification are compared for grades $G1$ and $G2$ in Figure 5.7 (d) and Figure 5.7 (e). The dashed lines represent the initial composition distribution of polystyrene by weight. The solid lines are the final distributions of polystyrene by weight after SIPN modification. Solid lines are simulated distribution based on the calculation of MWD of polyethylene, polystyrene and polyethylene-g-polystyrene, where PS MWD is simulated from the computed $\overline{Mw}$ and $\overline{Mn}$ based on the log-normal distribution. Note that crosslinking of polyethylene leads to a significant increase of polystyrene content in the soluble fraction, and the amount of increase does not exhibit dependence on the polymer chain length. Finally, note that the simulation results with our model agree well with the experimental data in Figure 5.7(d) and Figure 5.7(e). The simulation suggests that the crosslinking reactions generally take place at the end of the polymerization. A batch reactor is currently expected to be used for SIPN property control.

5.2.4 Effect of Process Conditions

Several reaction conditions can vary in the process, such as peroxide types, polyethylene types, component compositions, peroxide loading and reaction temperature. Sensitivity studies are carried out based on the kinetic model in order to understand the relationship between process conditions and product properties. The effect of reaction temperature and peroxide concentration are presented and discussed in this section.

(a) Gel content

(b) Polystyrene $\overline{Mw}$

(c) Grafting ratio

(d) Polystyrene composition distribution of Grade G1

(e) Polystyrene composition distribution of Grade G2
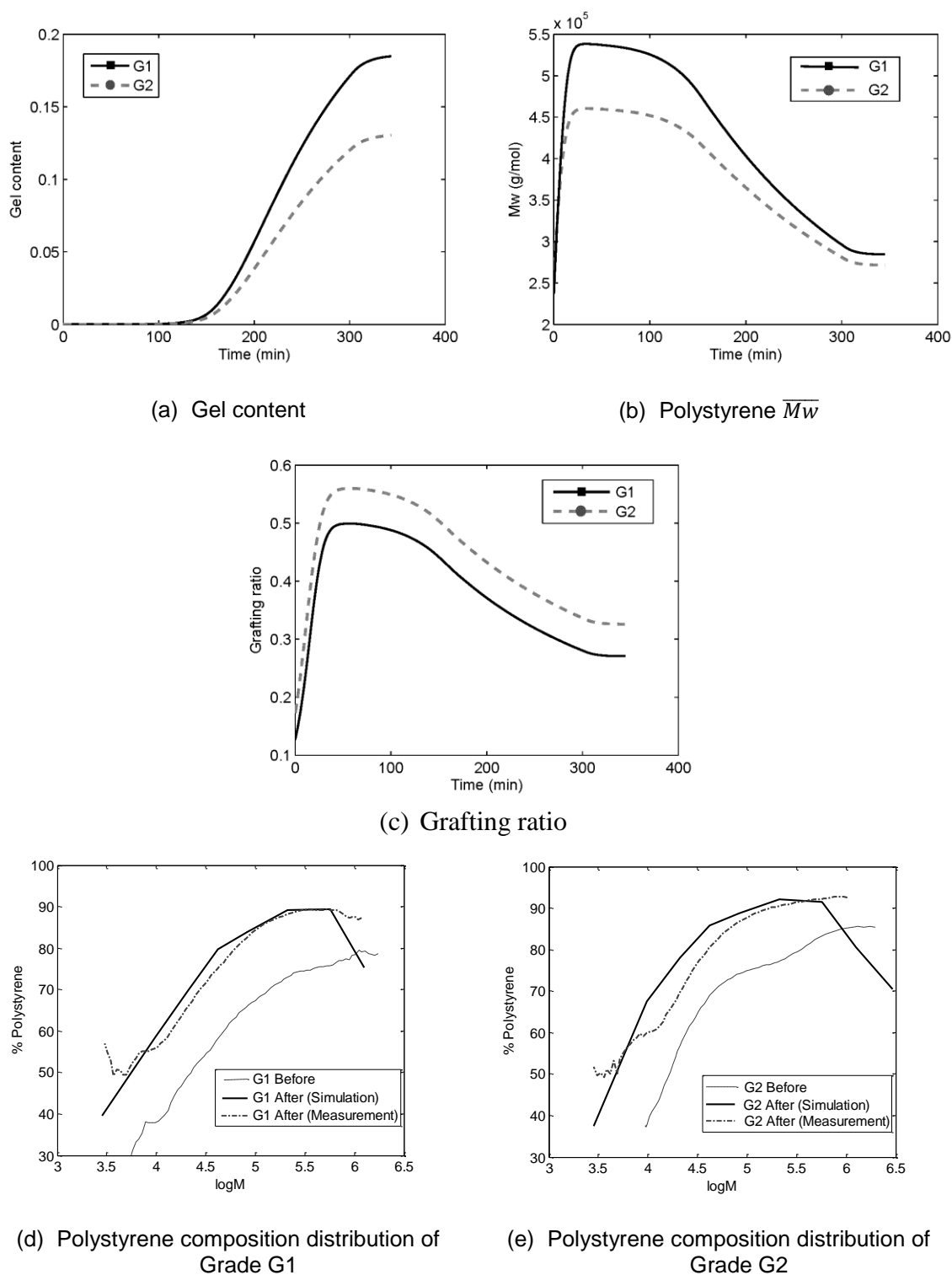
Figure 5.7 Predicted and experimentally measured SIPN properties for two grades of PES products

5.2.4.1 Effect of Reaction Temperature

Reaction temperature is one of the important controls in the process and has a strong effect on the inter-polymer properties. A set of simulations were run at increments of $10°C$ for different holding temperatures of the process for Grade $G1$. The output results are summarized in Figure 5.8. Figure 5.8 (a) shows that the gel content first increases with the increase in temperature, then starts to decrease for temperatures above 150℃ due to polymer degradation. Figure 5.8 (b) and Figure 5.8 (c) reflect the effect of degradation on the MW of free polystyrene and grafted-polystyrene. Both of their molecular weights decrease as the temperature increases. Figure 5.8 (d) presents the overall effect on the joint MWD. There is a significant increase of polystyrene soluble fraction from the condition of 120℃ to 140℃. However, distributions from the condition of 140℃ to 160℃ are similar, since both polyethylene crosslinking and polystyrene degradation reactions accelerate. Thus, low temperature slows down initiator decomposition, which leads to lower gel content. On the other hand, high temperature enhances polymer degradation, which could also lead to decrease of gel content. Joint MWD is affected by both of the effects. Hence, selecting an appropriate operating temperature is critical for product quality control.

(a) Gel content

(b) Polystyrene $\overline{Mw}$

(c) Grafting ratio

(d) Polymer composition
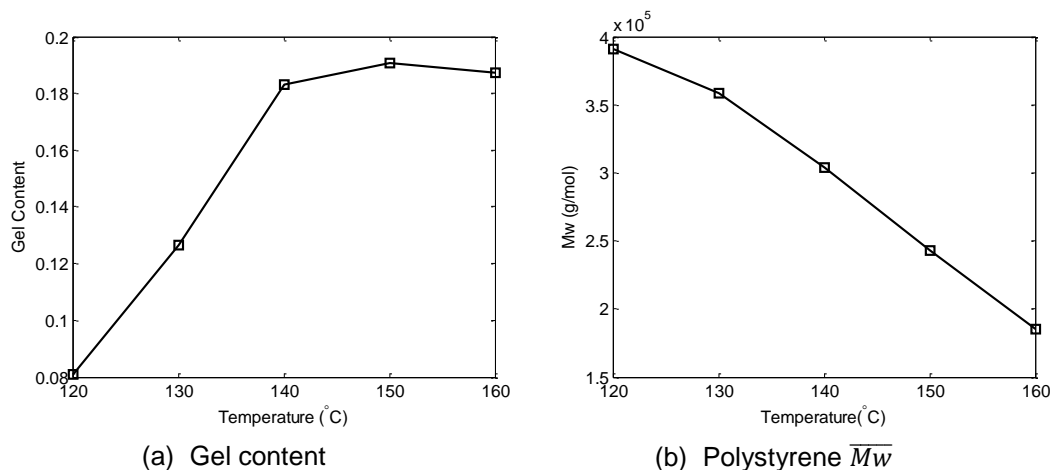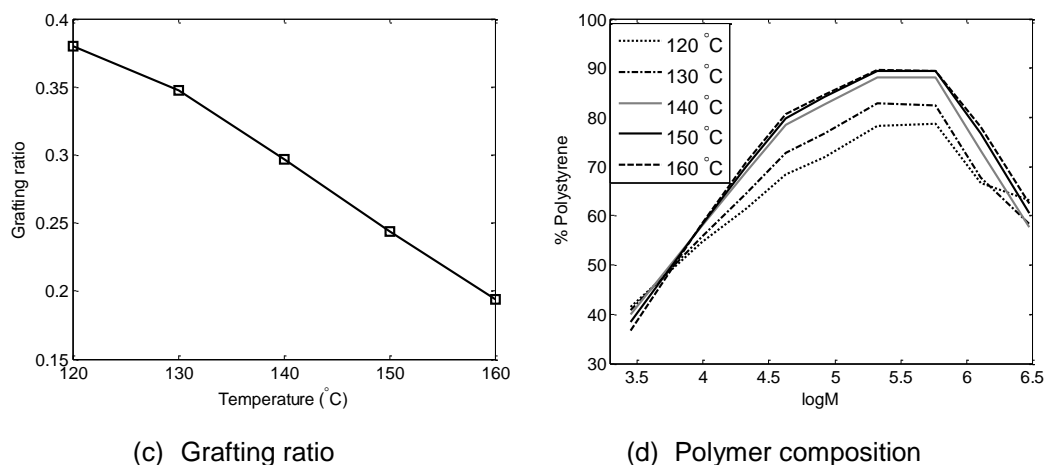
Figure 5.8 The effect of reaction temperature on PES properties

5.2.4.2 Effect of Peroxide Concentration

Peroxide concentration is also adjustable in the process. Simulations of initiator concentrations for $0.1, 0.5, 1, 2$ times that of the process for Grade $G1$ are shown in Figure 5.9, assuming initiator efficiency remains the same. At constant process temperature $143°C$, increasing the initiator concentration increases the overall gel content up to about 0.19, as shown in Figure 5.9(a), which is consistent with the gel content measurement in the lab. Also molecular weight of the soluble fraction continues to decrease, since MW of polystyrene, g-polystyrene and soluble polyethylene all decrease with enhanced degradation and cross-linking, as shown in Figure 5.9 (b). The decreasing rates appear to be close to linear with the initiator concentration, when initial efficiency is considered to be the same. Composition of the inter-polymer changes accordingly, as shown in Figure 5.9 (d). With specified product properties, reaction temperature and manufacturing policies can be optimized together to satisfy both quality and economic requirements.
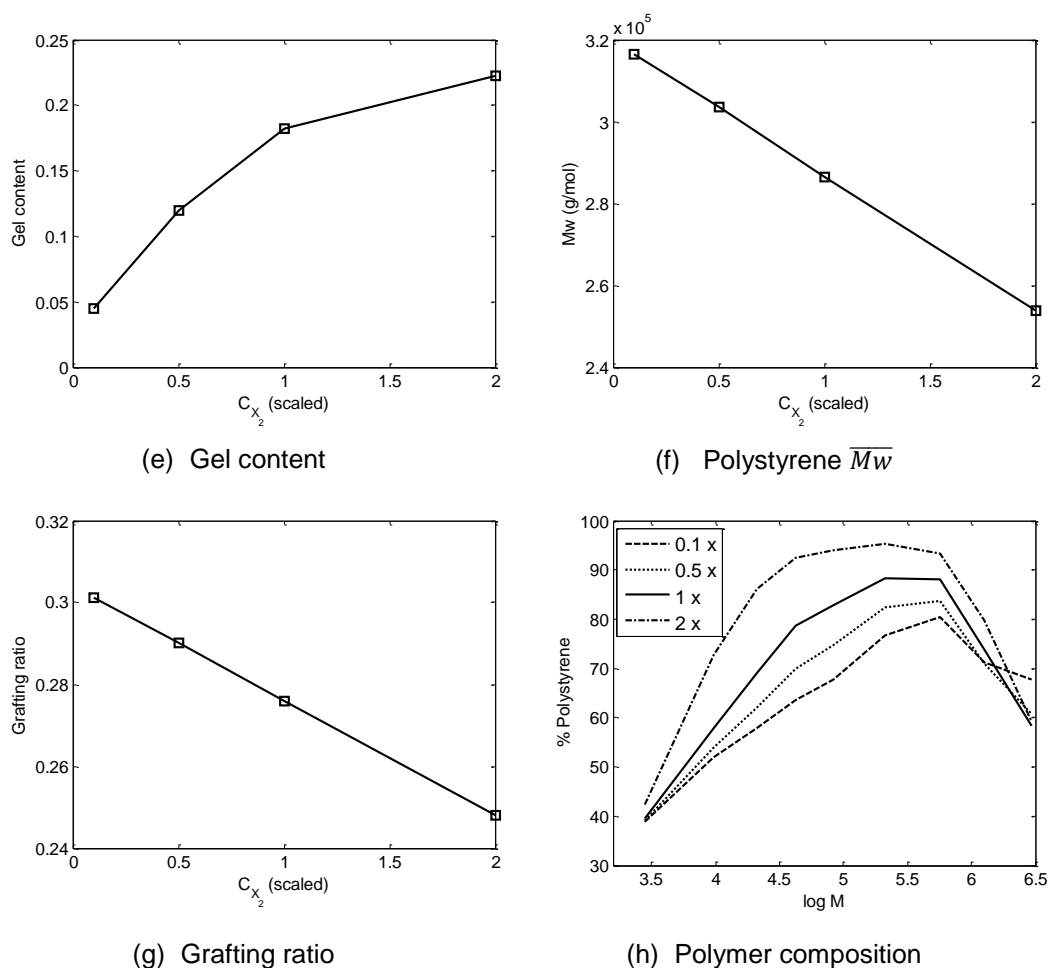
Figure 5.9 The effect of Initiator concentration on PES properties

5.3 Summary

A kinetic model for a SIPN process is proposed, where the use of a component decomposition strategy makes the modeling of the intricate polymer topology tractable. Continuous variable approximation and fixed pivot techniques are extended to solve the component population balance equations. Statistical assumptions are then employed to reconstruct the macromolecular formation. This leads to a detailed model with a manageable computational cost. In the presented model, gel content and joint molecular weight distribution are predicted throughout the entire reaction, and no breakpoint is needed for gel prediction. The model simulation is compared with PES Stage II process data. Good agreement is achieved both on

gel experiments and MWD measurements. This modeling framework can be extended to other binary systems and physical phenomena can be taken into account, together with the kinetic mechanism model for various process conditions. With appropriate modification of the polymerization mechanism, it is also possible to consider additional monomers in the modeling system. The general decomposition modeling approach can still be applied. Therefore, given desired macromolecular properties, the proposed model can serve as a basis for SIPN process design and optimization, and provides a promising approach for other polymer mixture systems.

Chapter 6

Parameter Selection and Estimation

From this chapter, foci are moved to computational strategies for large-scale nonlinear optimization, which are the challenges in polymerization model application. First, model-based quality control and process optimization is not possible until all the relevant model parameters are determined. Parameter estimation is a crucial but challenging step in model development. This chapter deals with parameter estimation problem in an over-parameterized system. A hybrid parameter selection and estimation approach is developed to reduce model distortion. Parameter estimation results for SIPN Stage I model are shown. Consistent predictions validate the model and the parameters we obtained.

6.1 A Hybrid Parameter Estimation Strategy

In free radical polymerization, apparent kinetic rates are dependent on the conversion regime. Kinetic parameters found in the literature show a high variability in their values (Almeida, et al., 2007) and no interpretation for free-radical polymerization is completely "model free" (Gilbert, 1992). Often the number of uncertain parameters is large, the system dynamics are complex and available analytical measurements are limited (Almeida, et al., 2007) .

As a result, determining a subset of estimable parameters and evaluating their goodness of fit is an important task in parameter estimation. Here, an effective approach for parameter selection and estimation is proposed. The approach employs an initial pre-selection that extends from Lund, et al. (2008), and a post optimal analysis following a simultaneous

parameter estimation strategy (Zavala, et al., 2008). With this approach, we can assess the influence and linear dependency of the parameters with little additional effort. The procedure is outlined in Figure 6.1.
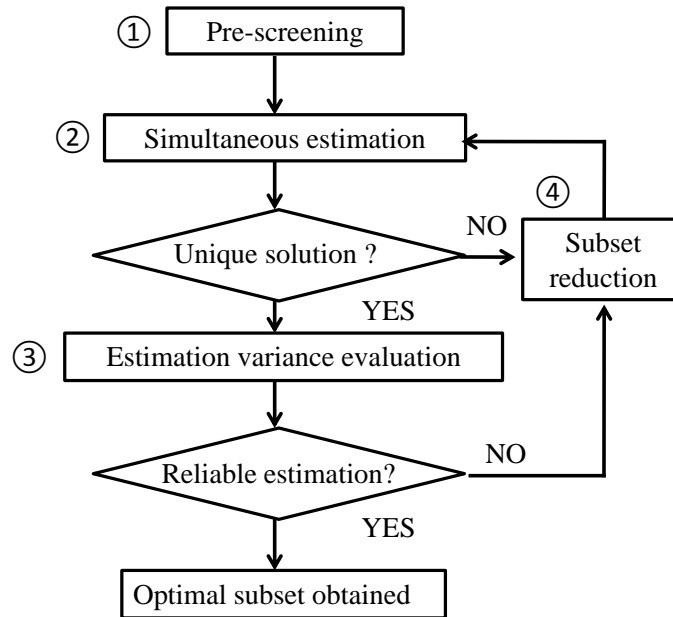
Figure 6.1 A diagram of hybrid parameter estimation procedure

Four steps are applied in this approach.

1. Select an initial subset by pre-screening. Based on parametric sensitivity at their nominal values, rank the parameters through approximated individual variance contribution. The cutoff threshold for the parametric variance is set to 3 orders of magnitude. Parameters with an estimated variance exceeding the threshold value are removed from the estimation set after pre-screening.

2. Simultaneous parameter estimation. The selected parameters are estimated simultaneously to obtain a unique estimation value within appropriate bounds. If the solution is not unique, go to step 4.

3. Estimation quality evaluation. Compute a reliability factor "β" based on scaled parameter variance estimation from post-optimal analysis and update the parameter ranking. If the largest β value (β_{max}) does not satisfy the reliability threshold β_U , then go to step 4. Otherwise, stop. The optimal subset is obtained.

4. Update the selected set by removing one of the parameters from the subset. If this step follows step 2, then the parameter with the largest $\Delta var \hat{\theta}_i$ (individual variance contribution) in the pre-screening list will be removed. If this step follows step 3, then the parameter with the largest β value (β_{max}) should be removed. Continue with step 2 and re-estimate a smaller subset of parameters.

The details of each step are discussed next.

6.1.1 Parameter Ranking and Pre-screening

The first step before solving any optimization problem is to pre-screen estimating parameters based on a local ranking strategy. Parameter estimability is an important but often overlooked step, when preparing to fit a mathematical model to a set of experimental data (Vajda, et al., 1989). However, a rigorous analysis of parameter subset selection for nonlinear models is generally computationally demanding. Approaches utilizing nominal sensitivity vectors for parameter selection help to provide effective means for parameter pre-screening. In particular, algorithms based on orthogonal factorization have clear geometric interpretation of linear dependency, and can be adapted easily. Here we use QR factorizations with a column permutation (QRcp) approach (Lund, et al., 2008), where the magnitude of the variance contribution for each parameter (assuming a Gaussian distribution) can be obtained in a particularly easy form. Parameter initial ranking based on QRcp approach is

used to select a large initial subset. More rigorous statistical inference can be further explored through optimization.

The QRcp algorithm is based on the analysis of a sensitivity coefficient matrix and the Cramer Rao inequality. In our system, the (scaled) sensitivity coefficient matrix for multi-response system is expressed as (Yao, et al., 2003) :

$$
S = \begin{bmatrix}
\frac{\theta_1^* \partial y_1}{y_1^* \partial \theta_1}\big|_{t=t_1} & \cdots & \frac{\theta_P^* \partial y_1}{y_1^* \partial \theta_P}\big|_{t=t_1} \\
\vdots & \ddots & \vdots \\
\frac{\theta_1^* \partial y_R}{y_R^* \partial \theta_1}\big|_{t=t_1} & \cdots & \frac{\theta_P^* \partial y_R}{y_R^* \partial \theta_P}\big|_{t=t_1} \\
\frac{\theta_1^* \partial y_1}{y_1^* \partial \theta_1}\big|_{t=t_2} & \cdots & \frac{\theta_P^* \partial y_1}{y_1^* \partial \theta_P}\big|_{t=t_2} \\
\vdots & \ddots & \vdots \\
\frac{\theta_1^* \partial y_R}{y_R^* \partial \theta_1}\big|_{t=t_N} & \cdots & \frac{\theta_P^* \partial y_R}{y_R^* \partial \theta_P}\big|_{t=t_N}
\end{bmatrix}
\tag{6.1}
$$

where $(\theta_1, \cdots, \theta_P)$ is a set of parameters to be estimated, $(y_1, \cdots, y_R)$ is a set of responses, θ_i^*, y_i^* are the reference values that scale θ_i and y_i, and $(t_1, \cdots, t_N)$ is a set of selected sample points in time. The elements of the matrix are individual parametric sensitivity coefficients, which are determined numerically.

We assume that measured output is a function of the parameters affected by measurement noise that follows a Gaussian distribution with zero mean and covariance matrix Σ. (Without loss of generality, the outputs in S were scaled so that the covariance matrix is reduced to I in the analysis.)

The Cramer Rao inequality, Equation (6.2), expresses a lower limit of the estimation variance of selected parameters.

$$\text{var } \hat{\theta} \geq \text{tr}(F)^{-1} \tag{6.2}$$

where F is the Fisher information matrix, defined by:

$$F(\theta) = E\left[\frac{\partial}{\partial\theta}\ln p(\tilde{y}|\theta)\frac{\partial}{\partial\theta^T}\ln p(\tilde{y}|\theta)\right] = \left(\frac{\partial y}{\partial\theta}\right)^T \Sigma^{-1}\frac{\partial y}{\partial\theta^T} = S^T S \tag{6.3}$$

It is shown by a recursive procedure that through a successive orthogonalization of S, individual variance contribution ($\Delta\text{var } \hat{\theta}_i$) can be associated with a measure of $S^T S$. Here, $\Delta\text{var } \hat{\theta}_i$ refers to an additional cost to the whole parameter set after inclusion of parameter θ_i in the ranked set of $\{\theta_1, \cdots, \theta_{i-1}\}$.

Thus, QR factorization with column permutation is carried out for S, as $SE = QR$, the permutation matrix E provides a reference ranking of parameters, while the matrix R offers a value of individual parameter variance.

Redefining R by extracting the diagonal, $R = D\bar{R}$, we evaluate

$$(E^T S^T SE)^{-1} = (\bar{R}^T D^T Q^T QD\bar{R})^{-1} = (\bar{R}^T D^2 \bar{R})^{-1} = \bar{R}^{-1} D^{-2} \bar{R}^{-T} = UD^{-2}U^T \tag{6.4}$$

where $D = \text{diag}[d_1, \cdots, d_p]$, $\bar{R}$ is upper unit triangular, and $U = \bar{R}^{-1}$. Then, the norm of the individual variance contribution of each parameter, $\Delta\text{var } \hat{\theta}_i$, is then given by:

$$\Delta\text{var } \hat{\theta}_i = \frac{\|u_i\|^2}{d_i^2} \tag{6.5}$$

where u_i is the ith column in U. Magnitudes of $\Delta\text{var } \hat{\theta}_i$ can be used as a criterion to determine the number of parameters to be estimated. More details can be found in (Lund, et al., 2008).

Notice that using one set of nominal parameter values to define the ranking is usually not sufficient and Lund, et al.(2008) suggested generating the sensitivities for as many values of

the parameter vector as available. Therefore, QRcp is only applied for preliminary set selection in our approach and only leads to elimination of the least sensitive parameters from the estimation. In this work, a variance range of 3 orders of magnitude is allowed in the pre-screening to keep the candidate parameter set large enough for simultaneous parameter estimation. The final parameter ranking and validation is left for the post-optimal analysis.

6.1.2 Simultaneous Parameter Estimation

In this step, optimal parameter values are determined and their qualitative influence is analyzed in order to reevaluate the parameter ranking. Here, the objective is to minimize the prediction error subject to constraints imposed by model equations and known bounds on the parameters (Li, 2003), in the form of (6.6).

$$
\begin{aligned}
\min_\theta \quad & \sum_{k=1}^{ND} (y(t_k) - y(t_k)^M)^T \Sigma^{-1} (y(t_k) - y(t_k)^M) \\
s.t. \quad & \text{Dynamic process model} \\
& y = h(z, x) \\
& \mathcal{F}(\frac{dz}{dt}; z(t); x(t); u(t); t; \theta) = 0 \\
& \mathcal{G}_s(z(t_s); x(t_s); u(t_s), t_s; \theta)) = 0 \\
& \text{Initial conditions: } z(0) = z_0 \\
& \text{Bounds: } z^L \leq z(t) \leq z^U \\
& x^L \leq x(t) \leq x^U \\
& \theta^L \leq \theta \leq \theta^U
\end{aligned}
\tag{6.6}
$$

where ND is the number of data sets, $k = 1 \cdots ND$, and $y(t_k), y(t_k)^M$ are simulation and measurement values at t_k, respectively. $\mathcal{F}$ are differential-algebraic constraints, $\mathcal{G}_s$ are additional point constraints at times t_s, z are differential variables, x are algebraic variables, $u(t)$ are control profiles, and θ are parameter vectors to be estimated.

For dynamic optimization problems, a comprehensive review can be found in (Biegler, 2007). Following (Kameswaran, et al., 2006), differential and algebraic variables are discretized using orthogonal collocation on finite elements, leading to a large-scale, structured nonlinear programming (NLP) problem of the form (6.7).

$$
\begin{aligned}
\min_{\chi \in R^n} \quad & f(\chi) \\
s.t. \quad & c(\chi) = 0 \\
& \chi^L \leq \chi \leq \chi^U
\end{aligned}
\tag{6.7}
$$

where χ represents the parameters and polynomial coefficients of the approximated state variable profiles, $\{f: \mathbb{R}^n \to \mathbb{R} \text{ and } c: \mathbb{R}^n \to \mathbb{R}^m\}$. The transcribed NLP model can be solved efficiently by a large-scale NLP solver. An interior point NLP solver, IPOPT (Wachter, et al., 2004) is used in our study. A unique local solution is necessary for the post-optimal analysis. If the KKT matrix of (6.6) is non-singular with appropriate inertia, it satisfies second-order sufficient conditions. In IPOPT, a quick, direct test for the uniqueness of the solution is through the output of the regularization value of the reduced barrier Hessian at the solution. If no regularization is required at the optimal point, then sufficient second order conditions are satisfied and the local solution and estimated parameters are unique. More details on this test can be found in Zavala, et al. (2008).

6.1.3 Estimation Quality Evaluation

Once optimal parameters are uniquely determined, the reduced Hessian, H^*, is extracted from the factorized KKT matrix, as described in Zavala, et al. (2008).

A reliability factor, β, is defined for the estimated parameters based on the obtained reduced Hessian information. β is the ratio of parameter variance to its estimated value:

$$\beta = \hat{\sigma}_{\theta_p}/|\hat{\theta}_p| \tag{6.8}$$

and $\hat{\sigma}_{\theta_p}$, the estimated standard deviation for parameter θ_p, can be computed following (Bard, 1974), based on the reduced Hessian matrix at the optimal point:

$$\begin{aligned} \hat{V}_\theta &= H^{*-1} \\ \hat{\sigma}_\theta{}^2 &= (\text{diag}(\hat{V}_\theta)) \end{aligned} \tag{6.9}$$

where $\hat{V}_\theta$ is the approximated covariance matrix. In practice, we set an acceptable threshold value of β as β_U. β_U is used as a user defined confidence level, and can be a scalar or vector depending on the parameter estimation requirement.

6.1.4 Selection Set Reduction

The selected parameter subset should be reduced under two scenarios, and is implemented differently in the pre-screening and post-optimal steps. In the pre-screening, insensitive parameters are removed from the QRcp ranking list to obtain a unique solution, while in the post-optimal step the parameter is removed if the β_{max} exceeds its threshold variance range β_U to improve the estimation quality.

When removed from the selection set, the parameter is fixed to its nominal value in the following parameter estimation run. While the goodness of fit for the reduced parameter set hardly changes, the uncertainty in the parameters can be greatly reduced. It is important to point out that the final selection may differ from the initial ranking in Step 1, since the sensitivity matrix changes at the new optimal solution. If the reliability threshold (β_U) is too low to be satisfied by any of the parameters, then additional measurements are probably required to meet the desired estimation criteria.

6.2 Results and Discussion

6.2.1 An Illustrative Example

We illustrate the parameter selection and estimation approach using a CSTR reaction model from Muske, et al. (2003). In addition, comparison with other approaches is discussed. The description of the example is provided here.
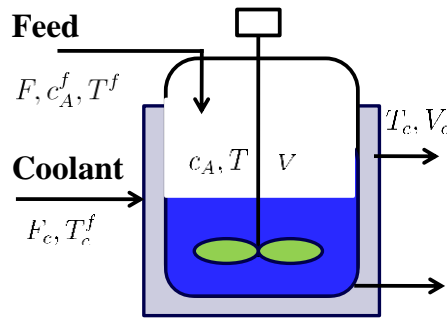
Figure 6.2 A CSTR example for parameter estimation

In a CSTR reaction system shown in Figure 6.2, component A undergoes a first-order, exothermic reaction to form a product component B

$$A \rightarrow B, \quad \mathcal{R}_A = k\exp(-E/RT)c_A \tag{6.10}$$
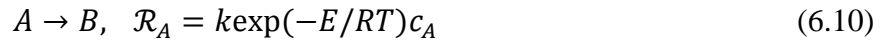
The CSTR system is described by the following three ODEs. Three state variables are concentration of component A (c_A), reactor temperature (T), and coolant temperature (T_c).

$$
\begin{aligned}
\dot{c}_A &= \frac{F}{V}(c_A^f - c_A) - \mathcal{R}_A \\
\dot{T} &= \frac{F}{V}(T^f - T) + \frac{\delta H}{\rho C_p}\mathcal{R}_A - \frac{hA}{\rho C_p V}(T - T_c) \\
\dot{T}_c &= \frac{F_c}{V_c}(T_c^f - T_c) + \frac{hA}{\rho_c C_{p_c} V_c}
\end{aligned}
\tag{6.11}
$$

The nominal values of the parameters are listed in Table 6.1.

Table 6.1 Nominal operating values of the CSTR example

Parameter	Variable	Value	Parameter	Variable	Value
Feed flow	F	$0.1\ m^3/h$	Activation energy	E/R	$255 K$
Feed temperature	T^f	$20°C$	Pre-exponential factor	k	$2.5 h^{-1}$
Feed composition	c_A^f	$2,500\ mol/m^3$	Coolant flow rate	F_c	$0.15\ m^3/h$
Reactor volume	V	$0.2\ m^3$	Coolant inlet temp	T_c	$10°C$
Heat transfer area	A	$4.5\ m^2$	Cooling jacket volume	V_c	$0.055\ m^3$
Fluid density	ρ	$1,025\ kg/m^3$	Coolant density	ρ_c	$1,000 kg/m^3$
Fluid heat capacity	C_ρ	$1.55 kJ/(kg \cdot C)$	Coolant heat capacity	C_{p_c}	$1.2 kJ/(kg \cdot C)$
Heat of reaction	δH	$160\ kJ/mol$			

Assume that only the reactor temperature measurements are available, and the sensor measurement noise is $\sigma^2 = \pm 1°C$. The objective of the parameter estimation problem is to estimate as many uncertain parameters as possible, while keeping the estimation variance within a 10% threshold ($\beta_U = 0.1$). Here, 12 sampling data (15 min/sample) of T is generated from the model with "true" parameter value. A random noise σ^2 is added to the generated data to simulate the process condition. Table 6.2 summarizes the parameter estimation results following the procedure described previously.

Table 6.2 Parameter selection result for the CSTR example

Ranked Parameters		$\text{var}(p_0)$	Estimation and β value for N_p parameters				(Chu, et al., 2007)
			$N_p = 4$	$N_p = 3$	$N_p = 2$	$N_p = 1$	
$\bar{T}^f$	(0.99)	0.0002	1.02(2.68)	0.92(0.31)	0.996(0.01)	1.001(0.01)	x
$\bar{c}_A^f$	(1.02)	0.0029	0.92(2.88)	1.03(0.09)	1.007(0.02)	x	x
$\bar{\rho}$	(0.99)	0.0701	0.92(0.47)	0.91(0.34)	x	x	x
$\bar{k}$	(1.10)	0.7710	0.88(3.14)	x	x	x	1.04
$\bar{E}$	(1.01)	7.0130	x	x	x	x	x
$\bar{T}_c^f$	(0.99)	32.2659	x	x	x	x	x
$\Delta \bar{H}$	(0.95)	.	x	x	x	x	x
$\bar{h}$	(1.05)	.	x	x	x	x	1.31
$\bar{\rho_c}$	(1.01)	.	x	x	x	x	*
Residual sum of squares			7.79	7.87	8.12	160.62	9.51

The value shown in the first column of the Table 6.2 is the "true" value of the 9 parameters (normalized by its nominal value in Table 6.1. Implementation details are described below.

- Step 0. A preparation step. The model is initialized with nominal parameters as shown in Table 6.2. Before solving any optimization problem, all the parameters in the estimation problem are normalized by their nominal values. Hence, all the parameters are approximately within the same range. Normalization enables easier comparison in this procedure.

- Step 1. Pre-screening. Perturbing the parameters around "1", we obtain local sensitivity information at the sampling points. The parameter ranking based on parameter variance contribution is shown in the 2nd column. Following the rule of a factor of 1,000, 4 parameters, T^f, c_A^f, ρ and k, are selected in the first step. All the rest parameters are fixed to nominal value 1.

- Steps 2 and 3. Simultaneous parameter estimation with variance approximation. When $N_p = 4$, the estimation results are shown in the 3rd column. The value in the bracket is the β ratio at current optimal point. As seen in the table, the estimation variances exceed the 10% threshold, indicating a further refinement of the selection pool is necessary.

- Step 4. Selection set reduction. As shown in the 4th and 5th column, k, ρ are sequentially removed from the simultaneous estimation and fixed to 1 in the following estimation problem. Until $N_p = 2$, T^f and c_A^f are selected, and both β values are within 10% range.

- Terminate and proceed to the optimal estimation selection. The parameter estimation procedure is terminated at $N_p = 2$. It indicates that at most two of the parameters could be estimated at the desired estimation accuracy, based on the available information. For comparison, the last column shows the result for $N_p = 1$. The increased residual sum of squares indicates a poor data fitting circumstance. It is because adjusting one parameter is not sufficient to fit the data.

This result is compared with the global sensitivity approach discussed in Chu, et al. (2007). From their results, three parameters are selected, which are k, h and ρ_c. However, in the estimation test, this subset shows higher estimation variance at the optimal point. Our hybrid parameter selection approach outperforms the previous approach.

6.2.2 Parameter Estimation for PES Stage I Model

We implemented the parameter estimation procedure for the Stage I model. Data are collected through sampling from an industrial PES pilot plant for styrene monomer and a polyethylene seed, which is extruded and screened to be monodisperse. Examples of the process examples can be found in patents (eg. Kitamori, 1979). Polyethylene seeds, with an average particle diameter of 0.8mm to 1.0mm, were suspended in the aqueous medium with suspending agent and strong agitation in a 10 L suspension reactor. An initial charge of styrene monomer and initiator mixture (typically 10% ~ 30% of the total amount of the recipe) was added to the reactor, and the reactor was brought to a desired temperature. The system was held for 1-2 hours until the seeds were well swollen. Thereafter, the remaining monomer and initiator were added continuously following a piecewise constant feeding strategy (see Figure 7.2) to begin polymerization inside the seed particles. The polymerization stage takes place at a constant temperature in the range of $85 \sim 90°C$ for a maximum of 10 hours.

Samples are taken during polymerization. For all pilot plant tests, no oscillatory or chaotic behavior was observed in the experiments.

The process model consists of Equations (4.22) - (4.30). Initial conditions are defined at the start of polymerization stage, and all the state variables are constrained with loose lower and upper bounds. Bounds on the parameters are set to a factor of 100 around their nominal values.

Four types of kinetic and physical parameters are present in the model.

1. Polymerization kinetic parameters: initiator efficiency "f", initiator decomposition rate "k_d", propagation rate "k_p", termination rate "k_t" and chain transfer rate "k_{fs}",

2. Transport properties: monomer effective diffusion coefficients "D_M", initiator effective diffusion coefficient "D_I",

3. Partial molar volume coefficients: "a_0^M", "a_1^M", "$a_0^{P_1}$", "$a_1^{P_1}$", "$a_0^{P_2}$", "$a_1^{P_2}$".

4. Initial conditions of the polymerization stage: initial weight average molecular weight "$\overline{Mw}_0$" and initial conversion ratio of monomer "$\bar{x}_{s_0}$". These initial conditions need to be estimated due to pretreatment during the seeding stage.

In the objective function of (6.6), data from 3 different grades of products are available. Based on the initial size of the seed, the total number of seed particles, $\mathbb{N}_{seed}$ are $1.3 \times 10^8, 7.9 \times 10^8$ and 8.0×10^8 , respectively. Each process includes $8 \sim 10$ samples during the reaction, which leads to a total of 26 data sets($ND = 26$). Also three types of property measurements are available at sample time t_k for each grade of resin.

1. Weight average molecular weight $\overline{Mw}_0$ of polystyrene, measured by GPC.

2. Styrene conversion ratio $\bar{x}_s$, measured by FTIR.

3. Average particle radius R, measured by a laser diffraction particle analyzer.

Hence, the multi-set parameter estimation problem based on (6.6) is formulated as (6.12).

$$
\begin{aligned}
\min_\theta \quad & \sum_{g=1}^{NG} \sum_{s=1}^{NS_g} (y(t_{gs}) - y(t_{gs})^M)^T \Sigma_y^{-1} (y(t_{gs}) - y(t_{gs})^M) \\
s.t. \quad & \{\text{Equation } (4.22) - (4.30)\}_g, \quad g = \{1, \cdots, NG\} \\
& \text{Initial conditions: } z_{g_0} \\
& \text{Bounds: } z_g^L \le z_g(t) \le z_g^U \\
& x_g^L \le x_g(t) \le x_g^U \\
& \theta^L \le \theta \le \theta^U
\end{aligned}
\tag{6.12}
$$

where $NG = 3$, denoting number of grades available, NS_g is the number of samples taken from each grade. y is the output vector of $[\overline{Mw}, \bar{x}_s, R]'$, and subscript gs refers to sample s in grade g measurement. Σ_y is set to be a diagonal matrix with the diagonal element as measurement variance of y. Equations (4.22)-(4.30) are applied for each grade. The initial condition z_0^g is specified from production recipes and initial sample measurements. θ refers to above 19 parameters.

To initialize the parameter estimation problem, nominal kinetic values are specified from (Curteanu, 2003). The effective diffusion rate refers to a similar diffusion system of toluene (Hong, et al., 1996), as shown in Table 6.2, and we assume the initiator has the same diffusion coefficient as the monomer. An initial guess of partial molar coefficients is approximated from the following equation:

$$
V = \sum_l (a_0^l + a_1^l \cdot \bar{c}_M) \cdot n_l
\tag{6.13}
$$

The initial conditions of the polymerization stage are based on sample measurements. These are scaled to one in Table 6.2 and listed along with the initial values for the other parameters.

Because the product is produced under isothermal conditions throughout the polymerization stage, the temperature variation for different grades is small ($\leq 5°C$). Hence, only pre-factors of the kinetic parameters are estimated and the activation energies are set to their literature values. The kinetic and physical parameters for different grades of product are estimated jointly, while the initial conditions for each polymerization stage are estimated individually, as a result of the difference in the pretreatment stage. The initial sensitivity matrix is computed from the simulation model for the above 19 parameters at their nominal values.

For the studied case, 20 shells were used for spatial discretization of the seed particle, which leads to 160 differential equations and 103 algebraic equations. Since Radau collocation is known to be suited for stiff ODEs, 3 point Radau collocation is used for the simultaneous approach with 15 to 25 unequally-spaced finite elements for each model. The model for a single data set contains around 12,000 to 20,000 variables after temporal discretization. To estimate model parameters that describe three process data sets, the multi-set parameter estimation problem leads to 50,411 variables. The parameter estimation is implemented in the modeling platform AMPL with the solver IPOPT 3.4 compiled with the METIS (Karypis, et al., 1999) package, running on a Linux box with Intel Core2 Quad CPU at 2.4 GHz.

Table 6.3 Results of parameter selection and estimation for Stage I model

RP	$\Delta\mathrm{var}\hat{\theta}_i$	EP(β) of SM			LM
		$Np = 13$	$Np = 12$	$Np = 11$	
k_p	0.017	1.0683(0.04)	1.0683(0.04)	1.0912(0.04)	1.0385(0.20)
$\overline{x_{s\,0}}^{I}$	0.134	1.1031(0.06)	1.1031(0.06)	1.0955(0.06)	1.1442(0.08)
a_0^{M}	0.167	0.8203(0.25)	0.8192(0.21)	1.0138(0.15)	0.9369(0.43)
f	0.270	0.7070(0.26)	0.7069(0.21)	0.7350(0.17)	0.7055(0.37)
$\overline{x_{s\,0}}^{II}$	0.393	1.0002(0.14)	1.0002(0.10)	1.0003(0.09)	1.0005(0.05)
$\overline{x_{s\,0}}^{III}$	0.495	0.9998(0.01)	0.9998(0.01)	0.9985(0.01)	0.9745(0.26)
$\overline{Mw_0}^{I}$	0.498	1.0655(0.04)	1.0654(0.04)	1.0380(0.04)	1.1367(0.58)
$\overline{Mw_0}^{III}$	0.495	1.5062(0.13)	1.5061(0.13)	1.5138(0.12)	1.4487(0.62)
$\overline{Mw_0}^{II}$	0.981	0.6473(0.25)	0.6471(0.25)	0.6118(0.26)	0.9666(1.00)
$a_0^{P_1}$	1.310	1.0548(0.21)	1.0537(0.21)	0.9973(0.22)	1.3521(1.50)
$a_0^{P_2}$	3.611	1.0412(0.08)	1.0422(0.08)	0.9820(0.08)	0.8864(1.12)
$a_1^{P_1}$	23.332	1.0033(0.35)	0.9997(0.33)	X	
a_1^{M}	6.117	0.4548(0.96)	X	X	
k_{fs}	69.192	X	X	X	
$a_1^{P_2}$	134.449	X	X	X	
k_t	410.389	X	X	X	
D_M	23995.3	X	X	X	
D_I	205781	X	X	X	
k_d	X	X	X	X	

RP: Ranked parameter
EP(β)   Estimated parameter value with β ratio
SM   Shell model
LM   Lumped model

The threshold ratio β_U is set to be 30%, and the optimized parameters for different selection sets are summarized in Table 3. The estimated values shown are scaled with their nominal values. The column of "$\Delta\mathrm{var}\,\hat{\theta}_i$" is computed through QRcp approach at the parameter initial guesses; this is Step 1 as discussed in section 6.1.1. Notice that, the initiator decomposition constant "k_d" and initiator efficiency "f" are dependent in the model, only one of the parameters is included for further analysis. In this case, f is included in the estimation, while k_d is fixed to its nominal value. In Step 1, "k_p" has the smallest variance contribution, with $\Delta\,var\,\hat{\theta}_i$ of 0.017, on the order of 10^{-2}. Following the 3 orders of magnitude cutoff rule, the threshold for $\Delta\mathrm{var}\,\hat{\theta}_i$ becomes orders of $10^3 \times 10^{-2} = 10$. Ranking the parameters according to $\Delta\mathrm{var}\,\hat{\theta}_i$ in Table 6.3, suggests that the initial subset could in-

clude parameters from "k_p" to "k_{fs}". From Table 6.3, "$a_1^{P_2}$" and the rest of parameters exceed the limit, and are removed from the pre-screening. Parameters ranked after "$a_1^{P_2}$" are removed from further analysis. Then, following the procedure of Step 2, 14 parameters are selected for simultaneous estimation. However, no unique solution can be obtained within the search region. "k_{fs}" is then removed from the subset and fixed to its initial guess based on the criteria in Step 4, and the remaining 13 parameters continue to be estimated to obtain a unique solution. The ratio β is computed from (6.8) at the solution point as shown in the 3rd column of the Table 6.3. The optimal parameter values are scaled by their nominal values for comparison and the β ratio is reported in parentheses. Notice that $\beta_{max} \geq 30\%$. The parameter with the largest "a_1^M" is removed at this step and fixed to 1. Consequently, estimation was done similarly for 12 and 11 parameters. Note that the reduced set with 11 parameters meets the requirement of 30% ratio of estimated variance, suggesting that the first 11 parameters can be reliably estimated based on the measurements. Hence, the selection and estimation procedure stops. Based on the estimation, the proposed model describes the particle evolution for all considered data sets very well.

The scaled comparison results are presented in Figure 6.3, with the data and model prediction shown for conversion ratio, weight average molecular weight and average particle radius. Model results compare favorably with experimental data as shown.

In order to study the importance of the diffusion reaction mechanism of the single particle system, we also run a parameter estimation study using a lumped model (LM), which reduced the multi-shell structure into a single core. The 11 selected parameters from the full model were estimated based on the reduced model with the same measurement data and objective function. The result obtained is compared in Table 6.3. The corresponding outputs for
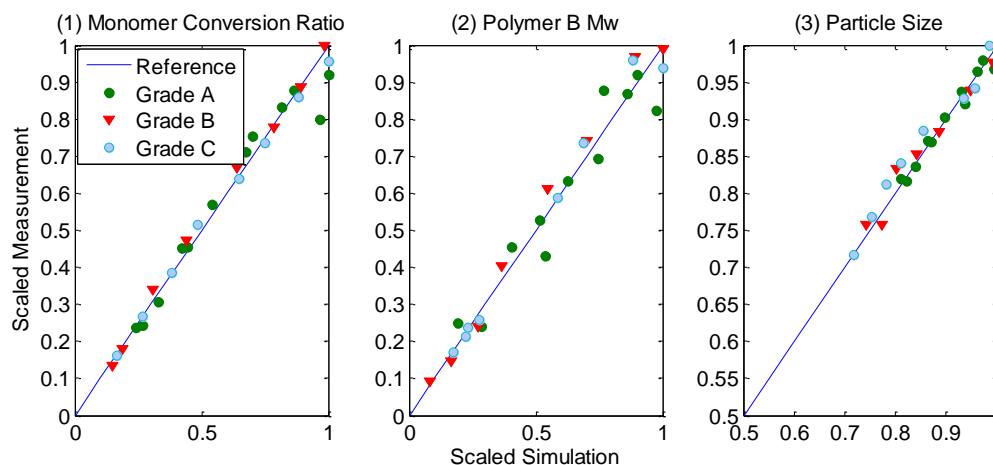
Figure 6.3 Result of parameter estimation for 3 grade products

Grade *A* product are also shown in Figure 6.4 as dashed lines. It may be observed that inclusion of the intra-particle dynamics does not change the average prediction significantly since the diffusivity is relatively high for styrene monomer in our system. However, due to the diffusion controlled kinetics, intra-particle distribution still plays an important role in the particle average properties. Notice that better predictions are achieved with the full model. The overall residual is reduced by 29% by using the shell model. This difference is also reflected in the parameter estimation results. From the comparison shown in Table 6.3, it is found that the estimated optimal parameter values are close in both cases. Nevertheless, the reliability ratio β is affected in the lumped model due to the lack of fit. Hence, fewer parameters could be regarded as reliably estimated from the reduced model.

6.3 Uncertainty Quantification before New Estimation

A successful parameter estimation procedure confirms output predictions within their measurement error. For this studied process, the model prediction satisfied such requirements through direct comparison with experimental data. When users want to use the simulation model for a different system without experimental data available, uncertainty quantification
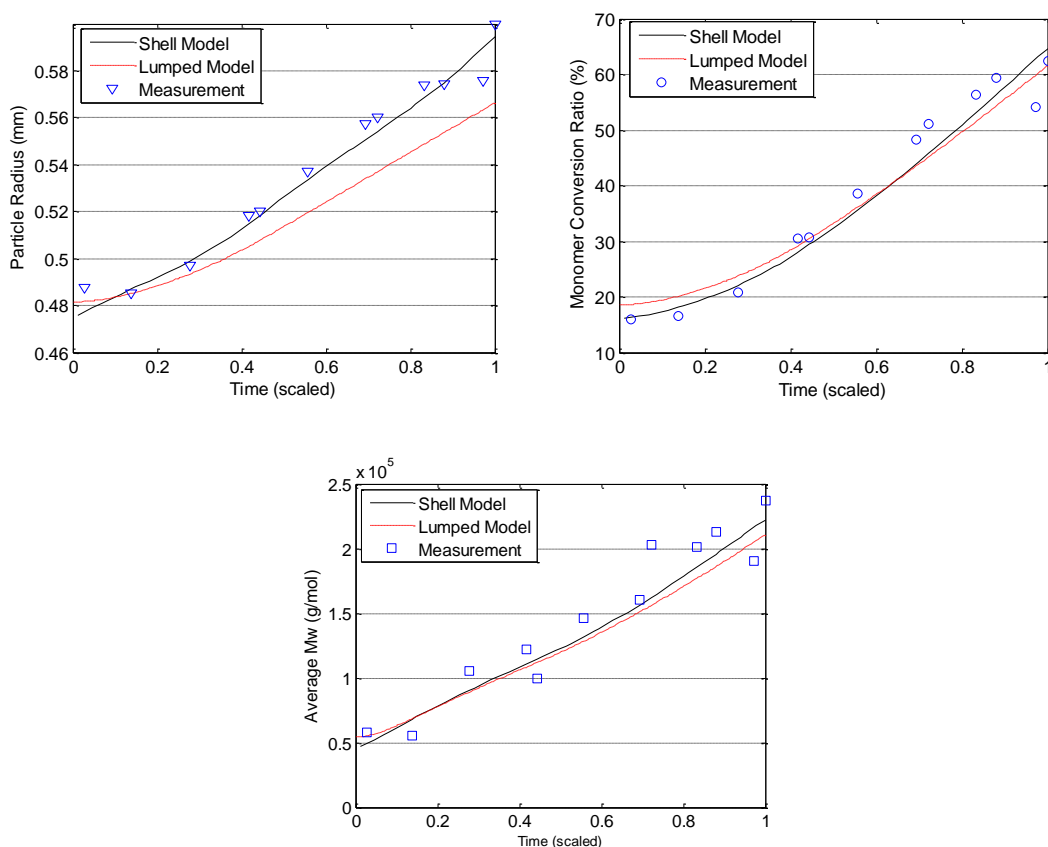
Figure 6.4 Comparison with the lumped model on parameter estimation results

of the model prediction is of importance when further actions are to be considered and valid conclusions are drawn. In this case, parameters are supplied using literature values without estimation from the process. Prior knowledge gives an uncertain range of the input parameters, and it is useful to access the estimation variance at the given conditions. Therefore, uncertainty quantification is shown for general use of the current model.

Assume that, the monomer is replaced with a different styrenic monomer. The kinetic mechanism of monomer polymerization remains the same, but model parameters are changed for this system. The uncertain parameters considered are k_p and f. The user supplies a nominal value for k_p from the literature, assuming the actual value follows a uniform distribution in the range of $[-10\%, +10\%]$ from its reference value, and f is assumed to vary

between 0.5 and 0.8. Monte Carlo simulation is carried out in the uncertain space of k_p and f. Prediction of $\overline{Mw}$ and $\overline{xs}$ is shown in Figure 6.5, accordingly.
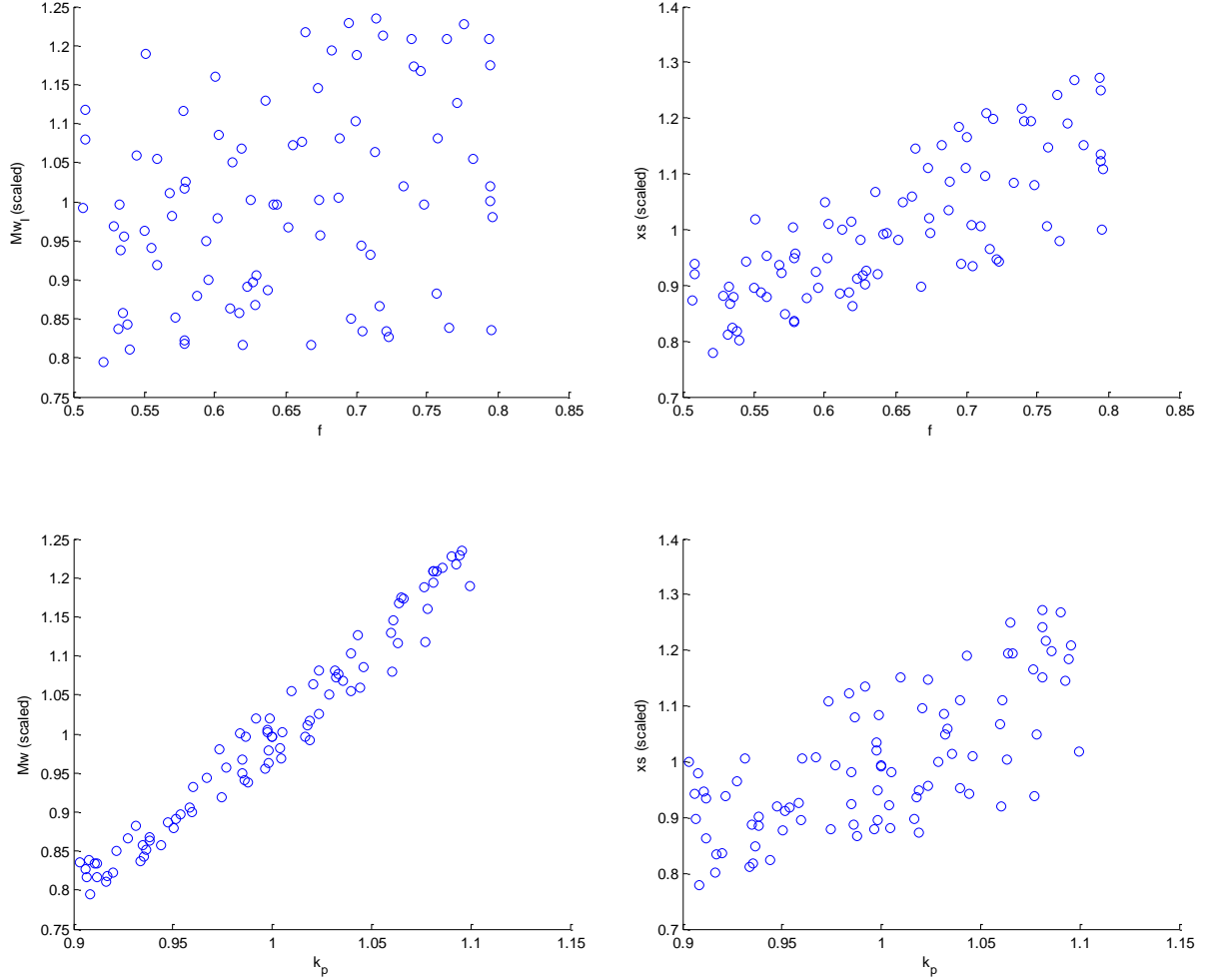
Figure 6.5 Scatter plot of simulation results under uncertainty

The true value of the outcome is expected to lie in the distribution as shown due to the uncertainty in model parameters. This again, shows that accurate propagation rate is more important to make a reliable prediction. This analysis can be convenient and useful for the user to decide if additional experiments are needed to satisfy the desired prediction accuracy. Discussion on optimal experimental design is beyond the scope of this work. Uncertainty

quantification helps to provide some intuition for new model predictions under different conditions.

6.4 Summary

In this chapter, a systematic approach is proposed to obtain reliable estimated parameters; this combines successive orthogonalization of the sensitivity matrix with post-optimal analysis derived from simultaneous parameter estimation. As a result, a subset of model parameters can be estimated with little additional computational effort.

The proposed model has been validated for the studied case of a PES system. The simulation results achieve excellent agreement with experimental measurements on particle size growth, polymerized polymer average molecular weight and monomer conversion ratio. Finally, an improved monomer feeding policy is obtained, which has been implemented and validated in a pilot plant. It validates the reliability of parameter estimation results. Prediction uncertainty analysis is demonstrated for new estimation problems, when the model is adapted for different processes at various conditions.

Chapter 7

Operation Policy Optimization

One of the main incentives of SIPN model development is to develop a minimum time oper-ation to meet product quality requirements within a defined molecular weight and composition. This chapter discusses optimization strategies for a single stage model and then for the integrated model. A special pattern of the optimal operation policy is revealed by the optimal solution. In addition, an algorithm for dynamic optimization with surrogate sub-models is developed, and applied to the complex integrated process model.

7.1 Optimization of Stage I - Singular Control Problem

Semi-batch feeding is a key time-limiting step in an SIPN process; therefore it is the main focus for optimization. The single particle model for the Stage I process which is developed in chapter 4 is first considered in the optimization.

The objective is to minimize the duration of Stage I, the polymerization stage, subjected to product quality constraints at the end of Stage I. The control variables are monomer and initia-tor feeding rates: "$F_M(t)$" and "$F_I(t)$". The optimization problem is formulated as follows:

$$
\begin{aligned}
&\min && t_I \\
&s.t. && \text{Stage I model } (4.22) - (4.30) \\
& && \text{Product quality constraints:} \\
& && \overline{Mw}^L \leq \overline{Mw}(t_I) \leq \overline{Mw}^U \\
& && \bar{x}_s^L \leq \bar{x}_s(t_I) \leq \bar{x}_s^U \\
& && \text{Control Bounds:} \\
& && F_M^L \leq F_M \leq F_M^U \\
& && F_I^L \leq F_I \leq F_I^U
\end{aligned} \tag{7.1}
$$

where $\overline{Mw}(t_I)$, $\bar{x}_s(t_I)$ are the weight average molecular weight and monomer conversion ratio at the end of Stage I, respectively. $\overline{Mw}^L$, $\overline{Mw}^U$, $\bar{x}_s^L$ and $\bar{x}_s^U$ are the lower and upper bounds on product quality and F_M^L, F_M^U, F_I^L and F_I^U are the lower and upper bounds of the monomer and initiator feed rates, respectively. The upper bounds of the feeding rate are obtained from the pilot plan study, and the lower bounds are set to zero. Exceeding the maximum feeding rate could violate operating assumptions and may form secondary particles. Only the lower bound of quality constraints is specified based on sample measurements from each grade.

Since F_M, F_I are variables with indefinite dimensions, without previous knowledge of the optimal solution, a piecewise constant function is applied for each feeding rate in the optimization problem. Figure 7.1 presents an optimal solution of F_M.
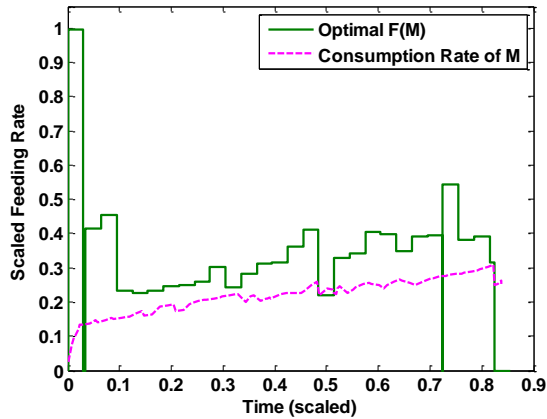
Figure 7.1 Optimal monomer feeding policy using piecewise constant formulation

However, as Figure 7.1 shows, the feeding rates present bang-bang and oscillatory behavior because of the inherent singular control properties of the dynamic optimization problem. Such solutions are not practical for plant operation. Strategy to reformulate this singular problem is discussed in the following.

7.1.1 Strategy for Reformulation of SIPN Singular Control Problem

Singular problems occur when the control appears linearly in the problem. General formulation of the optimal control problem is written as:

$$
\begin{aligned}
\min \quad & \Phi(z(t_f)) \\
s.t. \quad & \frac{dz}{dt}(t) = f(z(t), y(t), u(t), p), z(0) = z_0 \\
& g_E(z(t), y(t), u(t), p) = 0 \\
& g_I(z(t), y(t), u(t), p) \leq 0 \\
& h_E(z(t_f)) = 0, h_I(z(t_f)) \leq 0
\end{aligned}
\tag{7.2}
$$

where $y(t), z(t)$ are algebraic and differential states, respectively; z_{t_f} is the differential variable at final time; $u(t)$ is the time dependent control variable; p are time independent variables. One of the optimality conditions of problem (7.2) requires condition (7.3).

$$
\frac{\partial H(t)}{\partial u} = 0
\tag{7.3}
$$

where, $H = f(z, y, u, p)^T \lambda + g_E(z, y, u, p)^T \lambda + g_I(z, y, u, p)^T v_I$.

When $u(t)$ appears linearly in f, g_E and g_I. (7.3) is not explicit in the control variable $u(t)$. The optimal control profile would be either at its upper bound or its lower bound, which is known as a "bang-bang" solution, or the optimal solution is strictly between the control bounds. The evaluation of the Pontryagin Minimum Principle shows that optimal controls are composed of bang-bang and singular arcs. The optimal control problem induces a finite-dimensional optimization problem with respect to the switching times between bang-bang and singular arcs. However, reformulation of the control problem is required, and is considerably more complicated (Biegler, 2007). Non-smoothness regularization and prior smoothness assumptions are often applied in the problem formulation. However, several pitfalls of these approaches are found for various examples. The arc-parameterization is an

efficient method for solving the induced optimization problems and allows satisfaction of second-order sufficient conditions (SOSC). The key question is how to search for a suitable parameterization scheme for this problem.

To address this question, the solution of (7.1) is re-examined from process point of view. An interesting pattern of the solution is found for the SIPN process. In Figure 7.1, monomer consumption rate is plotted and compared with the optimal monomer feeding rate. It is found that the ratio of these two is kept at an almost constant level. It suggests that, the optimal policy maintains the system at a pseudo steady-state condition; the feeding rate could be a smooth function when it reaches the optimal pseudo steady-state, while it is discontinuous at the beginning and the end. This process insight helps to adopt a reduced order prior function for the monomer and initiator feeding rate. Hence, monomer feeding rate is defined to consist of 3 piecewise linear functions for the beginning, the pseudo steady-state and the end. The original singular control problem is reformed.

7.1.2 Results and Discussion

The new solution representation of feeding rate is then solved in the optimization problem (7.1). Figure 7.2(a) shows an optimal feeding policy with the maximum feeding rate scaled to 1. An implementable solution is obtained with little trade-off ($\leq 1\%$ lose) of the optimal efficiency. This optimal solution differs substantially from the original policy, and suggests a new pattern for the semi-batch operation. In Figure 7.2(a), the solid line is the computed optimal monomer feeding rate, and the dashed line is the monomer consumption rate. Comparing these profiles, again, we observe that the optimal feed rate and monomer consumption rate have the same trend. The monomer accumulation ratio is adjusted by the operation to remain nearly constant. This enables the process to meet particle quality and

productivity more efficiently. For the initiator feeding policy, higher concentration is preferred at the very beginning, and continued feeding is not required afterwards. This allows a higher polymerization rate earlier in the cycle. This pattern of optimal policies has been obtained with different quality constraints. For the optimal feeding policy, the same particle property requirements are met while saving 14% of the process time compared to the original feeding profile.

(a) Optimal monomer feeding rate   (b) Optimal initiator feeding rate
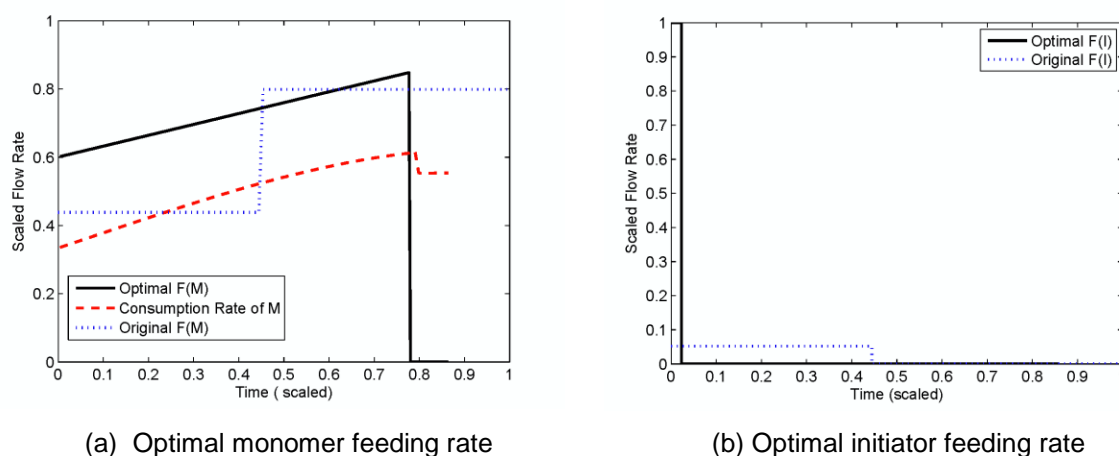
Figure 7.2 New optimal feeding policy for Stage I

We note that model prediction and experimental measurements based on the optimal feeding policy shown in Figure 7.2 also yields very good agreement, similar to that observed in Figure 6.5. Figure 7.3 shows the comparison of weight average molecular weight and monomer conversion ratio measured in the pilot plant test with model prediction for grade *A* product. Two quality constraints are satisfied in the reduced time from different evolution path. The consistency also validates our parameter estimation result in Chapter 5.

(a) Monomer conversion ratio

(b) Polystyrene $\bar{M}_w$
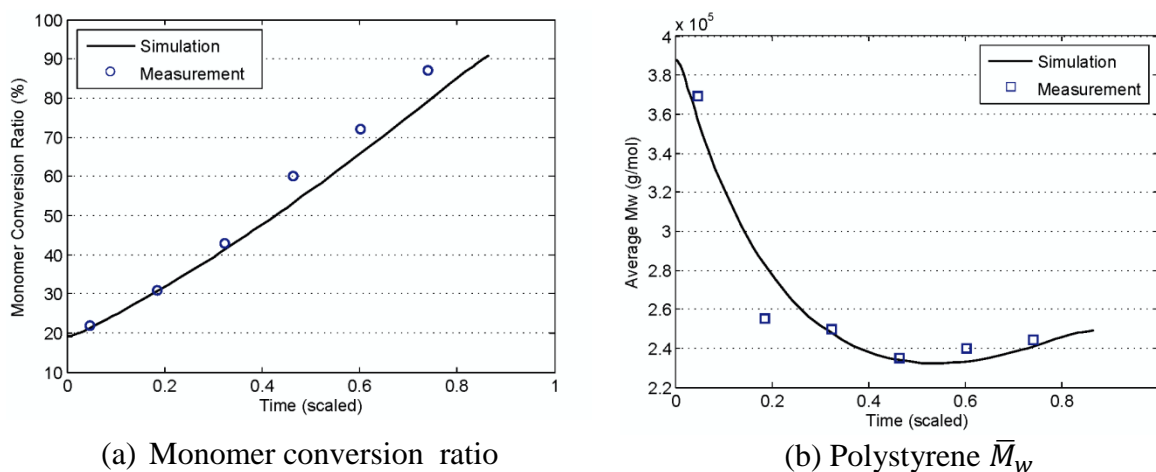
Figure 7.3 Comparison of model simulation and experiment for Stage I optimal policy

7.2 Optimization of Stage I and II -- Optimization with Surrogate Models

The optimization results shown previously do not include Stage II of the process. An improved optimization strategy is expected when the full process is considered. The final product quality indices include the SIPN gel content and the PS molecular weight at the end of Stage II. When conditions in the Stage II are allowed to be adjusted, i.e. introducing additional degrees of freedom, the end quality constraints in Stage I (e.g. PS Mw, styrene conversion) can be relaxed. However, the Stage II model is a large set of highly nonlinear and stiff DAEs; direct solution for the integrated process model is exceptionally challenging. A tailored approach is required to tackle this problem. In this section, an algorithm for using surrogate modeling in dynamic optimization is developed.

7.2.1 Strategy for Combining Stage II Model

We consider that Stage II reactions start from a uniform distribution of polymer and mono-mer mixture. This assumption is valid for PES process because the composition gradient at the end of Stage I is negligible and the monomer feeding is complete. As a result, average particle properties are used to link the two stage models to represent the integrated process. The full optimization problem is formulated as shown in (7.4). If the monomer concentration or polymer molecular weight gradient is significant before crosslinking, the Stage II model should include the dynamics in space as well. For a shell-represented particle, the bulk SIPN kinetic model can be used for each shell accordingly. The optimization problem (7.4) is a simplified case, which is suitable for the studied example.

$$
\begin{aligned}
\min \quad & t_I + t_{II} \\
s.t. \quad & \text{Stage I model } (4.22) - (4.30) \\
& \text{Stage II model } (5.19) - (5.32), (5.35) - (5.47) \\
& \text{Product quality constraints:} \\
& \quad \overline{Mw}_{end} \geq \overline{Mw}_{tar} \\
& \quad Gel_{end} \geq Gel_{tar} \\
& \text{Control bounds:} \\
& \quad v_c^L \leq v_c \leq v_c^U
\end{aligned}
$$

where v_c denotes all decision variables (control variables) in the process, including mono-mer and initiator feeding rate (F_M, F_I) present in Stage I, and crosslinking temperature(T,°C), crosslinking duration (t_{II}, min), crosslinking initiator mixture concentra-tion $(C_I^j, mol \cdot L^{-1}, j = 1 \cdots N_I)$ presenting in Stage II. Gel_{tar} and $\overline{Mw}_{tar}$ are targeted Gel content and PS $\overline{Mw}$ at the end of the process respectively. However, even without consider-ing the spatial variation, the integrated optimization problem still faces the challenge of computational complexity from Stage II. With 15 sectional grids for the representation of PE molecular weight distribution, Stage II kinetic model contains 45 nonlinear differential

equations. If solved directly with Stage I model together, the increased problem size, stiffness and nonlinearity becomes particularly difficult to handle.

One alternative approach is model reduction. It is noticed that the control variables in Stage II are not time dependent. This suggests a simplified model relationship as a surrogate model for the output prediction:

$$y_{II} = \mathcal{S}(v_c^{II}, x_0^{II}) \tag{7.4}$$

where output y_{II} are $\overline{Mw}_{II}$ and Gel content at the end of Stage II, v_c^{II} refers to the Stage II control variable, x_0^{II} is the initial condition of Stage II, and $\mathcal{S}$ is a surrogate model function, mapping the controls to the final output. Function (7.4) is then used to replace the original Stage II model in the optimization problem of (7.3) to alleviate the computational burden. This surrogate sub-model imbedded optimization strategy is the approach we will concentrate on.

The next three sub-sections are organized as follows. Section 7.2.2 briefly introduces surrogate modeling techniques and their applications in optimization. In section 7.2.3, a suitable surrogate modeling approach, Kriging, is suggested and discussed in more detail. An algorithm for Kriging-model-imbedded optimization is developed in section 7.2.4.

7.2.2 Surrogate Modeling

Surrogate model, also called response surface, metamodel, emulators, auxiliary models, etc., is a low computational burden alternative to the original simulation model. The surrogate model construction involves experimental design, model selection and model fitting. There is considerable flexibility in the form of the surrogate model. The key aspect of this approach is that use of a surrogate model trades accuracy for efficiency. Successful surro-

gate models must be computationally economical while maintaining the desired fidelity. The final goals of surrogate modeling could be Validation and Verification (V&V) of the simulation model, sensitivity analysis, and optimization of the simulated system (Kleijnen, 2009).

The surrogate models can be created through physics-based reduction or mathematical reduction. The physics-based reduction approach neglects some of the detail or complexity that is modeled in the original simulation. For example, in the Stage I model, the crosslinking effect is assumed to be negligible during polymerization. Hence, crosslinking reactions are not considered in the population balance equation, and the number of differential equations in the model is greatly reduced. On the other hand, the mathematical reduction approach does not interpret the physical meaning of the original model. Surrogate model is created by fitting a multidimensional surface function to a set of simulated data points, such as low-order polynomials, response surface model (RSM), neural networks (NN), radial basis functions (RBF), and Kriging modeling etc. Table 7.1 summarizes basic steps for approximating approaches from Simpson (2001). Various surrogate modeling approaches are derived from different combinations in each step.

Table 7.1 Surrogate modeling procedure

Experimental Design	Model Selection	Model Fitting
Factorial	Polynomial	Least Squares Regression
Central Composite	Splines	Weighted Least Squares Regression
Box-Behnken	Realization of a Stochastic Process	Best Linear Unbiased Predictor
D-Optimal	Kernel Smoothing	Best Linear Predictor
G-Optimal	Radial Basis Functions	Log-likelihood
Orthogonal Array	Network of Neurons	Back-propagation
Plackett-Burman	Rule-based or Decision Tree	Entropy
Hexagon		
Hybrid		
Latin Hypercube		
Random Selection		
Quasi-Random		

Surrogate models play an important role in aerospace engineering, architecture, mechanics and geostatistics for 2D/3D complex shape simulation, design and optimization. Surrogate modeling approaches are also shown to be important in general Input-Output approximation in k ($k \geq 3$) dimension, for engineering design and control. Several researchers compared the performance of alternative surrogate models for different problems in terms of approximation of the exact functions (Simpson, et al., 2001; Goel, et al., 2008; Peter, et al., 2008). It is generally believed that the Kriging method is superior in describing non-quadratic functions compared to general RSMs; and it is also superior in computational efficiency to NN approximation, which incurs a high computational cost for learning (Sakata, et al., 2003). For this reason, our focus is put on the Kriging approach. Optimization algorithm with the Kriging surrogate model is studied.

7.2.3 Kriging: Basics

Kriging was originally applied to the identification of optimum drilling locations for mining applications and has been applied frequently for 3-D visualization in geostatistical applications (Krige, 1951). While the Kriging approach is still an important methodology in geo-study, this mathematical method has gained popularity in many fields involving input-output modeling.

Kriging is an interpolation method using inverse distance weighting. It has been used for both deterministic simulation and random simulation. Here, we only consider the deterministic case, where the same input gives the same output prediction. The constructed model is considered to be exact at the sampling points, and the estimation error increases as it deviates from ns sampling points. Since the Kriging approach does not assume any predefined shape in the model reconstruction, it results in a global model with high accuracy, especially,

when the RSM model fails to fit the system as quadratic functions. It is also useful that both prediction value and its variance can be estimated from Kriging interpolation approach. A brief description of the Kriging approach is provided here. The interested reader can also refer to review articles (Barton, 1994; Van, et al., 2004; Kleijnen, 2009).

The Kriging predictor is represented as (7.5):

$$y(x) = Y(\beta, x) + Z(\beta, x) \tag{7.5}$$

$Y(\beta, x)$ is a regression problem as (7.7).

$$Y(\beta, x) \simeq F\beta \tag{7.6}$$

where F is the regression function, $F = [f_1(x), f_2(x), \cdots, f_p(x)]$, β is the regression coefficient. $Z(\beta, x)$ is assumed to be a stochastic Gaussian process with expected value zero $E(Z(x)) = 0$ and covariance $\text{cov}\left(Z(x_i), Z(x_j)\right) = \sigma^2 R(x_i, x_j)$. $R(x_i, x_j)$ is a spatial correlation function (SCF), considered in the form of (7.7).

$$R(\theta, x_i, x_j) = \prod_{k=1}^{nd} R_k(\theta_k, x_i^k - x_j^k) \tag{7.7}$$

Where nd is the number of inputs, θ_k are correlation parameters to be optimized, and x_i^k, x_j^k are the kth components of sample points x_i, x_j respectively. We maximize the likelihood of the observed data y generated from input x. The optimal solution of coefficient β and variance σ^2 are obtained as (7.9).

$$
\begin{aligned}
\beta^* &= (F^T R^{-1} F)^{-1} F^T R^{-1} Y \\
\sigma^2 &= \frac{1}{m} (Y - F\beta^*)^T R^{-1} (Y - F\beta^*)
\end{aligned}
\tag{7.8}
$$

The Kriging predictor is expressed as

$$y = F\beta + r^T R^{-1}(y - F\beta) \tag{7.9}$$

Where $r = [R(\theta, x_1, x), \cdots, R(\theta, x_n, x)]^T$.

When a function is smooth, the choice of regression function does not affect significantly the resulting metamodel fit because $Z(x)$ captures the most significant behavior of the function (Caballero, et al., 2008). But if we have better prior knowledge of the original model, more complex basis functions are recommended, which could better interpreter long range effect and improve the convergence of Kriging parameter optimization (Martin, et al., 2004).

There are many choices of SCF, for example, exponential function, exponential Gaussian function, Gaussian function, linear function, spherical function, cubic function, spline function, etc. The choice of SCF depends on the behavior of function near the origin, such as linearly or parabolic approach to the interpolation point. In general, the correlation function of form (7.11) is often a popular selection.

$$R_k = \exp(-\theta_k |x_i^k - x_j^k|^p) \tag{7.10}$$

where θ_k represents the importance of input k. The higher θ_k is, the less correlation input k has. p the model smoothness. When $p = 1$, it is an exponential correlation; when $p = 2$, it is a Gaussian correlation. We prefer to use Gaussian correlation for Kriging for the purpose of optimization, since the model function is continuous and differentiable. Since the Kriging technique optimizes both function and fitting parameters, it is considered to be more accurate than the fixed basis simulation.

Several optimization algorithms are developed based on the Kriging approach for black-box function and complex model optimization. Davis (2008) showed that a Kriging-RSM algorithm is more robust in finding the global optimal for a black-box function, compared

with other RSM based algorithms, such as DS-RSM(Direct search RSM approach), RSM-S, (Stand RSM based on local sub-region), RSM-G (Modified RSM based on global feasible region). The Kriging model helps to first locate a near optimal point and then the accuracy of the solution is further refined with the RSM model. Examples are shown for 2 to 10 design variables. The Kriging model is also applied as a meta-model with other rigorous models in flow sheet optimization. Caballero et al. (2008) proposed an algorithm for the use of the Kriging model in modular flow-sheet optimization. The Kriging model was re-evaluated in successive contraction or moving steps. It is considered to better handle highly constrained problems.

The main challenges of the Kriging model or other surrogate-model-based optimization include extension to high dimensionality and validation of solution optimality. For systems with many independent variables, there are well known issues of "curse of dimensionality". Surrogate models should be capable of approximating the global picture of the original model without exhausting the computational power. On the other hand, an accurate optimal solution should be retained with the surrogate model.

To address these challenges, an improved approach for surrogate-model based optimization is proposed. The advantages of the approach are due to its ability to:

- Apply an effective design and sampling technique to improve model robustness.

- Implement a well-defined termination step to identify a local optimal.

- Execute a simple refinement step.

7.2.4 Optimization with Kriging Metamodel

Figure 7.4 outlines the framework of surrogate model based optimization. In particular, Kriging metamodel is considered. The main steps involved are preparation and optimization; each step consists of several sub-steps.
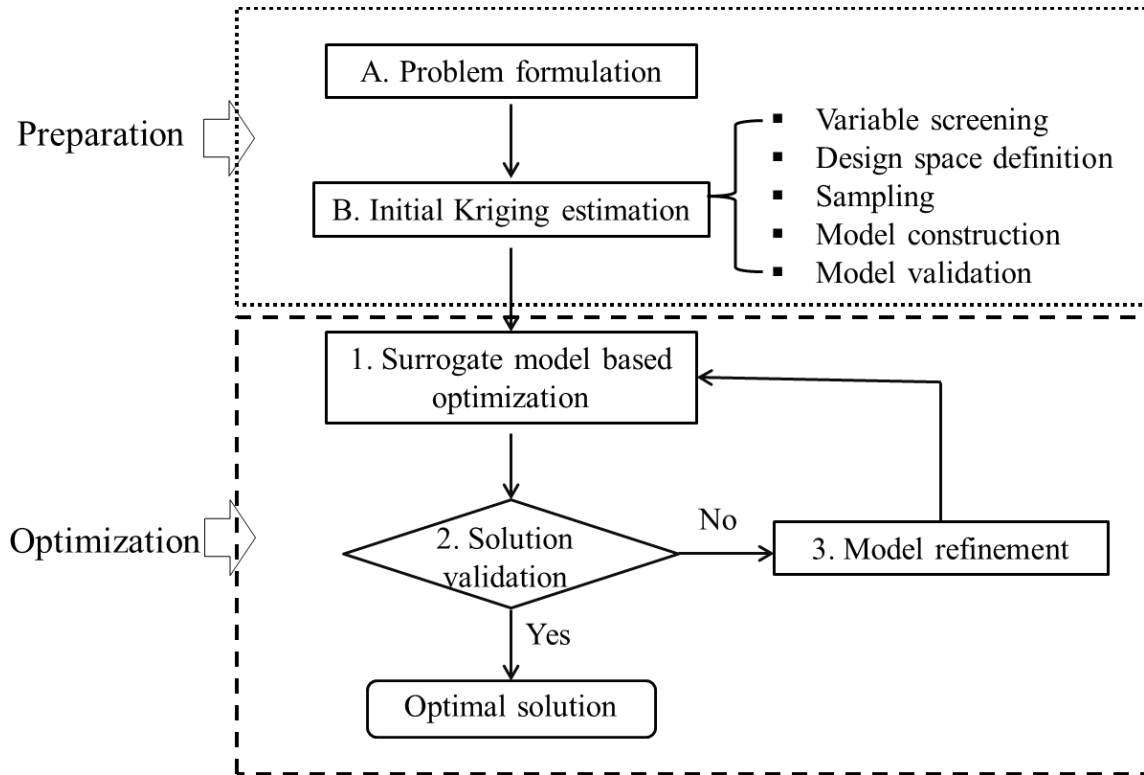
Figure 7.4 Diagram of surrogate model-based optimization framework

The optimization algorithm is summarized in the following box. Step 0 is the preparation step. In this step, the complex objective function or constraints in the original optimization problem are identified, and replaced with the surrogate model. Surrogate sub-model is denoted as $y^S = S(x)$. The original objective function is represented as $\mathcal{O}$. The optimization problem is formulated as a minimization problem. Steps 1 to 3 successively refine the surrogate model and optimized solution until it converges to a local optimal.

Algorithm 7.1 : Conditional refinement of Kriging-model-imbedded optimization solution

Step 0: Initialization. An initial guess $x_0 \in F$ and a Kriging model $\mathcal{S}_0$ of correlation parameter θ_0 , built from initial design $\{D_0, Y_0\}$. Set $k = 0$.

Step 1: Optimization of the reduce problem. Optimal solution based on $\mathcal{S}_k$ is obtained at x_k.

Step 2: Check for optimality conditions

   Step 2.1: Compare the output of Kriging model. If $|y^{act}(x_k) - y^s(x_k)| \le \epsilon_y$ is satisfied, go to step 2.2. Otherwise, go to Step 3.

   Step 2.2: Check objective value at perturbed solutions. If $\mathcal{O}(x_k \pm \epsilon_x) \ge \mathcal{O}(x_k)$ holds, local optimum of original problem is found. Otherwise, go to step 3.

Step 3: Update Kriging model. Set $D_{k+1} = \{D_k, x_k\}$, $Y_{k+1} = \{Y_k, y_k^{act}\}$.

If $\{\min_j |x_k^j - x_{k-1}^j| \le \delta, j \in \{1, \cdots, p\}, x \in R^p\}$, $\mathcal{S}_{k+1}$ is evaluated at θ_k . Otherwise, reestimate Kriging parameters. New model $\mathcal{S}_{k+1}$ is obtained at θ_{k+1}. Increase k by one and go to Step 1.

The procedure of each step is described next in detail.

- **Step 0. Preparation for optimization**

   1: Problem formulation

The first step is to formulate the optimization problem in its original form, identifying which part of the model can be replaced with the Input-Output function. The surrogate model can be used for the objective function directly, or for part of the constraints, based on the source of complexity and computational cost. This step forms a basis for the rest of the steps. Equation (7.11) shows an example where part of the model constraints (model of y) can be approximated by a surrogate model.

$$\begin{aligned}
min \quad & Q(x,p,y) \\
s.t.: \quad & \begin{cases} y = f(x,p) \\ h(x,p) = 0 \\ g(x,p) \geq 0 \end{cases}
\end{aligned} \qquad (7.11)$$

where x is the independent variable, y is dependent variable, p is model parameter, h and g are equality and inequality constraints accordingly. In this case, y is computed through a complex function f that is difficult to solve in the optimization problem. Inexpensive surrogate models $y = S(x,p)$ will be generated in the design space of x to replace the original model.

2: Initial Kriging estimation

The next step is to build an initial Kriging model $Y = S(x)$ in place of the original model in problem **Error! Reference source not found.**. Computational cost reduction in surrogate modeling and prediction accuracy improvement for the fitted model which are two important but contradictory issues need to be balanced in this step.

a. Variable screening

For problems rooted in geometric applications, independent variables are typically spatial dimensions. Variable screening is generally not necessary. However, when the surrogate model is applied for a general type function reduction with relatively large degrees of freedom, variable screening should be an important step to be taken into account. Effective variable screening strategy helps to reduce the cost in model evaluation while retaining satisfied accuracy. Only variables of certain significance should be considered in the design space, since inclusion of weak effect or linearly dependent variables significantly increase the computational cost and prediction variance as well. Therefore, this is a step where particular emphasis should be placed first.

Variable screening is an issue associated with sensitivity analysis. However, sophisticated sensitivity studies generally require ample coverage of the entire space, where variable screening is taken afterwards. In contrast, for the purpose of optimization, the algorithm seeks for a surrogate model to quickly locate a near optimal point, where more local properties could be explored. Hence, construction of surrogate models for optimization is considered to be different from building ones for sensitivity analysis. The step taken for variable screening in optimization is considered in the following ways. The discussion focuses on Gaussian correlation function. Most conclusions are applicable to other correlation functions.

(1) Model observation. Prior knowledge of the original model is helpful in defining the model structure. If there is access to the computer simulation model, primary analysis on linearly dependence and separability should be investigated.

(2) Correlation parameter analysis. In principle, θ_j is an indicator of the importance of input correlations. Therefore, θ_j is first examined based on the initial Kriging model, which is built from a relatively small number of design points. Two rules are applied to reduce the dimension of the Kriging model: (a) a small ratio of $\frac{\theta_{max}}{\theta_{min}}$; (b) to avoid θ reaching either the upper bound or lower bound. One observation of the Kriging approach is that estimation of θ is more difficult for non-isotropic function than for isotropic function. When $\frac{\theta_{max}}{\theta_{min}}$ is above the order of 10, the Kriging model is ill-conditioned. Numerical difficulty could be a dominant factor in obtaining θ value, consequently, leading to a poorly formulated model for optimization (refer to (Lophaven, et al., 2002b) for a detail discussion for θ computation). In particular, if

some θ goes to its lower bound, it is usually a weak effect or a separable input, since

its correlation is almost equally strong for all variables in the design space. If θ

reaches to its upper bound, some inputs might be separable.

(3) Mean square error comparison. When weak effect parameters are contained in the

Kriging model, estimated mean square error σ appears to be insensitive to the sample

size. This is also due to the small θ, which result in difficulties with factorization of R.

A rule of thumb is that the input dimension for Kriging is suggested to be kept as low as

possible. If the output is highly nonlinear, the dimension of the model should be even less.

For a system with multiple outputs (dependent variables), input variables are screened for

each output, and surrogate models are built accordingly. Usually, no more than 10 inputs

which have the same order of magnitude θ value will be considered as design variables.

Maintaining the problem in a low dimension helps to improve the model robustness.

b. Design space definition

It is well accepted that the design space should be as tight as possible to reduce the sam-

pling cost. For chemical process models, feasible operation ranges are considered for the

optimization variables.

c. Sampling

An appropriate sampling strategy is a key for efficient computation. Investigation of the

effect of different sampling methods on surrogate model simulation is carried out by several

groups. Simpson, et al. (2001) compared five experimental design types: Hammersley se-

quence sampling, Latin hypercube, orthogonal array, random design and uniform design,

and four approximation model types: Kriging approximation, multivariate adaptive regres-

sion splines, radial basis functions, second-order polynomial response surface for computer

experiments design and analysis. Detailed error analysis reveals that uniform designs provide good sampling for generating accurate approximations using different sample sizes while Kriging models provide accurate approximations that are robust for use with a variety of experimental designs and sample sizes. Caballero, et al. (2008) also highlighted some of the sampling approaches used in surrogate modeling. Variance reduction techniques, such as Latin hypercube sampling (Tang, 1993; Tang, 1994; Beattie, et al., 1997), Hammersley (Kalagnanam, et al., 1997) Hammersley (Hammersley, 1960), Halton (Halton, 1960), Sobol sequences (Sobol, 1967) are superior to simple Monte Carlo methods in prediction, because the uniformity of the sampling is improved in the variance reduction approaches so as to increase the gain of information for the unknown space. One criterion, so-called discrepancy, is introduced as a measure of the uniformity of the scattered sampling points in design space for different sampling strategies (Fang, et al., 1996; Santner, et al., 2002). Huang, et al. (2009) proposed a quasi-MC approach, the Number-Theoretical net method (NT-net), to further improve the discrepancy.

Many of the comparison results are based on one-shot design in spite of sequential properties in model building and the optimization loop. In our study, it is found that the Sobol sequence is a preferable choice because it allows new sample points to distribute uniformly with previous samples. Performance of low discrepancy is well kept during initial model fitting and update.

d. Kriging model construction

To fit the Kriging model based on the simulation points, computation packages are available. In particular, MATLAB "DACE" toolbox (Lophaven, et al., 2002) is well developed and freely available for Kriging model construction on computer experiments.

Selection of regression and correlation functions is problem dependent.

e. Initial model validation

To compare surrogate models, generalized mean square cross-validation error is often used as a measure of quality of fit (Goel, et al., 2007). A leave-one-out representation can be written as Equation (7.12)

$$GMSE = \frac{1}{n} \sum_i^n (y_i - \hat{y}_{(-i)})^2 \tag{7.12}$$

Where $\hat{y}_{(-i)}$ is the prediction at x_i using the surrogate model built from all samples but (x_i, y_i). The global cross-validation error is also known as the predicted residual sum of squares (PRESS) in polynomial response surface approximation terminology. $GMSE$ is also used in Caballero, et al.(2008) for initial Kriging model validation before optimization, but no discussion for initial model construction based on $GMSE$. We thus investigated the potential usage of error $(y_i - \hat{y}_{(-i)})^2$ for design improvement for optimization. However, as also pointed out in Goel, et al. (2007), high standard deviation of the surrogate model could suggest a high uncertain region, but small standard deviation does not necessarily prove the opposite. Thus, a quick check for error evaluation before applying more sophisticated analysis is to refer to the MSE value (σ^2) , Equation (7.9), predicted from the Kriging model. It is found that, the initial Kriging model does not require a small σ^2 in order to carry out optimization. Model refinement in Step 5 can help to improve its accuracy during optimization.

- **Step 1. Surrogate model based optimization**

Once a surrogate meta-model is obtained or updated, it is combined with the remaining rigorous model for the integrated optimization. A gradient based optimization algorithm can

be able to be applied to obtain a solution efficiently. In our case, the surrogate model is solved with other differential equations through a dynamic optimization approach.

Note that there could be multiple local optima for the nonlinear function. Optimization from multiple initial guesses is suggested to explore a global picture. If optimization converges to different local solution, each solution will be further compared.

- **Step 2. Optimal solution validation**

Though there are many discussions about validation of surrogate model simulation, little emphasis was put on validation of optimization solution based on surrogate models. Kleijnen (2009) pointed out that derivative information which is available from DACE should be used for checking the first-order optimality. But when the Kriging model is only used as part of the constraints, this conclusion does not apply. Empirical rules are often adapted, which could lead to a premature termination before converging to the true optimum.

In this study, there are two considerations to evaluate the solution. First, whether the solution is accurate according to the original model; second, whether this solution is a local optimal point as in the original optimization problem. The validation steps are designed to answer these two questions.

The first question can be easily answered by running a simulation at solution x^k. If the difference in output prediction is smaller than tolerance, $|y^{act}(x_k) - y^s(x_k)| \leq \epsilon_y$, a desired accuracy is validated. Otherwise, go the refinement step.

The second question is more challenging. Biegler, et al. (1985) proved that a necessary condition for an appropriate simplified model for optimization is that the gradients of the simplified and rigorous models be the same at the optimum. However, in many approaches,

this condition is not considered directly. In heuristic approaches (Caballero, et al., 2008; Davis, 2008), the algorithm is considered to converge if the optimal solution is the same in two successive major iterations. The authors expected the gradients to match the "true gradients" by excluding the possibility of the same but mismatched gradients in the iteration, assuming the Kriging model matches well with the local function. However, this conclusion may not be valid. Optimization could be terminated prematurely by taking the accuracy of the metamodel for granted. A systematic approach for optimality validation is required to address this problem. In this study, the first-order optimality conditions are directly taken into account by examining the gradient at the solution point. Therefore, this approach guarantees a local optimum if the condition is satisfied.

A simple approach is considered in the implementation. Simulations are run at perturbed solutions. If the relationship (7.13) holds (for minimization problem), x^* is validated to be a local optimum in the original model.

$$\mathcal{O}(x_k \pm \epsilon_x) \geq \mathcal{O}(x_k) \tag{7.13}$$

Otherwise, if the current solution fails to satisfy condition (7.13), continued iterations are required. We turn to Step 3 for surrogate model refinement.

- **Step 3. Surrogate model refinement**

Model refinement is an important step for optimization. In the case that $|y^{act}(x_k) - y^s(x_k)| \geq \epsilon_y$, it indicates a noticeable mismatch between the surrogate model and the original model. It can result from two possibilities. In an optimistic scenario, the Kriging model is able to locate a near-optimal point, but desired solution accuracy must be obtained by increasing the model local fidelity. Or, it might be the case that the initial surrogate model

fails to represent a correct contour in the space. Thus, the current solution stays far away from the true optimum. The surrogate model should be reconstructed to provide more information accordingly.

There are many possible strategies to update the surrogate model. We observe that by gradually adding new optimal points to the previous design following a combination of local and global strategy, an optimal solution can be found with few model simulations.

Local strategy refers to addition of the new optimal solution to the design without re-estimating Kriging parameters. It is applied when the new solution is close to the previous optimum, i.e. $\{\min_j |x_k^j - x_{k-1}^j| \leq \delta, j \in \{1, \cdots, p\}, x \in R^p\}$, where δ is a minimum distance between design samples in one dimension. It is based on the observation that a small distance between successive optimal points could result in a near optimal solution. Re-estimation of the Kriging parameter is not necessary in this case. Otherwise, a global strategy is performed, i.e. to re-fit Kriging parameters with the augmented points. Since the prediction error could result from high uncertainty in this un-sampled region, a re-estimated parameter could help to reduce the global prediction error. More results for comparison are shown in examples, demonstrating superior performance in computational cost.

7.3 Results and Discussion

7.3.1 An Illustrative Example

A modified Six-hump Camel Back function is used as an illustrative example. A minimization problem is considered as (7.15).

$$\min \quad f = \left(4 - 2.1x_1^2 + \frac{x_1^4}{3}\right)x_1^3 + x_1x_2 + (-4 + 4x_2^2)x_2^2 + 0.003x_3x_4 + 2x_5$$

$$\text{s.t.} \qquad\qquad -1.9 \leq x_1 \leq 1.9$$
$$-1.1 \leq x_2 \leq 1.1 \qquad\qquad (7.14)$$
$$0 \leq x_3, x_4 \leq 1$$
$$-1 \leq x_5 \leq 1$$

The original model only contains variables of x_1, x_2. Here, x_3, x_4, x_5 are augmented to the objective function in order to illustrate the variable screening step.

(1) Preparation for optimization

Assuming the original function is unknown, variable screening is carried out based on an initial correlation function analysis before getting into optimization. A 30 point Sobol sequence is generated from 5 dimensions after dropping the previous 2500 points. The initial Kriging model is built based on a constant regression function and Gaussian correlation function. Initial guess $\theta_0 = [10, 10, 10, 10, 10]$; lower and upper bound are $\theta_L = [0.1, 0.1, 0.1, 0.1, 0.1]$, $\theta_U = [20, 20, 20, 20, 20]$. The initial Kriging model gives $\theta^* = [1.7678, 0.3397, 0.1, 0.1, 0.1060]$, $\sigma^* = 6.1886$. Increasing the sample size to 50 points, the same θ^* is reached, but σ^* only reduces to 5.067. From the examination of the solution of θ^*, θ_3^* and θ_4^* are at the lower bound; θ_5^* is close to lower bound. It suggests that an ill-conditioned Kriging model is formed in this design space. In order to separate or remove variables from the design space, one-dimensional models are built for x_3, x_4, x_5 accordingly, maintaining the rest of variables fixed. In this case, fixed variables are set to 1. 10 points are sampled for each input. Figure 7.5 shows the scatter plot of each result.
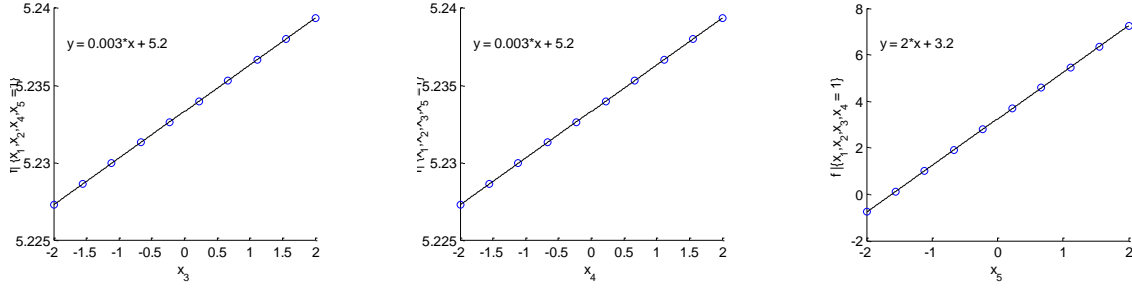
Figure 7.5   Fitting of one dimensional model for variable screening

A low order polynomial is used to fit the one dimensional model. In this case, a linear function is sufficient. From the result of reduced regression coefficients, $\beta_{x_3}, \beta_{x_4} \leq 0.01, \beta_{x5} = 5$. Thus, x_3, x_4 are identified as weak parameters, and x_5 is considered to be separable. The design space is consequently reduced to x_1, x_2. The original model is considered as in the form of (7.16), where x_3, x_4 are set to 0 in this case (as the minimum in Figure 7.5).

$$
\begin{aligned}
\min \quad & f = y + 2x_5 \\
s.t. \quad & y = S(x_1, x_2, x_3, x_4) \\
& -1.9 \leq x_1 \leq 1.9, \quad -1.1 \leq x_2 \leq 1.1 \\
& x_3, x_4 = 0 \\
& -1 \leq x_5 \leq 1
\end{aligned}
\tag{7.15}
$$

y is considered as the output in Kriging. Reduced Initial Kriging model is fitted based on 15 design points in 2 dimensions from SOBOL sequence after dropping the first 1400 points, as shown in Figure 7.6 (a). The regression constant is $\beta_0 = 0.0618$, and correlation function is Gaussian, $\theta_0 = [1.7678, 0.5256]$.
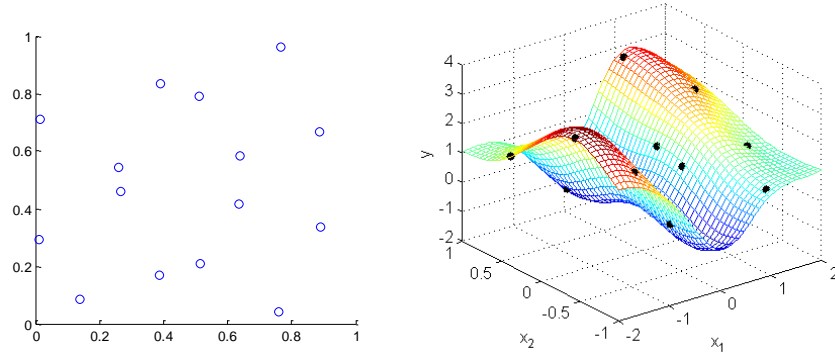
Figure 7.6 An initial design and Kriging model

(2) Surrogate model based optimization

The optimization problem is solved with "fmincon" in MATLAB. Desired accuracy of the final solution is set to be 5×10^{-3} ($\epsilon_x = 0.005$), prediction accuracy is set to be 2×10^{-3} ($\epsilon_y = 0.002$), and the minimum distance is $\delta = 0.01$. The actual value of y is shown in Figure 7.7. It has 2 global optima ($[x_1^*, x_2^*] = $[0.0898,-0.7126], [-0.0898, 0.7126]), and $y(x_1^*, x_2^*) = -1.0316$. Thus, the minimum of (7.15) locates at [0.0898,-0.7126, 0, 0, -1], [-0.0898, 0.7126, 0, 0, -1], and $f(x^*) = -3.0316$. The function is highly nonlinear in the feasible region.
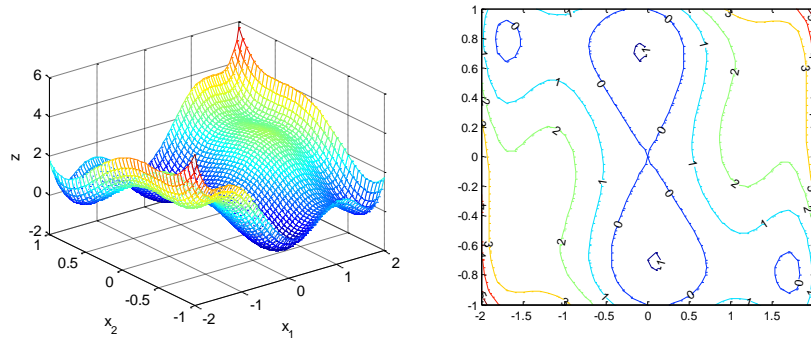
Figure 7.7 Surface and contour plot of six hump function in 2 dimensions

Table 7.2 summarized iteration results based on Algorithm 7.1. Figure 7.7 marks new solutions in the original design space. With only 5 additional points, the problem converged to the same optimal point as the original function with satisfactory accuracy. Another global optimum can be found with different initial guess in "fmincon".

Table 7.2 Summary of iterations of problem (7.16)

k	x		$y^s(x_k)$	$y^{act}(x_k)$	f
0	0	0	0	0	0
1	-0.1203	0.7417	-1.0198	-1.0217	-3.0217
2	-0.1192	0.7470	-1.0218	-1.0192	-3.0192
3	-0.1436	0.7385	-1.0259	-1.0162	-3.0162
4	-0.0984	0.7006	-1.0337	-1.0301	-3.0301
5	-0.0858	0.7128	-1.0322	-1.0316	-3.0316
optimum	-0.0902	0.7126	-1.0316	-1.0316	-3.0316
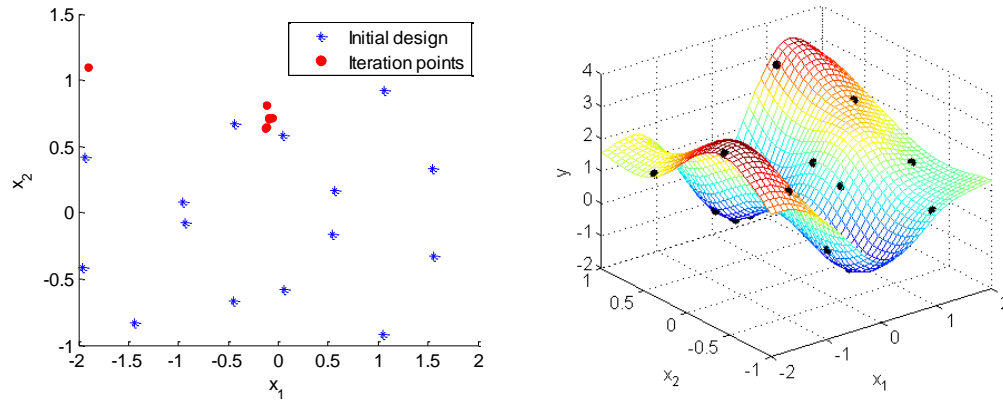
Figure 7.8 Solution iterations and Kriging prediction at convergence

It is interesting to compare the effect of different refinement strategies on solution convergence. Table 7.3 lists some of the results through three refinement approaches obtained from different initial guesses. It shows that it is possible to find an optimum without re-estimating the Kriging model, however more iterations are required for optimization. Therefore, the total number of simulations is larger. On the other hand, conditional refinement and

direct refinement approaches give similar results in this case. Some extra iterations in the direct approach are due to movement of optimum solutions between two global optima. Conditional refinement thus provides certain flexibility to switch rules depending on the distribution of the computational cost and condition of the Kriging model. The proposed approach is able to locate an optimum with few iterations even if the initial Kriging model is small.

Table 7.3 Comparison of different refinement strategies

	Conditional refinement			Fixed correlation			Direct refinement		
x_0	[1,1]	[0,0]	[0,1]	[1,1]	[0,0]	[0,1]	[1,1]	[0,0]	[0,1]
# Iter, $n_0 = 15$	6	8	8	15	16	11	6	9	9
# Iter, $n_0 = 20$	4	5	5	10	11	4	6	4	4
# Iter, $n_0 = 25$	6	5	6	7	9	4	6	5	6

To demonstrate the importance of valid termination criteria, solutions based on the heuristic termination rule and the optimality validation rule are compared. Here, $tol_x = 0.005$, which is the same as ϵ_x. It is found that when a fixed Kriging model is used for optimization, the heuristic rule could terminate at a non-optimum point, or points without sufficient accuracy. Introducing the test for optimality ensures the solution quality. Table 7.4 shows some examples of the comparison, where $\hat{x}^*$ is the solution indicated at termination. Initial Kriging model is based on 25 Sobol points. Compared to the true optimum, [0.0898,-0.7126], the heuristic rule terminates the optimization problem incorrectly.

In next section, we would like to apply this algorithm to the complex integrated model to find an improved operation policy.

Table 7.4 Comparison of different termination criteria

$n_0 = 25$	Termination criteria							
	$\|x_k - x_{k-1}\| \leq tol_x$				Optimality validation			
x_0	1.9	-1.0	-1.8	1.0	1.9	-1.0	-1.8	1.0
Iterations	0.0952	-0.6389	-0.1378	0.5810	0.0952	-0.6389	-0.1378	0.5810
	0.1315	-0.8163	-0.1072	0.7930	0.1315	-0.8163	-0.1072	0.7930
	1.1940	-0.9179	-0.1705	0.7569	0.0864	-0.7084	-0.1705	0.7569
			-0.1386	0.7296	0.0514	-0.7198	-0.1191	0.7195
			-0.0950	0.7059	0.0897	-0.7099	-0.0970	0.7084
					-0.0858	0.7500	-0.0941	0.7088
$\hat{x}^*$	1.1983	-0.9216	-0.0978	0.7063	0.0904	-0.7117	-0.0899	0.7128

7.3.2 Optimization with Stage II Surrogate Model

The original optimization problem for an integrated process is described in **Error! Reference source not found.**. Six potential input variables in the Stage II surrogate model are: Temperature, $(T, °C)$, Stage II duration (t_{II}, min), two initiator mixture concentration ($C_I^1, C_I^2, mol \cdot L^{-1}$), conversion ratio ($\bar{x}_s$, %), and $\overline{Mw}$ at the beginning of the stage II ($\overline{Mw}_{II_0}$, $kg \cdot mol^{-1}$). T, t_{II}, C_I^j are control variable in Stage II only. $\bar{x}_s$ and $\overline{Mw}_{II_0}$ are connection variables to the Stage I model. Optimization of the connection variables would affect the solution of both stages. The two outputs considered are: Gel_{end} (Gel content at the end of Stage II) and $\overline{Mw}_{end}$ (PS $\overline{Mw}$ at the end of Stage II). Kriging models are fitted for them separately.

Following the proposed algorithm, 6 input variables were screened for the outputs of Gel_{end} and $\overline{Mw}_{end}$. Based on the results of Figure 5.8 and Figure 5.9, a first order polynomial is used as the regression function, and the Gaussian function is assumed for the correlation function. The range of input variables is set from 50% to 150% compared to its nominal value. Simulations are taken at 30 initial design points. It is interesting to note that correlation parameters reach their upper bound in the initial Kriging model for Gel content,

suggesting that all inputs are separable. In addition, $\overline{Mw}_{II_0}$ has little impact in the regression function, suggesting it may be removed from the model. Linear regression analysis further validates this conclusion. Therefore, the surrogate model for Gel content becomes a linear function of T, C_1, C_2, t_{II} and $\bar{x}_s$. The model of $\overline{Mw}_{end}$ presents higher nonlinearity. Linear regression is no longer sufficient. Input T appears to be separable. Therefore, the Kriging model for $\overline{Mw}_{end}$ is built based on other five inputs. The integrated optimization problem is formulated as follows:

$$
\begin{aligned}
\min \quad & t_I + t_{II} \\
s.t. \quad & \text{stage I model} \\
& \text{Stage II surrogate model:} \\
& \quad \{\, \text{Gel}_{end} = S_1(v_c^{II}); \ \overline{Mw}_{end} = S_2(v_c^{II}) \,\} \\
& \quad Gel_{end} \geq Gel_{tar} \\
& \quad \overline{Mw}_{end} \geq \overline{Mw}_{tar} \\
& \text{Control bounds} \\
& v_c^L \leq v_c \leq v_c^U
\end{aligned}
\tag{7.16}
$$

Notice that t_{II} is one of the inputs, and also present in the objective function. The optimization problem will push t_{II} to its lower bound, if all the constraints could still be satisfied. It turns out to be the case in this problem.

A nice feature of the Stage II surrogate model is that the function is close to linear in the design space. After the initial optimal solution is obtained for the integrated process, only one refinement step is sufficient to satisfy the optimality condition. An example of the solution is shown in Figure 7.9. The new optimal solution reduces the process time by 23.4% over the original recipe.

Optimization based on surrogate sub-model provides a cost effective way to solve this large complex problem.
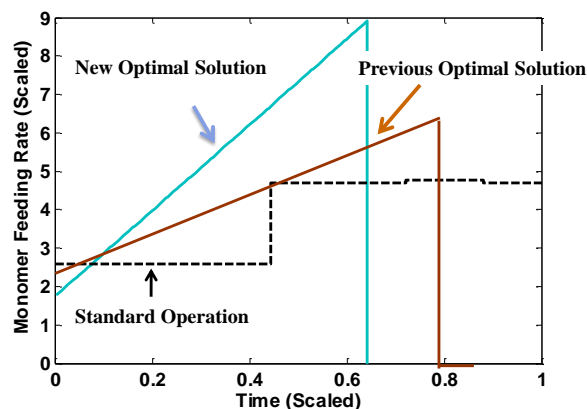
Figure 7.9 Optimal monomer feeding policy based on the integrated model

7.3.3 Sensitivity study

It is also interesting to know how sensitive the optimal solution is to the change of quality constraints. Therefore, a series optimization is run and compared. Figure 7.10 shows the change of monomer feeding rate to the change of final product properties.
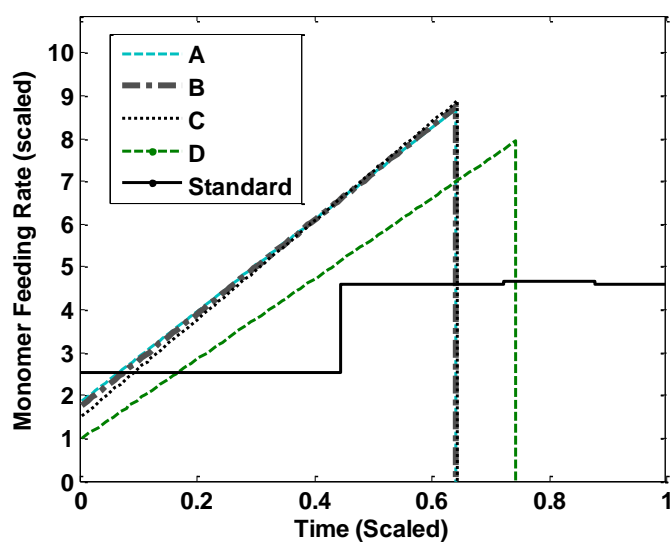
	Gel_{tar}	$\overline{Mw}_{tar}$
A	Gel_{std}	$\overline{Mw}_{std}$
B	$+6\% \, Gel_{std}$	$\overline{Mw}_{std}$
C	$+18\% \, Gel_{std}$	$\overline{Mw}_{std}$
D	Gel_{std}	$+15\% \overline{Mw}_{std}$

Figure 7.10 Sensitivity study for the optimal policy

In Figure 7.10, solutions A, B, C and D correspond to different final quality criteria $(Gel_{tar}, \overline{Mw}_{tar})$. Denote nominal quality values as $Gel_{std}, \overline{Mw}_{std}$. Selected values for the

four cases are listed in the notation table above. It is found that optimal monomer feeding rates are not sensitive to the final Gel content constraint, but to PS Mw quality constraints. In general, higher PS Mw requires slower monomer feeding rate, and lower initiator concentration. In general higher quality constraints result in longer processing time. Gel content and PS Mw quality have different effects on the optimal feeding profile. The constraint of PS $\overline{Mw}$ dominates the Stage II optimization solution.

Finally, it should be noted that the prediction is based on constant initiator efficiency. In practice, initiator efficiency would change from run-to-run. In addition, more information is needed to understand the reactivity of different initiator radicals. Therefore, there is considerable uncertainty of the prediction due to possible deviations from the simplified assumptions. For example, if the initiator efficiency changes from 0.3 to 0.7, Gel_{end} will increase by 40%, and PS $\overline{Mw}_{end}$ decreases by 12%.

Optimal solutions as shown in Figure 7.9 were implemented in the pilot plant experiments. Preliminary analytical analyses show good agreement with the model prediction. With the assistance of model-based optimization, more aggressive operation policies are obtained, and shown to be valid and economical in production.

7.4 Summary

Semi-batch feeding is the main time-limiting step in the SIPN process. Model-based optimization is carried out to explore an optimal operation policy which retains satisfactory polymer properties with minimum process duration. A special pattern of optimal feeding policy is revealed through dynamic optimization combined with process knowledge. New profile representation is applied to reformulate the SIPN singular control problem. Further-

more, Kriging, a surrogate modeling approach is introduced to alleviate the difficulty in optimizing the integrated multi-stage process model. The stiff DAE sub-model is replaced by low order Kriging models. Computational strategy for dynamic optimization with surrogate sub-models is developed. The obtained optimal feeding policies are implemented in the pilot plant, and show significant efficiency improvement compared to the original recipe.

Chapter 8

Multi-Scenario Optimization

Improvement of model-based applications is an iterative process. For example, the accuracy of the estimated parameter should be improved when additional process information becomes available. On the other hand, the effectiveness of the optimal strategy could be improved if the uncertainty of the model parameters is taken into account. Consequently, the need for information expansion leads to formulating multi-scenario optimization problems, which are large-scale yet structured. A two-stage decomposition algorithm is developed in this chapter, focusing on parameter estimation problem from multiple data sets. The new algorithm shows significant improvements on robustness for ill-conditioned problems, which is particularly usefully for the application of polymerization process models.

8.1 Introduction of Multi-scenario Optimization

Multi-scenario optimization is an important class of optimization problems, which are especially useful in process design, parameter estimation and optimization under uncertainty. A general formulation of the multi-scenario problem can be written in the form of (8.1):

$$
\begin{aligned}
min \quad & \sum_{i=1}^{NS} f_i(v_i^l, v^g) + w(\,v^g) \\
s.t. \quad & \left. \begin{array}{l} H_i(v_i^l, v^g) = 0 \\ G_i(v_i^l, v^g) \leq 0 \end{array} \right\} \qquad i \in \{1, \cdots, NS\}
\end{aligned} \tag{8.1}
$$

where NS is the number of scenarios, and the subscript i ($i \in \{1, \cdots, NS\}$) denotes an individual scenario in the set. In particular, one "scenario" refers to a complete model representation, which consists of a set of equality constraints (H_i) and inequality constraints (G_i). For dynamic problems, H and G are a discrete representation of original DAE or PDAE models. The important relationship between each scenario is through the global variables, v^g, which are present in all the scenarios, while the differences among scenarios are the local variables, v^l, which can vary from scenario to scenario. The objective function of the multi-scenario optimization is typically expressed in a summation form, where f_i represents functions dependent on both local and global variables, w represents functions that only depend on global variables. It is a convenient formulation when a common decision is to be found over a set of different conditions.

For optimization of a few small-size scenarios, problem (8.1) might be solved directly through general purpose NLP algorithms. However, for a large-scale problem with a realistic size of scenarios, the size of multi-scenario optimization can easily grow intractably. For example, dynamic models lead to large-scale single scenarios after discretization, and a large number of scenarios are required as a discrete representation of multivariable distribution. In such cases, even a few scenarios could exceed current solution limits through a direct solution approach. This is due to numerical instability and the limitations of computational power.

Therefore, a decomposition method is proposed to address this problem. The solution of the multi-scenario problem is divided into an outer problem and an inner problem. While efficient algorithms can be applied at each stage by taking advantage of its particular struc-

ture, the robustness of the solution is improved by the decomposition as well. This technique enables to solve complex multi-scenario problems with up-to-date computational technology.

We focus on multi-set parameter estimation problem to illustrate the decomposition algorithm. The framework can be extended to the problem of Optimization Under Uncertainty (OUU).

8.2 Parameter Estimation with Multiple Data Sets

One important class of the multi-scenario optimization problem is parameter estimation from multiple data sets. It is in the form of (8.2) when the sum of least squares formulation is applied.

$$
\min_{\theta:\, \theta^L, \theta^S} \quad \sum_{i=1}^{NS} (y_i - y_i^m)^T \Sigma_i (y_i - y_i^m)
$$
$$
s.t. \quad \left.\begin{array}{l} y_i = f_i(x_i, \theta_i^L, \theta^G) \\ h_i(x_i, \theta_i^L, \theta^G) = 0 \\ g_i(x_i, \theta_i^L, \theta^G) \le 0 \end{array}\right\} \qquad i \in \{1, \cdots, NS\} \tag{8.2}
$$

where $\theta \in \mathcal{R}^{n_\theta}$ are the parameters to be estimated, which is further classified into global parameters, θ^G, and local parameters, θ_i^L. x_i correspond to local variables in i^{th} scenario. $y_i, y_i^m \in \mathcal{R}^{n_y}$ are dependent variables and corresponding measurements in the ith scenario. f_i, h_i, g_i are equalities and inequalities define the sub-model of ith scenario, which can be the same or different functions. NS is the number of data set, i.e. scenario, in parameter estimation.

In principle, the solution algorithm for a single scenario optimization problem can be applied in the same way as the multi-scenario problem. However, there are several cases when customized algorithm is required to handle the increased dimensionality and complexity of

the problem. For example, the error-in-variables-measured (EVM) formulation usually leads to a large-scale problem for every single scenario, as shown in Equation (8.3), considering $u_t = u_t^* + \eta_t$, $y_t = y_t^*(x^*, \theta) + \epsilon_t$.

$$\min \quad \sum_{i=1}^{NS} (y_i - y_i^m)^T \Sigma_y^{-1} (y_i - y_i^m) + \sum_{i=1}^{NS} (u - u_i^m)^T V_u^{-1} (u_i - u_i^m)$$

$$s.t. \quad \left. \begin{array}{l} y_i = f_i(u_i, x_i, \theta_i^L, \theta^G) \\ h_i(x_i, u_i, \theta_i^L, \theta^G) = 0 \\ g_i(x_i, u_i, \theta_i^L, \theta^G) \le 0 \end{array} \right\} \quad i \in \{1..NS\} \tag{8.3}$$

Where η is error in x, and ϵ is error in y, Σ_y and V_u are the covariance for ϵ and η respectively. The EVM function accounts for errors in all the measured variables, both dependent and independent variables, implementing simultaneous parameter estimation and data reconciliation. Though there are clear advantages of EVM consideration, the size of the optimization problem could soon become too large to handle. Furthermore, it is often the case that data are collected from a large number of scenarios for a dynamic system, resulting in a structured large-scale parameter estimation problem. As model-based optimization is being applied for more and more realistic industrial problems, the issues of increasing problem size and complexity attract considerable attention. The following section introduces two main classes of solution algorithms which take advantage of the multi-scenario structure in parameter estimation.

8.2.1 NLP Solution Algorithm

The multi-scenario formulation leads to a nested NLP problem. Several NLP algorithms are developed for efficiently handling the nested structure through decomposition. The decomposition strategy can be generally divided into two groups: sequential approach with external decomposition and simultaneous approach with internal decomposition. The gain in

computational efficiency through parallel computing has also been a strong motivation for the decomposition algorithm. Problem level decomposition might conform to the existing numerical techniques to a new architecture, while algebraic level decomposition often introduces new paradigms in devising solution strategies. The following sections review these two types of decomposition algorithm in more detail.

8.2.1.1 Sequential Approach

Sequential approaches are explicit decomposition strategies. The needs of developing the decomposition strategy first arise from the EVM formulation with multiple data sets. Rod, et al. (1980) developed an iterative algorithm, which originates from the fact that the model parameters (θ^G) are common to the set of experiments, while the incidental parameters (θ^L, x_i) are specific to individual experiments. The routine searches for the minimum of the maximum likelihood objective function in an iterative manner. Optimization of the model parameter (θ^G) is solved in inner loop 1, given incidental parameters, and then optimization of incidental parameters is performed in the loop 2, given the model parameters. An outer loop 3 checks the effect of the changes of the incidental parameters on θ^G and return to loop 1 until the convergence of all parameters is reached. Reilly et al. (1981) studied a Bayesian formulation of EVM problem through a nested approach. For a given set of parameters, the constraint equations are linearized or successively linearized at measured variables. A Lagrangian method is used for optimization. Explicit calculation of the reconciled measurements is not necessary. Kim et al. (1990) further improved the robustness of the algorithm by a two-stage approach, where a set of decoupled NLPs instead of the linearized model is solved in the inner problem for independent and state variables. Dovi et al. (1989) proposed a constrained variation approach to decouple the problem. All the state and local

parameters (x_i and θ^L) are eliminated by model simulation and optimality conditions. The optimization problem is carried out in terms of linking parameters θ^G only. The problem size is greatly reduced and selection of NLP algorithms becomes more flexible. However, the price to pay is that an increased amount of information is required for the first and second derivatives of the equations that describe the model. Faber et al. (2003) extended the work of Dovi et al. (1989) and Kim et al. (1990) by presenting a nested three-stage algorithm. The upper stage is an NLP with only the parameters (θ^G) to be estimated. The middle stage consists of multiple sub-NLPs in which the independent variables of each data set are treated as optimization variables. In the lower stage the dependent variables and their sensitivities are computed through a simulation step. In this approach, only Jacobians of the model equations are required at the lower stage by simulation. User supplied derivative information is not required for its implementation. A schematic representation of (Faber, et al., 2003) is shown in Figure 8.1.

Upper Stage:
Main NLP

$$\min_{\theta} f = \sum_{i=1}^{NS} f_i = \sum_{i=1}^{NS} (y_i - \hat{y}_i)^T \Sigma_y^{-1} (y_i - \hat{y}_i) + (u_i - \hat{u}_i) V_u^{-1} (u_i - \hat{u}_i)$$

$$s.t. \quad \theta_l \leq \theta \leq \theta_u$$

Middle Stage:
Sub-NLP

$$\min_{\mu_i} f_i = (y_i - \hat{y}_i)^T \Sigma_y^{-1} (y_i - \hat{y}_i) + (u_i - \hat{u}_i) V_u^{-1} (u_i - \hat{u}_i)$$

$$s.t. \quad g_i(x_i, y_i, u_i, \theta) \leq 0$$

Lower Stage:
Simulation step

$$h_i(x_i, y_i, u_i, \theta) = 0$$

$$i \in \{1, \cdots, NS\}$$
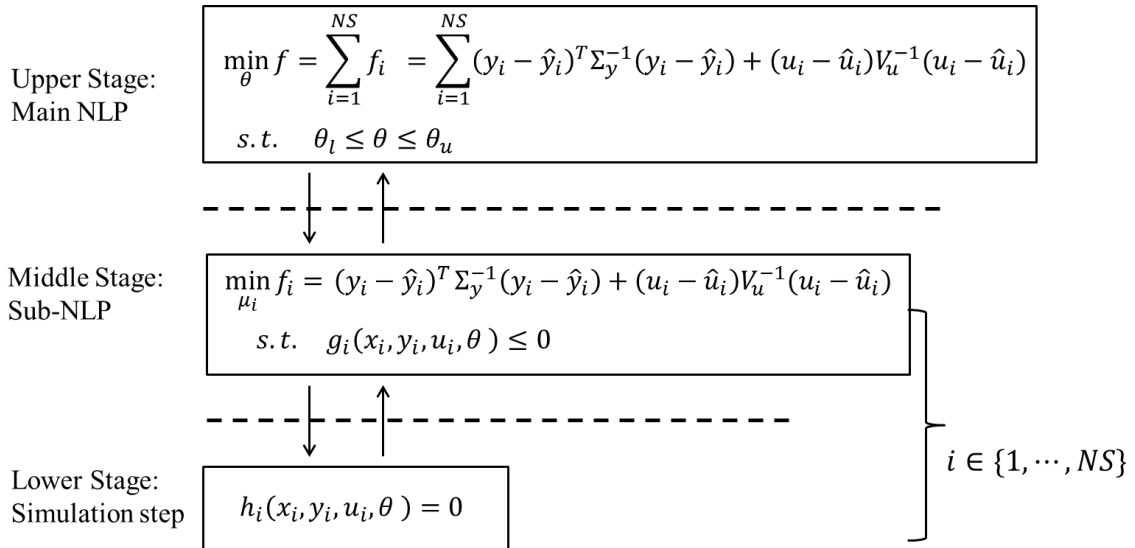
Figure 8.1 A framework of the multi-stage sequential approach

The main advantages of the sequential approach include that few mathematical manipulations are required and implementation is easy to carry out with standard NLP software. However, the limitation of current sequential approaches is the computational difficulty and efficiency in evaluating Jacobian and Hessian information from the decomposed problem. Hence, the sequential approach often suffers limited scaling properties.

8.2.1.2 Simultaneous Approach

In contrast, another class of solution strategy is the simultaneous approach with internal decomposition. Exploring a particular matrix structure in general purpose algorithms is of great interest for NLP problem, because of its potential for fast parallel computing.

Lootsma and Ragsdell (1987) reviewed hierarchical problems with linking variables in nonlinear optimization, and commented on the promising approaches for solving large-scale well-structured constrained problems. Tjoa and Biegler (1991, 1992) developed a reduced Hessian SQP method for solving the EVM problem. By introducing new variables and additional constraints to each data set, a range and null space decomposition was applied. The approach was shown to be more efficient than general purpose NLP solver MINOS 5.2 and contemporaneous RND SQP. An internal decomposition algorithm was further improved as the development of parallelization of linear algebra. The Interior-Point Algorithm, in particular, which is mainly limited by the efficiency of linear algebra, significantly benefits from the parallel implementation of linear algebra kernels (Migdalas, et al., 2003). Gondzio (2004) developed full-space approaches for linear and quadratic programming problems by exploiting nested block-structure. The idea for block structure decomposition is then extended to nonlinear nonconvex problems. Zavala et al. (2008) developed an interior-point method with Schur complement decomposition strategy implemented in parallel computing architectures

for parameter estimation of an industrial polymerization model. An NLP solver, SCHUR-IPOPT, which is a modification of standard IPOPT, is designed for large-scale general non-linear optimization problems. Successful applications of SCHUR-IPOPT algorithm have been reported for industrial-scale problems. To show the convergence properties of internal decomposition, the algorithm in Zavala et al. (2008) is outlined here.

The dynamic multi-scenario problem is first translated into a large-scale, general NLP problem through a full discretization approach as discussed in Chapter 5. The problem can be written as:

$$
\min_{x_k, d} \quad \sum_{k=1}^{NS} f_k(x_k, d)
$$
$$
\left.\begin{array}{c} c_k(x_k) = 0 \\ S_k x_k \geq 0 \\ D_k x_k - \overline{D}_k d = 0 \end{array}\right\} \quad k \in \{1, \cdots, NS\} \tag{8.4}
$$

where x_k contains all the parameters and variables corresponding to the discretization of the DAEs for a particular scenario k, d is a linking variables vector (e.g. global parameter θ^L). D_k and $\overline{D}_k$ extract and assign linking components. Inequalities in (8.4) are added to the objective function to formulate a barrier function in IPOPT. Then, a primal-dual approach is applied to solve the Karush-Kuhn-Tucker(KKT) condition of the barrier function. As a result, one block bordered diagonal structure is generated at the iteration:

$$
\begin{bmatrix}
W_1 & & & & & A_1 \\
& W_2 & & & & A_2 \\
& & W_3 & & & A_3 \\
& & & \ddots & & \cdots \\
& & & & W_{NS} & A_{NS} \\
A_1^T & A_2^T & A_3^T & \cdots & A_{NS}^T & \delta_1 I
\end{bmatrix}
\cdot
\begin{bmatrix}
\Delta v_1 \\
\Delta v_2 \\
\Delta v_3 \\
\vdots \\
\Delta v_{NS} \\
\Delta d
\end{bmatrix}
=
\begin{bmatrix}
r_1 \\
r_2 \\
r_3 \\
\vdots \\
r_{NS} \\
r_d
\end{bmatrix}
\tag{8.5}
$$

Where $\mathcal{L}_k^l = f_k(x_k^l) - \mu \sum_j \ln\left[(S_k x_k^l)^{(j)}\right] + c_k(x_k^l)^T \lambda_k + \left[D_k x_k^l - \bar{D}_k d\right]^T \sigma_k$, $r_k^T = -[(\nabla_{x_k}\mathcal{L}_k^l)^T, (c_k^l)^T, (D_k x_k^l - \bar{D}_k d^l)^T]$, $\Delta v_k^T = [\Delta x_k^T, \Delta \lambda_k^T, \Delta \sigma_k^T]$, $A_k^T = [0, 0 - \bar{D}_k^T]$, $r_d = \sum_{k=1}^{NS} \bar{D}_k^T \sigma_k^l$ and

$$W_k = \begin{bmatrix} H_k^l + \delta_1 I & \nabla_{x_k} c_k^l & D_k^T \\ (\nabla_{x_k} c_k^l)^T & -\delta_2 I & 0 \\ D_k & 0 & -\delta_2 I \end{bmatrix} \text{ for } k = 1, \cdots, NS.$$

The key step is to solve (8.3) in parallel by computing Δd through forming Schur complement.

$$[\delta_1 I - \sum_{k=1}^{NS} A_k^T (W_k)^{-1} A_k]\Delta d = r_d - \sum_{k=1}^{NS} A_k^T (W_k)^{-1} r_k \qquad (8.6)$$

Once Δd is known, the remaining variables can be found by solving the following:

$$W_k \Delta v_k = r_k - A_k \Delta d, k = 1, \cdots, NS. \qquad (8.7)$$

The internal decomposition algorithm is well-suited for well-conditioned systems, i.e. KKT matrix has the correct inertia, and δ_1 and δ_2 are 0 or close to 0 during iteration. In principle, this parallel computing framework enjoys a good complexity property, and is capable of handling a large number of scenarios. Zavala et al. (2008) argued that the advantage of this decomposition strategy is that it retains the same convergence properties as the original IPOPT, since the core NLP algorithm is not altered in the decomposition. However, excessive computation cost and poor convergence behavior are observed for large-scale nonlinear and ill-conditioned systems. Increasing the number of scenarios in this case often leads to failed solutions even with the original IPOPT. The robustness of the decomposition is challenged for highly nonlinear and ill-conditioned problems. When examining the solution output from IPOPT, it is found that this behavior is mainly attributed to the difficulties in the inertia correction step, which occurs in the matrix factorization. Matrix inertia is used

to verify the optimality conditions, and should be kept constant throughout the iteration. Nonzero δ_1 and δ_2 values are included to temporally modify the singularity and non-descent conditions in order to return a proper KKT inertia. Without regularization, a successful step Δd is easy to obtain at each iteration. However, when the full KKT matrix or W_k is ill-conditioned, determination of appropriate δ_1 and δ_2 values becomes particularly difficult for this large matrix.

8.2.2 A Two-stage Decomposition Algorithm

In this work, we present a new two-stage decomposition algorithm for large-scale multi-scenario nonlinear problems. It is a hybrid algorithm extended from both sequential and simultaneous approaches. It aims to combine the advantages of easy manipulation as in the sequential approach and high efficiency for large degrees of freedom as in the simultaneous approach. The ill-conditioned system can be handled more robustly in this approach. The optimization variables are divided into two levels, as global variable and local variable. In the outer problem, there are only global variables (θ^G), namely, variables sharing the same value for all the scenarios. The dimension of the optimization problem (d^G) is generally small. In the inner problem, the degrees of freedom are local variables (θ^L), which are variables allowed to vary in different scenario. The dimension of separate variables (d^{L_i}) and stage variables in a single scenario problem can be large.

Figure 8.2 illustrates the basic idea of the two-stage approach based on formulation (8.2). Extension to the EVM problem is also straightforward, as long as the objective function (F) can be decoupled as a function of inner problem objective functions from each scenario (f_j). Here, $\theta^G_{(k)}$ represents global parameters at iteration k. θ^{L_j} is local variable in j^{th} scenario.

h_i and g_i represent constraints in scenario j. The objective function gradient and Hessian (optional) with respect to θ^G, as $\nabla_{\theta^G} f_i$ and $\nabla_{\theta^G}^2 f_i$, are obtained from the inner stage, and passed to the outer stage for optimization.
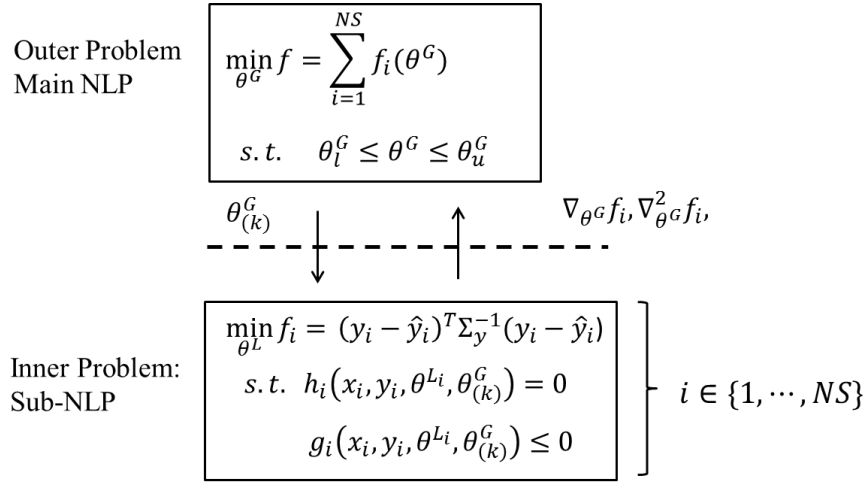
Figure 8.2 A framework of two-stage decomposition approach for multi-scenario optimization

The algorithm is outlined as follows:

- Step 1. Identify global parameters, θ^G, in the multi-scenario problem. Set the iteration counter for the outer NLP as $k = 0$. Initialize all variables in the optimization.

- Step 2. At each iteration k:

    o Solve the inner optimization problem at fixed linking parameter $\theta_{(k)}^G$. In this case, inner problem, sum of least squares or EVM is solved.

    o Evaluate objective function, gradient and Hessian (optional) with respect to $\theta_{(k)}^G$ at inner optimization solution.

- Step 3. Stop, if optimality condition of the outer NLP is satisfied at $\theta_{(k)}^G$. Otherwise, call a constrained NLP solver to update $\theta_{(k)}^G$. $k \leftarrow k + 1$. Return to Step 2.

The main difference of this approach with previous sequential approaches lies in Step 2, which is capable of handling the large-scale single-scenario problem efficiently, as well as obtaining the gradient and Hessian information cheaply. A simulation step is no longer necessary. Compared with the simultaneous approach, updating $\theta_{(k)}^G$ is equivalent to solve Δd in Equation (8.5) after converging each block structure of W_k. Since the ill-conditioned properties are handled in the inner problem, the outer NLP is generally well-conditioned in θ^G. Therefore, more robust convergence properties are expected. The implementation details are presented in the following.

8.2.2.1 Sensitivity Analysis of Inner Optimization Problem

One of the key components in this two-stage algorithm is an efficient derivative evaluation approach at the solution of the inner optimization problem. In this work, exact first order information is computed by taking advantage of NLP sensitivity analysis. A package named "*s*IPOPT" (Pirnay, et al., 2011) (previously named "AsNMPC") is adapted for this usage.

"*s*IPOPT" is an add-on for the standard IPOPT. It was designed to facilitate the implementation of the advance-step NMPC algorithm developed by Zavala (2008). It is essentially a sensitivity analysis step for the NLP problem. The value of state variables at a perturbed parameter value is estimated by a first order Taylor expansion, where the first derivative of state variable with respect to parameter is obtained from KKT matrix at the current solution point. For its usage in the two-stage algorithm, sensitivity of the inner objective function with respect to the global parameter, $\frac{\partial f}{\partial \theta_{(k)}^G}$, is the gradient information required for the outer optimization problem. It can be retrieved readily through the NLP sen-

sitivity. Here, the solution strategy of "sIPOPT" is briefly described. Interested readers can refer to (Zavala, et al., 2008) for more details.

"sIPOPT" computes a perturbed NLP solution in addition of the nominal solution based on KKT matrix at optima. For example, a general NLP problem is written as (8.8),

$$\begin{aligned} \min_{x} \quad & f(x, \theta) \\ s.t. \quad & c(x, \theta) = 0 \\ & x \geq 0 \end{aligned} \tag{8.8}$$

where θ is a parameter vector with a fixed value, x is the variable vector. Denote the optimal solution of (8.7) at θ as $x^*(\theta)$. As-NMPC computes an additional solution $\hat{x}^*(\theta')$ after the convergence of nominal problem, which is an approximated solution of (8.7) at user specified θ'. $\hat{x}^*(\theta')$ has a first order accuracy compared to the true value of $x^*(\theta')$. It is shown to be particularly useful for fast online updates of state variables when the perturbation of the system parameter is small. For our purpose of computation, the first derivative of x with respect to θ at the optimal point, $\frac{\partial x}{\partial \theta}|_\theta$, is computed through (8.9).

$$\frac{\partial x}{\partial \theta}|_\theta = \frac{\hat{x}^*(\theta') - x^*(\theta)}{\theta' - \theta} \tag{8.9}$$

$\frac{\partial x}{\partial \theta}|_\theta$ obtained above is an exact first derivative, if strict complementarity, LICQ and SSOC hold. Since our interest is to recover $\frac{\partial x}{\partial \theta}|_\theta$, not to accurately estimate the state of $\hat{x}^*(\theta')$, we don't require θ' to be in the neighborhood of θ. Therefore, θ' is set to be $(\theta + 1)$ regardless of the nominal value of θ. (8.9) is reduced to (8.10).

$$\frac{\partial x}{\partial \theta}|_\theta = \hat{x}^{*\prime}(\theta + 1) - x^*(\theta) \tag{8.9}$$

The reason for allowance of an arbitrary choice of θ' is because $\frac{\partial x}{\partial \theta}|_\theta$ is solved prior to

estimating $\hat{x}^*(\theta')$ in the sIPOPT solver. The underlining mechanism for computing $\frac{\partial x}{\partial \theta}|_\theta$ is

equivalent to evaluating the exact first derivative at the optimum. The derivation is summa-

rized below.

The Lagrange function of problem (8.8) is defined as (8.11).

$$\mathcal{L} = f(x) - v^T x + \lambda^T c \tag{8.11}$$

where v and λ are Lagrange multipliers for bounds and the equality constraints. At the opti-

mal point, the KKT condition is satisfied. We have $\nabla_{\{x,\mu,\lambda\}}\mathcal{L} = 0$. Denoting $s = [x, v, \lambda]$, we

have $\varphi = \nabla_s \mathcal{L} = 0$. Considering ϕ is a function of model parameter θ and s, Equation (8.12)

holds at the nominal parameter value θ at the optimal solution s^*.

$$\varphi(s^*(\theta), \theta) = 0 \tag{8.12}$$

Applying the implicit function theorem to (8.12), Equation (8.13) is obtained.

$$K^*(\theta)\frac{\partial s^*}{\partial \theta} = -\frac{\partial \varphi(s^*(\theta), \theta)}{\partial \theta} \tag{8.13}$$

where $K^*(\theta)$ is the KKT matrix of the primal-dual system at $s^*(\theta)$. A nice property of (8.13)

is that $K^*(\theta)$ is already factorized at the optimal solution. Solving this linear system with

different right hand sides only costs a single back-solve. Matrix factorization, which is the

most expensive step in the interior point algorithm, is not required. In the sIPOPT calcula-

tion, the right hand side of (8.13) is substituted by $-\frac{\partial \varphi(s^*(\theta), \theta')}{\partial \theta}$ in order to compute $\frac{\partial s^*}{\partial \theta}$. If

the solution satisfies strict complementarity, LICQ and SSOC at the nominal θ value, θ' is

at some neighboring region of θ, then the activity set of inequality equations does not

change at θ', and equation (8.13) would be first-order accurate in terms of state estimation. $\hat{s}(\theta')$ is the estimated solution at θ', which is reported as output in sIPOPT.

$$\hat{s}(\theta') = s^*(\theta) + \frac{\partial s^*}{\partial \theta}(\theta' - \theta) \tag{8.14}$$

Therefore, Equation (8.9) can be used to recover $\frac{\partial x_*}{\partial \theta}$ based on sIPOPT solution. This feature enables to tackling the gradient evaluation problem in the conjugation of the multi-stage algorithm efficiently. The global variable, θ^G, though fixed in the inner optimization problem, is defined as an artificial variable for sIPOPT processing. Thus, solution of the objective function at a new set of global parameter values can be solved in this manner. At the end of each iteration, the inner optimization problem returns a function value and a gradient vector with respect to the linking variables.

8.2.2.2 NLP Algorithm for Outer Optimization Problem

In principle, any general NLP solver could be used for the outer optimization problem. Nevertheless, the outer problem is a simple bound-constrained problem in the form of (8.15),

$$\begin{aligned} \min \, & f(\theta) \\ \text{subject to:} \quad & \theta_L \leq \theta \leq \theta_U \end{aligned} \tag{8.15}$$

where, θ corresponds to global parameters for all the scenarios. Therefore, the choice of the outer NLP solver is considered particularly for the bound-constrained problem, which allows more efficient implementation for this problem structure. Several NLP algorithms are available. Here L-BFGS-B (Zhu, et al., 1997) and TRON (Lin, et al., 1999) are used in this work, which is briefly described in the following.

"L-BFGS-B" is a limited-memory quasi-Newton code for bound-constrained optimization. At each iteration, a search direction is computed in two steps. Active variables are first identified through a gradient projection approach; then free variables are computed to approximately minimize a quadratic function. See the details of L-BFGS-B in Byrd et al.(1995). Since Hessian is updated through a limited memory BFGS approximation, no Hessian information needs to be extracted from the inner optimization problem. The exact first derivative, $\frac{df_j}{d\theta_{(k)}}$, is directly provided from the output of the inner optimization solution. L-BFGS-B is considered to be efficient for unconstrained optimization.

"TRON" is a trust region Newton method for the solution of large bound-constrained optimization problems. The search direction is computed through a preconditioned conjugate gradient method with an incomplete Cholesky factorization. A projected search approach keeps the constrained variables in bounds during iterations. TRON is suitable for solving large-scale problems for its efficiency of examining feasible sets by generating a small number of minor iterations.

Besides the gradient information, the Hessian is required for TRON's algorithm. Hence, an additional routine should be included to evaluate the Hessian from the inner problem. Notice that, one does not need to compute the Hessian matrix directly. Instead, the Hessian vector product is used in the computation. Hessian vector product refers to "$H \cdot s$", where H stands for Hessian matrix of "$\frac{\partial^2 f}{\partial^2 \theta^L}$", and "$s$" is the search direction. It can be approximated by a finite different scheme, such as central difference.

$$\mathrm{H} \cdot \Delta\theta \approx \frac{G(\theta + \epsilon\Delta\theta) - G(\theta - \epsilon\Delta\theta)}{2\epsilon} \tag{8.16}$$

where $G(\theta)$ is the gradient of f with respect to x. Each Hessian vector product calculation

requires two gradient evaluations, i.e., two inner problem solutions.

8.3 Results and Discussion

8.3.1 α-Pinene Isomerization Example

α-Pinene model which contains 5 estimating parameters is taken from the COPS (Large-

Scale Optimization Problems) collection, discussed in (Dolan, et al., 2000; Box, et al., 1973;

Tjoa, et al., 1991; Averick, et al., 1991). A brief summary of the example is provided here.

The model describes the reaction scheme of thermal isomerization of α-pinene (Y_1) to di-

pentene (Y_2) and alloocimene (Y_3), which yields α $-$and β $-$pyronene (Y_4) and a dimer (Y_5),

as shown in the Figure 8.3.
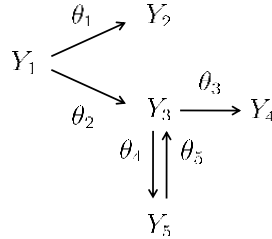
Figure 8.3 Reactions of α $-$Pinene example

Five ordinary differential equations are considered in the model, as shown in.

$$
\begin{aligned}
\frac{dy_1}{dt} &= -(\theta_1 + \theta_2)y_1 \\
\frac{dy_2}{dt} &= \theta_1 y_1 \\
\frac{dy_3}{dt} &= \theta_2 y_1 - (\theta_3 + \theta_4)y_3 + \theta_5 y_5 \\
\frac{dy_4}{dt} &= \theta_3 y_3 \\
\frac{dy_5}{dt} &= \theta_4 y_3 - \theta_5 y_5
\end{aligned}
\tag{8.17}
$$

The objective function of parameter estimation problem is set to be a sum of squares function. ODE system (8.17) is discretized at 2-point Radau collocation points, and transformed to NLP. For illustration purposes, assume that θ_4 and θ_5 are local parameters, $\theta_1, \theta_2, \theta_3$ are linking parameters. Data sets are generated based on the same value of $\theta_1, \theta_2, \theta_3$, but different values of θ_4 and θ_5. Therefore, the degree of freedom is 2 for the inner NLP, and the degree of freedom is 3 for the outer NLP.

$$\text{Outer NLP:} \quad \min_{\theta_1, \theta_2, \theta_3} \quad f = \sum_{i=1}^{NS} f_i(\theta_1, \theta_2, \theta_3) \tag{8.18}$$
$$s.t. \quad \theta_L \le \theta_1, \theta_2, \theta_3 \le \theta_L$$

$$\text{Inner NLP:} \quad \min_{\theta_4, \theta_5} \quad f_i = \|y(\tau) - z\|^2$$
$$s.t. \quad \text{Discrete model of (8.17)} \tag{8.19}$$
$$\theta_L \le \theta_4, \theta_5 \le \theta_U$$

For the outer NLP, the termination criteria of L-BFGS-B are set to be: $pg_{tol} = 1 \times 10^{-5}$. (Stop when $(\max\{|\text{proj } g_i|, i = 1, \cdots n_\theta\} \le pg_{tol})$, where proj g_i is the ith component of the projected gradient.) The termination criteria of TRON are set to be: $g_{tol} = 1 \times 10^{-5}$; $f_{rtol} = 1 \times 10^{-12}$; $fev\_\max = 200$. For the inner NLP, IPOPT V3.9 trunk 1955 was used for this task. Default termination setting was applied for solution accuracy. In addition, solutions from direct approach are also compared. IPOPT V3.9 is used for computation. Results from L-BFGS-B, TRON and direct solution approach are summarized in Table 8.1. nh is a adjusting parameter used to change the problem size; nv is the total number of variables; I^O is the number of major iterations in L-BFGS-B; T is wall-clock time in seconds; I^I_{max} is the max number of iterations for an inner NLP; t is the maximum

solution time for an inner NLP; nf is the number of function evaluations in TRON; I^D is the number of iterations by direct solution approach using IPOPT.

Table 8.1 A comparison of α- pinene example

	NLP Statistics		L-BFGS-B				TRON				Direct	
NS	nh	nv	Outer		Inner		Outer		Inner		IPOPT	
			I^O	$T(s)$	I^I_{max}	$t(s)$	nf	$T(s)$	I^I_{max}	$t(s)$	I^D	$t(s)$
10	120	21660	11	31.28	121	2.2	24	53.31	6	0.04	9	2.33
	1200	128160	11	509.24	438	82.5	24	850.36	8	1.71	11	82.5
20	120	43320	11	56.77	121	2.1	17	91.87	6	0.04	15	9.29
	1200	256320	11	948.84	438	86.6	19	1388.5	8	1.7	19	349.1
30	120	64980	11	83.11	121	2.1	20	139.01	6	0.04	15	14.4
	1200	384480	11	1388.78	438	83.4	19	2191.2	8	1.7	19	891.3

It is seen from Table 8.1, that the decomposed problems, in general, are insensitive to the increased problem size, in terms of total number of iterations for the inner NLP and outer NLP. Notice that the L-BFGS-B algorithm takes many more iterations at some of the steps than the others. For example, the maximum number of iterations for a single scenario problem with 21660 variables reaches to 121. This is due to a large step size generated from the outer NLP. It is difficult for Inner NLPs to converge from a poor starting point. In contrast, the number of iterations in TRON is more regular for the inner NLP, since trust-region properties insure the reliability of generated steps. However, convergence is much slower, and the cost in evaluation of Hessian also slows down the overall process. Comparing the wall-clock time, the direct solution approach performed the best for this example. Since both inner NLP and direct NLP problem are well-conditioned, no inertia correction was observed in the iteration. Direct solution should be a good choice even for a very large problem size.

Yet, it is also worth to noting that the solution time shown above is from sequential imple-mentation of the inner problem. In fact, the two-stage NLP is naturally suitable for parallel computing. Inner NLPs can be handled independently, while the Outer NLP is usually in a low dimension requiring few interactions. Therefore, in a parallel processing framework, the solution time for main iteration would be dominated by the most expensive inner NLP problem. Extra savings from parallel computing would be significant for problems with a large number of scenarios.

8.3.2 Marine Population Dynamics Example

A marine population dynamics model is also taken from COPS, studied in Rothschid, et al. (1997). The model describes the population of a marine species at each stage as a function of time. Parameter estimation is carried out to determine stage specific growth and mortality rates. Population at n_s stage is described as following:

$$y'_j = g_{j-1}y_{j-1} - (m_j + g_j)y_j, \quad 1 \le j \le n_s \tag{8.20}$$

Where m_j and g_j are the unknown mortality and growth rate at stage i with $g_0 = g_{ns} = 0$. Notice that initial conditions for the differential equation are also unknown to this system. Therefore, it is treated as local parameters in the multi-scenario formulation. m_i and g_i are considered to be linking parameters in this case. The model is discretized at a 2-point La-grange collocation point. nh is the number of finite elements used for discretization.

$$\min \sum_{i=1}^{NS} \|y(\tau_i; m, g) - z_i\|^2 \tag{8.21}$$

Decomposing the problem into two stages, we have

$$\text{Outer NLP:} \quad \min_{m_i, g_i} \quad f = \sum_{i=1}^{NS} f_i(m, g) \tag{8.22}$$
$$s.t. \qquad m, g \geq 0$$

$$\text{Inner NLP:} \quad \min_{y0_i} \qquad f_i = \|y_i(\tau) - z_i\|^2$$
$$s.t. \qquad \text{Discrete model of (8.17)} \tag{8.23}$$
$$y_0^L \leq y_0 \leq y_0^U$$

The same termination criteria are used for the marine population problem. Table 8.2 summarizes the computational results based on the three approaches.

Table 8.2 Marine population dynamics solution comparison

	NLP Statistics		L-BFGS-B				TRON				Direct	
NS	nh	nv	Outer		Inner		Outer		Inner		IPOPT	
			I^O	$T(s)$	I^I_{max}	$t(s)$	nf	$T(s)$	I^I_{max}	$t(s)$	I^D	$t(s)$
10	200	32160	13	35.0	7	0.42	19	85.3	5	0.10	31	12.2
	400	64160	13	89.4	12	1.2	19	148.8	7	0.41	21	21.0
	800	128160	13	188.16	15	3.4	19	350.5	8	1.04	30	72.8
20	200	64320	13	88.3	7	0.6	14	144.2	5	0.03	15	20.9
	400	128320	13	210.2	12	4.2	16	334.9	8	0.30	20	66.2
	800	256320	13	364.4	17	6.3	15	734.1	8	0.95	18	241.1
30	200	96480	13	196.0	11	0.22	18	355.1	5	0.08	21	34.3
	400	192480	13	422.1	14	3.5	19	615.9	5	0.22	25	130.2
	800	384480	13	754.2	19	5.2	19	1269	8	0.36	19	820.8

In this example, similar observations are shown. The solution time in the decomposition method began to be comparable to direct solution approach when the number and size of the scenario increased.

8.3.3 Application to Parameter Estimation of Stage I model

In chapter 6, we have shown that properties of three different grades of products can be predicted with the same set of kinetic parameters. Simultaneous optimization was applied to

obtain the parameter estimation solution. To extend the model application and improve the parameter accuracy, it is interesting to consider a broader range of products which share the same or part of the kinetic mechanisms. However, the resulting large-scale highly nonlinear NLP is particularly difficult to solve.

Parameter estimation of the Stage I model shares some similarities as with example of marine population dynamics model in terms of the classification of global and local parameters. Initial conditions varied in each scenario due to the swelling pretreatment before polymerization. In addition, initiator efficiency also changes at different process conditions. Kinetic parameters are considered to be the same for the same system. Since experimental data are not all available at this time, simulated data are used to examine the use of the algorithm. PS $\overline{Mw}$, styrene conversion ratio and particle size are simulated at different feeding rates and initial conditions. Parameters of interests include kinetic parameters for all the scenarios. Hence $\theta^G = \{k_p, a_l^0\}, l = \text{PS, Sty, PE.} \quad \theta^L = \{\overline{Mw}_i, \overline{xs}_i, f\}. \quad i = \{1, \cdots, NS\}$. Table 8.3 summarizes the result from two different solution approaches.

Table 8.3 Multi scenario solution of Stage I model

	NLP Statistics	L-BFGS-B				Direct	
		Outer		Inner		IPOPT	
NS	nv	I^O	$T(s)$	I^I_{max}	$t(s)$	I^D	$t(s)$
3	37811	2	781.1	200	386.2	10	40.6
4	50414	2	365.7	22	60.6	26	171.7
5	63017	3	488.6	22	52.5	32	274.3
6	75620	3	3152	200	364.2	132*	1163*
7	88223	3	4133	200	591.8	x	x
8	100826	3	3450	77	281.1	x	x
9	113429	3	4099	34	116.1	x	x
10	126032	3	4122	55	143	x	x

* Converged with inertia correction
x Failed to converge

It is found that the direct-solution approach starts to experience difficulties as the number of scenarios increases. For the Stage I model, when ns is below 5, the direct solution was still able to proceed from temporarily linear-dependent points. However, when ns reaches 6, regulation and re-factorization of ill-conditioned KKT matrix becomes the most expensive and difficult step in the iteration. The process terminated at a point after 132 iterations, with $rg = 10^{10.1}$ in the KKT matrix. When ns goes above 7, the direct solution terminated with an error message without a solution. In comparison, the two-stage decomposition approach remains capable, and insensitive to the increased problem size. This feature provides a good basis for implementing larger and more difficult parameter estimation problems in the future.

8.4 Summary

A two-stage decomposition algorithm is developed for multi-scenario dynamic optimization problems. Decision variables (which are the degrees of freedom) are decomposed into global variables and local variables. Local variables, which are separable, are solved at the inner stage given the value of global parameters. Then global parameters are updated at the outer stage based on the sensitivity analysis from the inner NLP. An efficient approach for NLP sensitivity evaluation adapted from the sIPOPT package enables determination of the exact first derivative without expensive computational cost. Bound-constrained NLP optimization, which is separated from inner NLP optimization, alleviates the difficulty resulting from ill-conditioned scenarios. The trust region type algorithm is considered to handle ill-conditioned global variables more robustly, but slow convergence is observed in TRON. Larger scenarios of the SIPN process model are studied. Improved robustness and capability compared to the direct solution approach is shown with the proposed algorithm. Adaption of the two-stage decomposition algorithm for parallel computing is also straightforward.

Considerable gain in computational efficiency is expected for parallel processing of large-scale inner problems.

Chapter 9

Conclusions and Future Research Directions

Model-based optimization provides a systematic, efficient and cost effective way to facilitate innovative advancement and operational effectiveness in chemical engineering. In particular, the polymer industry has seen great potential for advanced modeling and optimization tools in supporting decision making.

This thesis work focuses on the synergy of modeling and optimization tools for complex system study. A Semi-Interpenetrating Polymer Networks process is studied as a representative example for the development of model-based optimization in polymer industry. SIPNs are a class of specialty polymers in the IPN family, which are of great importance because of their broad applications. However, challenges in SIPN product quality control and productivity improvement stimulate new advances on mathematical modeling and optimization tools.

We have successfully built effective models for the SIPN process, and implemented new operation policies for process improvement based on the tools we developed in this work. Modeling of the SIPN process provides a comprehensive understanding of the relationship between process conditions and SIPN macromolecular properties. Furthermore, it enables process optimization to be carried out effectively. On the other hand, by developing advanced computational tools, unknown parameters are obtained and validated based on

process data, and novel optimal operation policies are explored. The combination of the

power of modeling and optimization demonstrates a promising direction for future research.

9.1 Summary of Contributions

This thesis contributes in both modeling and optimization areas, and makes an effective in-

tegration of both tools for model-based optimization. Major contributions of this thesis are

summarized from two aspects, as shown in Figure 9.1.

Effective modeling approaches		**Advanced computational tools**
• Multi-stage modeling framework for complex process study.		• Parameter subset selection and estimation.
• Modeling of seeded suspension polymerization process.	**Mathematical modeling** / **Optimization**	• Solution profile representation.
• Comprehensive kinetic models for SIPN composite.		• Optimization with surrogate sub-models.
		• Decomposition algorithm for multi-scenario dynamic optimization.

Figure 9.1 Summary of main contributions

9.1.1 Mathematical Modeling

- ***A multi-stage modeling framework for complex process study***

Polymerization processes usually contain multiple chemical and physical phenomena.

Getting a unified model to include all the phenomena does not seem to be practical nor nec-

essary for the purpose at hand. The multi-stage representation presents an effective way to

decouple modeling difficulties. Thus, different key effects are considered at each stage.

Complex problems are broken down into manageable pieces so that effective solution ap-

proaches can be developed accordingly. Linkages between sub-models are kept for constructing an integrated model.

As for SIPN process modeling, a two-stage model is built to understand the complex SIPN dynamics. Two key features of IPN, "Interpenetrating" and "networking", are decoupled in different modeling stages. Temperature is the factor for the stage partition in this work. At a low temperature (80~90℃), the main consideration is the monomer diffusion and the particle growth. A generalized particle growth model is developed to describe inter-particle and intra-particle dynamics under semi-batch operation. Simplified polymerization scheme is adapted since networking reactions are negligible at this temperature. "Interpenetrating" properties are able to be represented. Then, at a high temperature (130~150℃), all the reactions start to take place, while the particle growth is stabilized because of the completion of monomer feeding. The key effect becomes the SIPN kinetics in this stage. A SIPN kinetic model is constructed to consider detailed kinetic mechanisms including polymerization, crosslinking, grafting, degradation and polymer interaction when diffusion is insignificant. "Networking" characteristics come to be attainable. Construction of a model from essential building blocks facilitates comprehensive representation for complex systems.

This multi-stage modeling methodology is readily generalizable for more complex system analysis. Different factors can be used to divide different modularized stages. The complexity of sub-models can be significantly reduced, while the predictability of the model is little affected.

- ***Single particle model for seeded suspension polymerization process***

The seed polymerization technique is receiving increasing attention and becoming a promising technique for novel material development. Its advantages in particle size control

and versatile customizable properties make it a competitive choice in many areas of application. However, due to the complexity of the particle growth, the efforts toward modification and control are not intuitively obvious and many experimental observations remain unexplained. Modeling intricate particle growth and morphology, which is significant for the design and operation of particulate processes, was not yet developed.

In this work, a generalized single particle growth model is developed in order to facilitate this progress. To depict the special features of seed polymerization, the interactions of external mass transfer and internal diffusion are considered with polymer kinetic model and connected with the macro-scale feeding strategy for further purposes of optimal control. Different from traditional single particle models, the particle size growth is modeled in a more rigorous way, where the seed property and the dynamic density change are taken into account. In particular, the morphology evolution of these complex polymer particles is simulated along with realistic kinetic phenomena, where the apparent kinetic rates are dynamic functions of the states that reveal more insights about the polymer properties.

Numerical simulations are performed through a special discretization approach. The single particle is discretized into a certain number of moving shells. The coupled differential-integral-algebraic equations are transformed to be differential-algebraic equations. The resulting model leads to an efficient simulation study and enables its further application in optimization.

- *Comprehensive SIPN kinetic models*

The properties of IPNs are found to be closely related with their network structure and joint molecular weight distribution. While specific polymer structure is desired for various applications, poor control of the process condition can prevent the formation of the desired

structure, so as to affect their ultimate properties. This is an incentive to develop a systematic mathematical model to understand and control of such processes, and to provide insights for the material design. Since polyethylene is the largest commodity polymer product nowadays, IPN modification of polyethylene is of particular interest. A polyethylene/polystyrene semi-I IPN process is chosen as a case study in this work, and discussed in detail.

A comprehensive kinetic model is developed, which involves simultaneous crosslinking, grafting and degradation, to predict SIPN gel content and molecular weight development simultaneously up to full conversion. Computational expense has been reduced considerably through a new component-decomposition strategy. Continuous variable approximation is applied for monomer polymerization and grafting reactions. Discrete population balance approach is introduced for simulation of crosslinking reaction as well as simultaneous chain transfer and chain scission. Multiple representations of population balance models, including a novel fixed pivot technique, are adapted, providing comprehensive information on the MWD and gel content of the IPN to predict product properties. The final inter-polymer formulation is reconstructed through a statistical approach.

This SIPN kinetic model is extendable to the full IPN process as well as other polymer composite systems. The simplicity and effectiveness of the multi-population balance representation can be easily adapted to general purpose computational packages.

9.1.2 Optimization

- *Parameter selection and estimation*

Using large-scale nonlinear programming tools, we have developed parameter ranking, selection and estimation strategies to improve estimation and prediction quality. Often, only

a portion of parameters can be estimated reliably due to inherent model structure and data availability. Improper inclusion of estimating parameters would lead to large distortions of the model prediction. In this work, parameter estimability is investigated in parameter estimation. A hybrid approach to select and identify parameters in nonlinear dynamic system is presented.

Local sensitivity analysis is used for initial parameter screening. A primary parameter ranking is obtained through a QRcp (QR decomposition with column permutation) approach. Weak-effect parameters are removed from the selected subset. Then parameter estimation is carried out for the selected parameters simultaneously. The effect of prior ranking as well as parameter uncertainty is minimized. Moreover, by applying the NLP sensitivity analysis, the covariance matrix of the estimated parameter from a maximum likelihood formulation can be extracted easily from a pre-factored KKT matrix. This approach enables statistical inference and systematic pruning of parameter selection to be conducted within this model building study. Satisfied parameters are identified with little additional cost.

This parameter estimation procedure is successfully applied to the SIPN process model study. A sub-set of parameters is selected and estimated reliably, which demonstrates diffusion limited features of polymer reactions and molecular weight distributions (MWD) in the development of the complex polymer network. This approach can be implemented with standard parameter estimation processes efficiently.

- *Surrogate model based optimization*

Polymerization models often contain highly nonlinear and stiff DAEs, which are particularly difficult to optimize through the direct transcription (full discretization) approach compared with other dynamic optimization problems. The difficulties in realizing optimiza-

tion for the full SIPN model make requests for alternative approaches for complex system optimization.

Surrogate modeling is a low cost substitution for evaluating computationally expensive models. Among different modeling approaches, Kriging is chosen in this work for its superior performance in both prediction accuracy and construction efficiency. Several important questions are brought up in Kriging-model-based optimization. First, does the Kriging model used for optimization need to have the same accuracy as for simulation? Second, does the optimal solution based on surrogate models converge to the same optimal point as the original model? Last but not least, how is the surrogate model refined efficiently to find a satisfactory optimal solution?

A framework of surrogate-model-based optimization is developed to address the above questions. The comparison results show that constructing the Kriging model for optimization could start from a relatively small number of initial design points. Variable screening should be implemented before exhaustive design and simulation. Second, the optimal solution should be validated in a systematic way. Examination of KKT conditions at the solution point prevents premature termination in the optimization loop. The optimization approach based on surrogate models therefore returns to a local optimum of the original optimization problem through the solution validation step. Finally, a conditional refinement approach is presented. Total number of function evaluations can be reduced significantly.

Optimization with surrogate models enables integrated optimization strategies to be employed for multi-stage process models. The Stage II sub-model of the two-stage SIPN process is replaced by two Kriging models for process optimization. The newly proposed operation policy further improves the productivity significantly.

- *Multi-scenario dynamic optimization*

Parameter estimation based on multiple data sets leads to large-scale multi-scenario optimization problems. When a single scenario model is complex and the number of scenarios is large, resulting optimization problem is often difficult to solve with off-the-shelf optimization tools. In addition, polymerization process models are often ill-conditioned. Solution convergence is the main concern in this case.

A two-stage decomposition algorithm is developed to improve the solution robustness and capability. This two-stage structure is based on the formulation of the parameter estimation problem for global parameters and local parameters accordingly. Global parameters share the same value for all the scenarios, while local parameters vary in different scenarios. Therefore, local parameters can be solved in the inner stage given global parameters; global parameters can be updated in following search step using sensitivity from the inner stage model.

In this work, the inner optimization problem takes advantage of an efficient interior point NLP algorithm and fast NLP sensitivity analysis to provide exact derivative information, while the outer optimization problem is solved with a bound constrained algorithm in a low dimension to better handle ill-conditioned variables in the system. The computational complexity in each stage has good scaling properties for problems with a large number of scenarios. Parameter estimation with multiple data sets with the proposed algorithm outperformed a direct solution approach in terms of convergence. A test problem based on SIPN Stage I model is shown. The robustness of this algorithm allows handling a growing number of data sets and applying for future model improvement.

9.1.3 Model Validation and Implementation

Moreover, these models were developed in close conjunction with an industrial experimental program which validated the model. The predictive model enabled dynamic optimization of the process in order to control the product quality and reduce the production time. The optimal results were validated in the pilot plant and indicated that significant performance gains (around 20%) can be obtained with novel operating strategies for this polymer process. This integrated model-based optimization framework demonstrates great potential for polymerization process model-based applications.

9.2 Recommendations for Future Work

- *Model formulation enhancement*

    1) Establish structure-property relationship for SIPN products

IPNs and other polymer products in general, are specified by end-use properties when used in practice, such as density, tensile modulus, impact strength, electric properties, thermal stability, optical properties etc. The relationship between basic parameters of polymer macromolecular structure and end-use properties would be an important link to be included in future process optimization for product improvement and process design. Current SIPN quality indices, such as $\overline{Mw}$ and Gel content, might be modified in such optimization problems based on obtained correlations. New characteristics may need to be considered to characterize the complex polymer composite.

    2) Consideration of various optimization criteria

Besides improvements in the mechanistic modeling, various optimization objectives are also worthy of consideration. In this work, productivity is the main focus in the optimization

problem. Reaction duration is minimized to reach a maximum production capability. In practice, other objective functions can be of interest as well. For example, an economic based objective function permits the user to explicitly evaluate operational cost and production value. Energy consumption based optimization is also of interest, since the reactor undergoes several cycles of heating and cooling. Novel operating strategies may be explored with a detailed reactor model and focused objective.

- *Efficient and robust bound-constrained NLP algorithm*

Bound-constrained NLP optimization is an important step in the two-stage decomposition approach for multi-scenario optimization problems. We have seen that a trust region algorithm has the advantage of retaining a good iteration for inner NLP, without generating a wild step. However, convergence is slower and more function evaluations are required in total. The efficiency of the bound-constrained NLP algorithm can be improved without sacrificing the nice trust region properties by adapting newly developed research in this area. Here, Adaptive Cubic Overestimation (ACO) (Cartis, et al., 2009) is a promising approach to be used. Consider the solution for smooth function f(x) in (9.1) with bound constraints,

$$\min_{x \in F} f(x) \tag{9.1}$$

A cubic model $m(x)$ is solved at iterate x_k within feasible region F.

$$m_k(x_k + s) = f(x_k) + <g_k, s_k> + \frac{1}{2} <s_k, B_k s_k> + \frac{1}{3}\sigma_k \|s_k\|^3 \tag{9.2}$$

where $<\cdot,\cdot>$ donotes the Euclidean inner product, $g_k \overset{\text{def}}{=} \nabla_x f(x_k)$, B_k is a symmetric matrix approximating $\nabla_{xx} f(x_k)$. σ is a non-negative regularization parameter, which is updated analogous to the trust region method. Good global and local convergence properties and worst-case iteration complexity bounds are shown by ACO approach, superior to the classi-

cal trust-region algorithm. This would be a good direction to take to improve the convergence rate of the two-stage algorithm.

- *NLP sensitivity implementation*

NLP sensitivity analysis is shown to be useful for implementing the two-stage decomposition algorithm for complex problems. However, several issues are suggested for improvement when it is realized on different platforms. Introducing artificial variables and equalities is necessary for including parameters of interest in the KKT structure. However, disabling variable substitution for the entire problem could have negative effects on the convergence compared to the original problem. Many manual tasks are required to incorporate current NLP sensitivity analysis into the model. A flexible and well-specified approach to incorporate KKT sensitivity calculation is worth developing for better implementation. In addition, extracting Hessian information of the parameter more efficiently is also an interesting topic.

- ***Optimization under uncertainty with the two-stage decomposition algorithm***

The parameter estimation problem is one of the foci for multi-scenario optimization in this work, whereas, the usage for the Optimization Under Uncertainty (OUU) problem is worth further investigated. OUU for a dynamic process as shown in (9.2) (Samsatli, et al., 1998), can be reformulated into an equivalent deterministic problem as a multi-scenario NLP problem as shown in (9.3)

$$\min_{u,v,\tau} \mathrm{E}_{\theta}\{\Phi(\dot{x}, x, y, u, v, \tau; \theta)\} = \min_{u,v,\tau} \int_{\theta \in \Theta} \Psi(\theta)\Phi(\dot{x}, x, y, u, v, \tau; \theta)d\theta \qquad (9.3)$$

$$s.t. \qquad J_0(\dot{x}(0), x(0), y, u(0), v, \tau; \theta) = 0$$

$$h(\dot{x}, x, y, u, v, t; \theta) = 0$$

$$g(\dot{x}, x, y, u, v, t; \theta) \leq 0$$

where x are the differential state variables, $\dot{x}$ their derivatives with respect to time, y the algebraic state variables, u the time-dependent optimization parameters (controls), v the time-invariant optimization parameters, t time, T the final time, θ the uncertain model parameters over the domain Θ, Ψ the joint probability density function (PDF), Φ a performance metric to be optimized, and $E\{\Phi\}$ the expected value of Φ. The equations J_0 represent the initial conditions of the system. Discretization of the distribution $\Psi(\theta)$ allows problem (9.3) to be represented as (9.4).

$$\min_{u, v, \tau} P = \sum_{k=1}^{ns} w_k f(s, u, v, \tau, \theta_k)$$

$$\begin{cases} H_k(s, u, v, t, \theta_k) = 0 \\ G_k(s, u, v, t, \theta_k) \leq 0 \end{cases} \quad k = 1, \cdots, NS$$

(9.4)

where s represents discretized state variables and their derivatives; H_k and G_k are equality and inequality constraints in scenario k after discretization.

The main difference between (9.4) and (8.1) is that inequalities can become active in different scenarios. Since the inequality constraints are more commonly associated with performance requirements (e.g., product purity specifications), equipment limitations, and safety regulations, the inner problem can become infeasible as well. Direct application of the previous two-step decomposition algorithm will challenge the sensitivity calculation, since the sensitivity might be undefined if the active set of inequalities is changed. Potential application of "soft" constraints, where some violation of inequality can be tolerated, or penalizing infeasibility in the outer NLP objective function could be considered. Depending on the problem specification, one-sided or two-sided penalties might be defined. The result-

ing challenge is to handle ill-conditioned outer NLPs after decomposition. Recovering from a poor search step is important for the success of the algorithm. Including some heuristic to customize the outer NLP algorithm might be useful for this extension.

- ***On-line parameter estimation /optimization for batch operation***

Modeling and optimization studies are carried out off-line for the SIPN process in this work. Accommodating uncertainty in policy design is a challenging task, since the process optimization solution is obtained based on previously estimated parameter values, where uncertainties are unavoidable. A more rigorous optimization strategy would be based on online process optimization where uncertainty of parameters can be significantly reduced. Realization of this improvement will rely on the development of online monitor systems and incorporation of "soft sensors" from model prediction. Performance of model-based optimization can be improved by such advances for complex polymer manufacture.

In summary, model-based optimization is a rich field to explore. Advanced nonlinear programming tools and more sophisticated process modeling strategies will help to facilitate innovative developments in many different ways.

A. Appendix

A.1. Notation

a_0^l =   partial molar volume coefficient of species l, $m^3 \cdot \text{mol}^{-1}$

a_1^l =   partial molar volume coefficient of species l, $m^3 \cdot \text{mol}^{-1}$

A_1 =   first order gel factor coefficient, $2.57 - 5.05 \times 10^{-3} \cdot \text{T} \cdot \text{K}^{-1}$

A_2 =   second order gel factor coefficient, $9.56 - 1.76 \times 10^{-2} \cdot \text{T} \cdot \text{K}^{-1}$

A_3 =   third order gel factor coefficient, $-3.03 + 7.85 \times 10^{-2} \cdot \text{T} \cdot \text{K}^{-1}$

C_l =   concentration of species l, $\text{mol} \cdot L^{-1}$

$\bar{C}_n$ =   number average chain length

C_{PS} =   concentration of polystyrene, $\text{mol} \cdot L^{-1}$

$\bar{C}_w$ =   weight average chain length

C_{X_2} =   concentration of peroxide, $\text{mol} \cdot L^{-1}$

$C_{X\bullet}$ =   concentration of peroxide primal radical, $\text{mol} \cdot L^{-1}$

D_l =   effective diffusion coefficient for species l, $m^2 \cdot s^{-1}$

f =   fraction

$F_l(t)$ =   molar absorption rate of reactant l by each particle, $\text{mol} \cdot s^{-1}$

$\mathbb{F}_l(t)$ =   molar feeding rate of reactant l to the reactor, $\text{mol} \cdot s^{-1}$

g^C =   the lowest grid defining a gel, referring to the critical gel size

I =   Initiator species

J =   diffusion flux, $\text{mol} \cdot m^{-2} \cdot s^{-1}$

L_i =   chain length of the ith section divider

L_{max} =   maximum chain length of the section divider

M   =   monomer species

M_0 =   average molecular weight of polymer segments

$\bar{M}_A$ =   average molecular weight of the repeating unit of polymer A, $\text{g} \cdot \text{mol}^{-1}$

$\bar{M}_B$ =   average molecular weight of the repeating unit of polymer B, $\text{g} \cdot \text{mol}^{-1}$

$\overline{Mn}$ =   number average molecular weight, $\text{g} \cdot \text{mol}^{-1}$

$\overline{Mw}$	=	weight average molecular weight, $\mathrm{g} \cdot \mathrm{mol}^{-1}$
$\overline{Mn_r}$	=	number average molecular weight at particle radius position r , $\mathrm{g} \cdot \mathrm{mol}^{-1}$
$\overline{Mw_r}$	=	weight average molecular weight at particle radius position r , $\mathrm{g} \cdot \mathrm{mol}^{-1}$
N_g	=	number of grids
$\mathbb{N}_{seed}$	=	total number of seed particles in the reactor
k_{bA}	=	rate constant of polymer A chain scission, s^{-1}
k_{bB}	=	rate constant of polymer B chain scission, s^{-1}
k_{fb}	=	rate constant of hydrogen abstraction from polymer A by radical B, $m^3 \cdot \mathrm{mol}^{-1} \cdot s^{-1}$
k_{fs}	=	rate constant of polystyrene chain transfer rate, $m^3 \cdot \mathrm{mol}^{-1} \cdot s^{-1}$
k_I	=	rate constant of peroxide dissociation, $m^3 \cdot \mathrm{mol}^{-1} \cdot s^{-1}$
k_{IM}	=	rate constant of initiation of monomer double bond, $m^3 \cdot \mathrm{mol}^{-1} \cdot s^{-1}$
k_{HA}	=	rate constant of hydrogen abstraction from polymer A by peroxide radical, $m^3 \cdot \mathrm{mol}^{-1} \cdot s^{-1}$
k_{ha1}	=	rate constant of reversible hydrogen abstraction for polymer A, $m^3 \cdot \mathrm{mol}^{-1} \cdot s^{-1}$
k_{ha2}	=	rate constant of reversible hydrogen abstraction for radical A, $m^3 \cdot \mathrm{mol}^{-1} \cdot s^{-1}$
k_{HB}	=	rate constant of hydrogen abstraction from polymer B by peroxide radical, $m^3 \cdot \mathrm{mol}^{-1} \cdot s^{-1}$
k_{hb1}	=	rate constant of reversible hydrogen abstraction for polymer B, $m^3 \cdot \mathrm{mol}^{-1} \cdot s^{-1}$
k_{hb2}	=	rate constant of reversible hydrogen abstraction for radical B, $m^3 \cdot \mathrm{mol}^{-1} \cdot s^{-1}$
k_t	=	rate constant of polystyrene radical termination, $m^3 \cdot \mathrm{mol}^{-1} \cdot s^{-1}$
k_{ta}	=	rate constant of radical A termination, $m^3 \cdot \mathrm{mol}^{-1} \cdot s^{-1}$
k_{ta}^0	=	rate constant of radical A termination in ideal system without a gel effect, $m^3 \cdot \mathrm{mol}^{-1} \cdot s^{-1}$
k_{tca}	=	rate constant of radical A combination termination, $m^3 \cdot \mathrm{mol}^{-1} \cdot s^{-1}$
k_{tca}^0	=	rate constant of radical A combination termination in ideal system without a gel effect, $m^3 \cdot \mathrm{mol}^{-1} \cdot s^{-1}$
k_{tcb}	=	rate constant of radical B combination termination, $m^3 \cdot \mathrm{mol}^{-1} \cdot s^{-1}$
k_{tcb}^0	=	rate constant of radical B combination termination in ideal system without a gel effect, $m^3 \cdot \mathrm{mol}^{-1} \cdot s^{-1}$
k_{tda}	=	rate constant of radical A disproportion termination, $m^3 \cdot \mathrm{mol}^{-1} \cdot s^{-1}$

k_{tda}^0 = rate constant of radical A disproportion termination in ideal system without a gel effect, $m^3 \cdot mol^{-1} \cdot s^{-1}$

k_{th} = rate constant of styrene thermal initiation, $m^6 \cdot mol^{-2} \cdot s^{-1}$

k_p = rate constant of styrene polymerization, $m^3 \cdot mol^{-1} \cdot s^{-1}$

k_Q = a class of rate constants which are molecular weight dependent

κ_Q = rate constant of chain length 1 accordingly

P = Pressure, Pa

$P(s)$ = terminated polymer (dead polymer) with s repeating unit

$p(s)$ = concentration of $P(s)$, $mol \cdot L^{-1}$

$p^{(i)}$ = concentration of ith moment of polymer P, $mol \cdot L^{-1}$

R = particle radius, m

r = Intra-particle radial position, m

$R^{\bullet}(s)$ = polymer radical (live polymer) with s repeating unit

$r(s)$ = concentration of $R^{\bullet}(s)$, $mol \cdot L^{-1}$

$r^{(i)}$ = concentration of ith moment of radical $R^{\bullet}$, $mol \cdot L^{-1}$

s = number of repeat units in polymer

t = time, s

t_I = duration of the Stage I, s

t_{II} = duration of the Stage II, s

v_l = consumption rate of species l, $mol \cdot m^{-3} \cdot s$

V = volume of the system, m^3

$\overline{V}_l$ = partial molar volume of species l, m^3

w_{gel} = weight of gel content, g

w_{total} = total weight of polymer, g

X_2 = peroxide species

$X^{\bullet}$ = primal radial generated by peroxide dissociation

x_s = styrene monomer conversion ratio

$\bar{x}_s$ = overall monomer conversion ratio of the particle

z_i = representative chain length in the ith grid

Greek letters

α = adjustable parameter for rate constant of termination combination

γ_g = grafting ratio

δ_i = Kronecker delta function. If $i = 0$, $\delta_i = 1$; if $i \neq 0$, $\delta_i = 0$.

μ_i = i^{th} moment of either polymer A or polymer B

$\Gamma(n, n')$ = kernel function of R_{gB} chain scission, which is the probability producing a fragment of chain length n radical $R_{gB}^{\bullet}(n)$ from a chain length n' radical $R_{gB}^{\bullet}(n')$

$\Omega(n, n')$ = kernel function of R_B chain scission, which is the probability producing a fragment of chain length n radical $R_B^{\bullet}(n)$ from a chain length n' radical $R_B^{\bullet}(n')$

Subscripts and superscripts

A = crosslinked polymer, polyethylene in the studied case

B = linear polymer, linear polystyrene in the studied case

AgB = polymer A with grafted component B

gB = grafted component, grafted-polystyrene in the studied case

gel = gel content

g = grade

(i) = i^{th} moment of the distribution

(i) = i^{th} grid (italic)

L = lower bound

P_1 = seed polymer

P_2 = in situ polymerized polymer

U = upper bound

Bibliography

Adolph, V. and Wayne, P. 1987. Modified styrenic polymer beads. *4652609* U.S., Mar 1987. Patent.

Adolph, V. and Wayne, P. 1987. Process for producing modified styrenic polymer beads of high strength foamable articles. *4659745* U.S., 1987. Patent.

Advani, S. G. and Sozer, E. M. 2002. Process modeling in composites manufacturing. New York Basel : Marcel Dekker, Inc., 2002.

Alizadeh, M., et al. 2004. Modelling of fluidized bed reactor of ethylene polymerization. *Chem. Eng. J.* 2004, Vol. 97, pp. 27-35.

Almeida, A., Wada, K. and Secchi, A. 2007. Simulation of styrene polymerization reactions: kinetic and thermodynamic modeling. *Braz. J. Chem. Eng.* 2007, Vol. 25, pp. 337-349.

Andrzejewska, E., et al. 2005. Chain length dependent termination in radical cross-linking polymerization. *Macromolecules.* 2005, Vol. 46, 15, pp. 5437-5446.

Arai, K. and Saito, S. 1976. Simulation model for the rate of bulk polymerization over the complete course of reaction. *J. Chem. Eng. Jpn.* 1976, Vol. 4, pp. 302-313.

Arzamendi, G. and Asua, J. M. 1995. Modeling gelation and sol molecular weight distribution in emulsion polymerization. *Macromolecules.* 1995, Vol. 28, pp. 7479-7490.

Asteasuain, M., Sarmoria, C. and Brandolin, A. 2002a. Peroxide modification of polyethylene. Prediction of molecular weight distribution by probability generating functions. *Polymer.* 2002, Vol. 43, 8, pp. 2363-2373.

Asteasuain, M., Sarmoria, C. and Brandolin, A. 2002b. Recovery of molecular weight distributions from transformed domains. Part I: Application of pgf to mass balances describing reactions involving free radicals. *Polymer.* 2002, Vol. 43, pp. 2513-2527.

Aster, R., Borchers, B. and Thurber, C. 2005. *Parameter estimation and inverse problems.* Third. s.l. : Elsevier Academic Press, 2005.

Asua, J. M., et al. 2004. Critically evaluated rate coefficients for free-radical polymerization, 5. *Macromol. Chem. Physic.* 2004, Vol. 205, 16, pp. 2151-2160.

Asua, J. 2007. *Polymer reaction engineering.* s.l. : Willey-Blackwell, 2007.

Athawale, V. D. and Raut, S. S. 2002. New interpenetrating polymer networks based on uralkyd/poly(glycidylmethacraylate). *Eur. Polym. J.* 2002, Vol. 38, pp. 2033-2040.

Averick, B. M., Carter, R. G. and MoršŠ, J. J. 1991. The Minpack-2 test problem collection. 1991.

Aylsworth, J. W. 1914. Superior-sounding disc (molded phenol and formaldehyde mixed with wood-flour and a solvent into a heat-resistant disc). *1111284* U.S., 1914.

Bailagou, P. E. and Soong, D. S. 1985. Major factors contributing to the nonlinear kinetics of free radical polymerization. *Chem. Eng. Sci.* 1985, Vol. 40, pp. 87-104.

Ballard, M. J., Napper, D. H. and Gilbert, R. G. 1984. Kinetics of emulsion polymerization of methy methacrylate. *J. Polym. Sci: Polym. Chem.* 1984, Vol. 22, 11, pp. 3225-3253.

Bamford, C. H. and Jenkins, A. D. 1960.. 1960. The coupling of polymers. Part 1. - Size distributions and intrinsic viscosities. 1960, Vol. 56, pp. 907-931.

Bard, Y. 1974. *Nonlinear parameter estimation.* s.l. : Academic Press, New York and London, 1974.

Barton, R. 1994. Kriging interpolation in simulation: a state of art review. *Proceedings of the 1994 Winter Simulation Conference.* 1994.

Batte, A., et al. 1999. Calculation of molecular weight distributions in free-radical polymerization with chain branching. *Macromol. Theor. Simul.* 1999, Vol. 8(5), pp. 498-512.

Beattie, S. D. and Lin, D. K. 1997. *Designing computer experiments: rotated factorial designs.* s.l. : Department of Statistics, The Pennsylvania State University, University Park, PA., 1997.

Beck, J. V. and Arnold, K. J. 1977. *Parameter estimation in engineering and science.* s.l. : Addison-Wesley Publishing Company, 1977.

Berchtold, K. A., et al. 2001. The significance of chain length dependent termination in cross-linking polymerizations. *Polymer.* 2001, Vol. 42, 11, pp. 4925-4929.

Beuermann, S., et al. 1997. Critically evaluated rate coefficients for free-radical polymerization, 2. Propagation rate coefficients for methyl methacrylate. *Macromol. Chem. Physic.* 1997, Vol. 198, 5, pp. 1545-1560.

Biegler, L. T. 2007. A Survey of simultaneous dynamic optimization strategies. *Chem. Eng. Process.* 2007, Vol. 46, pp. 1043--1053.

Biegler, L. T. 2002. Advances in simultaneous strategies for dynamic process optimization. *Chem. Eng. Sci.* 2002, Vol. 57, pp. 575-593.

Biegler, L. T. 2007. An overview of simultaneous strategies for dynamic optimization. *Chem. Eng. Process.* 2007, Vol. 46, pp. 1043-1053.

Biegler, L. T., Grossmann, I. E. and Westerberg, A. W. 1985. A note on approximation technique used for process optimization. *Chemput. Chem. Eng.* 1985, Vol. 9, pp. 201-206.

Bokis, C. P., Ramanathan, S. and Franjione, J. 2002. Physical properties, reactor modeling, and polymerization kinetics in the low-density polyethylene tubular reactor process. *Ind. Eng. Chem. Res.* 2002, Vol. 41, pp. 1017-1030.

Bovey, F. and Kolthoff, I. 1950. Mechanism of emulsion polymerizations. iv. kinetics of polymerization of styrene in water and detergent solutions. *J. Polym. Sci. Pol. Chem.* 1950, Vol. 5, p. 487.

Box, G. E., et al. 1973. Some problems associated with the analysis of multiresponse data. *Technometrics.* 1973, Vol. 15, 1, p. 33.

Brandolin, A. and Sarmoria, C. 2004. Prediction of molecular weight distributions by probability generating functions. Application to industrial autoclave reactors for high pressue polymerization of ethylene and ethylene-vinyl acetate. *Polym. Eng. Sci.* 2004, Vol. 41, 8, pp. 1413-1426.

Brun, R., Reichert, P. and Kunsch, H. R. 2001. Practical identifiability analysis of large environmental simulation models. *Water Resour. Res.* 2001, Vol. 37, pp. 1015-1030.

Buchelli, A., et al. 2005. Modeling fouling effects in LDPE tubular polymerization reactors. 1. Fouling thickness determination. *Ind. Eng. Chem. Res.* 2005, Vol. 44, 5, pp. 1474-1479.

Budde, U. and Wulkow, M. 1991. Computation of molecular weight distributions for free radical polymerization systems. *Chem. Eng. Sci.* 1991, Vol. 46, p. 549.

Burgos, J. M. and Horne, J. K. 2007. Sensitivity analysis and parameter selection for detecting aggregations in acoustic data. *ICES J. Mar. Sci.* 2007, Vol. 64, 1, pp. 160-168.

Byrd, R. H., Lu, P. and Nocedal, J. 1995. A limited memory algorithm for bound constrained optimization. *SIAM J. Sci. Stat. Comp.* 1995, Vol. 16, 5, pp. 1190-1208.

Caballero, J. A. and Grossmann, I. E. 2008. An algorithm for the use of surrogate models in modular flowsheet optimization. *AICHE J.* 2008, Vol. 54, 10, pp. 2633-2650.

Camacho, E. and Bordons, C. 2007. Nonlinear model predictive control: an introductory review. *Assessment and Future Directions of Nonlinear Model Predictive Control.* s.l. : Springer Berlin / Heidelberg, 2007. Vol. 358, pp. 1-16.

Canu, P. and Ray, W H. 1991. Discrete weighted residual methods applied to polymerization reactions. *Comput. Chem. Eng.* 1991, Vol. 15, 8, pp. 549-564.

Cartis, C., Gould, N. I. M. and Toint. Ph. L. 2009. An adaptive cubic regularization algorithm for nonconvex optimization with convex constraints and its function evaluation complexity. *Technique Report.* 2009.

Casey, B. S., et al. 1992. Effects of diffusion control on the propagation and transfer rate coefficients in free radical polymerization. *Macromolecules.* 1992, Vol. 25, pp. 7063-7065.

Chaimberg, M and Cohen, Y. 1990. Kinetic modeling of free-radical polymerization: a conservational polymerization and molecular weight distribution model. 1990, Vol. 29, p. 1152.

Chen, Chau-Chyun. 2002. An industry perspective on polymer process modeling. *CAST Communications.* 2002.

Cherbanski, R., Milewska, A. and Molga, E. 2007. Saftety aspects in batch reactors for styrene suspension polymerization. *Ind. Eng. Chem. Res.* 2007, Vol. 46, 18, pp. 5898-5906.

Cheung, P. C. and Balke, S. T. 1997. Reactive extrusion of polypropylene/polyethylene blends: kinetic model development. *Ind. Eng. Chem. Res.* 1997, Vol. 36, pp. 1191-1201.

Chiu, W. Y., Carratt, G. M. and Soong, D. S. 1983. A computer model for the gel effect in free-radical polymerization. *Macromolecules.* 1983, Vol. 16, 3, pp. 348-357.

Choi, K. Y. 1993. Modeling of polymerization processes. [book auth.] C. J. Pereira and E. R. Becker. *Compter Aided Catalyst Design.* New York : Marcel-Dekker, 1993, pp. 335-387.

Chu, Y. and Hahn, J. 2007. Parameter set selection for estimation for nonlinear dynamic systems. *AICHE J.* 2007, Vol. 53, 11, pp. 2858-2870.

Chylla, R. W. and Haase, R. 1993. Temperature control of semibatch polymerization reactors. *Comput. Chem. Eng.* 1993, Vol. 17, 3, pp. 257-264.

Crowley, T. J. and Choi, K. Y. 1997. Calculation of molecular weight distribution from molecular weight moments in free radical polymerization. I*nd. Eng. Chem. Res.* 1997, Vol. 36, pp. 1419-1423.

Crowley, T. J., et al. 2000. Control of particle size distribution described by a population balance model of semibatch emulsion polymerization. *J. Process Contr.* 2000, Vol. 10, 5, pp. 419-432.

Curteanu, S. 2003. Modeling and simulation of free radical polymerization of styrene under semibatch reactor conditions. *Cent. Eur. J.* 2003, Vol. 1, pp. 69-90.

Davis, E. F. 2008. *Modeling and Optimization of Process Engineering Problems Containing Black-Box Systems and Noise.* Ph.D. thesis, the State University of New Jersey. 2008.

de Gennes, P. G. 1982a. Kinetics of diffusion-controlled processes in dense polymer systems. I. Nonentangled regimes. *J. Chem. Phys.* 1982a, Vol. 76, p. 3316.

de Gennes, P. G.. 1982b. Kinetics of diffusion-controlled processes in dense polymer systems. II. Effects of entanglements. *J. Chem. Phys.* 1982b, Vol. 76, p. 3322.

Denbigh, K G. 1947. Continuous reactions. Part II. The kinetics of steady state polymerisation. *Trans. Faraday. Soc.*1947, Vol. 43, p. 648.

Deuflhard, P. and Wulkow, M. 1989. Computational treatment of polyreaction kinetics by orthogonal polynomials of a discrete variable. *IMPACT Comput. Sci. Eng.* 1989, Vol. 1, p. 269.

Dolan, E. D. and MoršŠ, J. J. 2000. Benchmarking optimization software with COPS. 2000.

Dovi, V. G. and Paladino, O. 1989. Fitting of experimental data to implicit models using a constrained variation algorithm. *Comput. Chem. Eng.* 1989, Vol. 13, pp. 731-735.

Doyle, F. J., Harrison, C. A. and Crowley, T. J. 2003. Hybrid model-based approach to batch-to-batch control of particle size distribution in emulsion polymerization. *Comput. Chem. Eng.* 2003, Vol. 27, pp. 1153-1163.

Dube, M. A., et al. 1997. Mathematical modelling of multicomponent chain-growth polymerization in batch, semi-batch and continuous reactors: a review. *Ind. Eng. Chem. Res.* 1997, Vol. 36, 4, pp. 966-1015.

Duerksen, J. H. and Hamielec, A. E. 1968. Polymer reactors and molecular weight distribution. IV. Free-radical polymerization in a steady-state stirred-tank reactor train. *J. Polym. Sci. Pol. Lett.* 1968, Vol. C25, p. 155.

Eriksson, J. 1996. Optimization and regularization of nonlinear least squares problems. *Ph.D. Dissertation, Umeå University, Umeå, Sweden.* 1996.

Faber, R., Li, P. and Wozny, G. 2003. Sequential parameter estimation for large-scale systems with multiple data sets. 1. Computational framework. *Ind. Eng. Chem. Res.* 2003, Vol. 42, pp. 5850-5860.

Fang, K. T. and Wang, Y. 1996. *Number-Theoretical Methods in Statistics.* Beijing, China : Scientific Publishing Inc., 1996.

Fiorentino, Stefano. 1997. Nonlinear chain-length distributions in free-radical polymerization. *Ind. Eng. Chem. Res.* 1997, Vol. 36, pp. 1283-1301.

Flory, P J. 1936. Molecular size distribution in linear condensation polymers. *J. Am. Chem. Soc.* 1936, Vol. 58, p. 1877.

Flory, P J. 1953. *Principles of Polymer Chemistry.* s.l. : Cornell University Press, Ithaca, 1953.

Friis, N. and Hamielec, A. E. 1976. Gel effect in emulsion polymerization of vinyl monomers. *ACS Symp. Ser.* 1976, Vol. 24, pp. 82-91.

Frisch, H. L. 1985. Interpenetrating polymer networks. *Brit. Polym. J.* 1985, Vol. 17, 2, pp. 149-153.

Frisch, K. C., et al. 1974. Morphology of a polyurethane-polyacrylate interpenetrating polymer networks. *Polym. Eng. Sci.* 1974, Vol. 14, 1, p. 76.

Ghosh, P., Chattopadhyay, B. and Sen, A. K. 1998a. Modification of low density polyethylene (LDPE) by graft copolymerization with some acrylic monomers. *Polymer.* 1998a, Vol. 39, pp. 193-201.

Ghosh, P., Gupta, S. K. and Saraf, D. N. 1998b. An experimental study on bulk and solution polymerization of nethy methacrylate with responses to step changes in temperature. *Chem. Eng. J.* 1998b, Vol. 70, pp. 25-35.

Gilbert, R. 1992. Consistent values of rate parameters in free radical polymerization systems. *Pure Appl. Chem.* 1992, Vol. 64, pp. 1563-1567.

Goel, T., et al. 2008. Comparison of surrogate models for turbomachinery design. *Wseas Trans. Fluid Mech.* 2008, Vol. 3, 1, pp. 10-1007.

Goel, T., et al. 2007. Ensemble of multiple surrogates. *Struct. Multidiscip. O.* 2007, Vol. 33(3), pp. 199-216.

Gonçalves, O., et al. 2009. Secondary particle formation in seeded suspension polymerization. *Polymer.* 2009, Vol. 50, pp. 375-381.

Gonçalves, O., et al. 2008. Synthesis of PS/PMMA core-shell structured particles by seeded suspension polymerisation. *Macromolecules.* 2008, Vol. 41, pp. 6960-6964.

Gondzio, J. and Grothey, A. 2004. Exploiting structure in parallel implementation of interior-point method for optimization. *Technical Report MS-04-004, School of Mathematics, The University of Edinburgh.* 2004.

Grosser, J. H., Doherty, M. F. and Malone, M. F. 1987. Modeling of reactive distillation systems. *Ind. Eng. Chem. Res.* 1987, Vol. 26, pp. 983-989.

Gu, H., et al. 2009. Surrogate models for shape optimization of underwater glider. *Proceedings of the 1994 Winter Simulation Conference.* 2009.

Gupta, N. and Srivastava, A. K. 1994. Interpenetrating polymer networks: a review on synthesis and properties. *Polym. Int.* 1994, Vol. 35, 2, pp. 109-118.

Halton, J. H. 1960. On the efficiency of certain quasi-random sequences of points in evaluating multi-dimensional integrals. *Numer. Math.* 1960, Vol. 2, pp. 84-91.

Hamielec, A. E., et al. 1991. Kinetics of free radical modification of polyolefins in extruders - chain scission, crosslinking and grafting. *Can. J. Chem. Eng.* 1991, Vol. 69, pp. 611-618.

Hamielec, A. E. 1987. Polymer reactors and molecular weight distribution: Part II. Free radical polymerization in a batch reactor. *AICHE J.* 1967, Vol. 13, 6, pp. 1087-1091.

Hammersley, J. 1960. Monte Carlo Methods For Solving Multivariable Problems. *Proceedings of the New York Academy of Science.* 1960, Vol. 86, pp. 844--874.

Hong, S. and Duda, J. L. 1996. Penetrate Transport in Polyethylene-Polystyrene Semi-Interpenetrating Polymer Networks. *J. of Appl. Polym. Sci.* 1996, Vol. 65, pp. 51--57.

Huang, W., Phoomboplab, T. and Ceglarek, D. 2009. Process capability surrogate model-based tolerance synthesis for multi-station manufacturing systems. *IIE Trans.* 41, 2009, pp. 302-322.

Hui, A. W. and Hamielec, A. E. 1972. Thermal polymerization of styrene at high conversions and temperatures. An experiment study. *J. of Appl. Polym. Sci.* 1972, Vol. 16(3), pp. 749-769.

Huskic, M. and Sebenik, A. 1993. Characterization of crosslinked ethylene-vinylacetate copolymers. *Polym. Int.* 1993, Vol. 31, 1, pp. 41-44.

Ito, K. 1980. Estimation of molecular weight in terms of the gel effect in radical polymerization. *Polym. J.* 1980, Vol. 12, 8, pp. 499-506.

Kahovec, J., et al. 1997. Source-based nomenclature for non-linear macromolecules and macromolecular assemblies. *Pure Appl. Chem.* 65, 1997, p. 2511.

Kajimura, M. and Kaisha, S. 1981. Process for producing expandable thermoplastic resin beads using polypropylene as nucleus. *4303757* U.S., Dec 1981. Patent.

Kalagnanam, J. R. and Diwekar, U. M. 1997. An efficient sampling technique for off-line quality control. *Technometrics.* 1997, Vol. 39, 3, pp. 308-319.

Kameswaran, S. and Biegler, L. T. 2006. Simultaneous dynamic optimization strategies: recent advances and challenges. *Comput. Chem. Eng.* 2006, Vol. 30, pp. 1560--1575.

Karypis, G. and Kumar, V. 1999. A fast and high quality multilevel scheme for partitioning irregular graphs. *SIAM J. on Sci. Comput.* 1999, Vol. 20, pp. 359--392.

Keramopoulos, A. and Kiparissides, C. 2002. Development of a comprehensive model for diffusion-controlled free-Radical copolymerization reactions. *Macromolecules.* 2002, Vol. 35, pp. 4155-4166.

Kichatov, B. V., Korshunov, A. M. and Assorova, P. V. 2003. Particle size distribution of the product of suspension polymerization. *Theor. Found. Chem. Eng.* 2003, Vol. 37, 3, pp. 306-309.

Kim, D. H. and Kim, S. C. 1984. Dicumyl peroxide-initiated crosslinking reaction of low density polyethylene. *Polym. Soc. Kor.* 1984, Vol. 8(1), pp. 44-52.

Kim, I. W, Liebmann, M. J. and Edgar, T. F. 1990. Robust error-in-variables estimation using nonlinear programming techniques. *AICHE J.* 1990, Vol. 36, 7, pp. 985-993.

Kim, Y. C. and McCoy, B. J. 2000. Degradation kinetics enhancement of polystyrene by peroxide addition. *Ind. Eng. Chem. Res.* 2000, Vol. 39, pp. 2811-2816.

Kimura, T. 1962. Molecular weight distribution of irradiated polymers. *J. Phys. Soc. Jpn.* 1962, Vol. 17, 12, pp. 1884-1890.

Kiparissides, C. 1996. Polymerization reactor modeling: a review of recent developments and future directions . *Chem. Eng. Sci.* 1996, Vol. 51, pp. 1637-1659.

Kiparissides, C. 2006. Challenges in particulate polymerization reactor modeling and optimization: a population balance perspective. *J. Process Control* 2006, Vol. 16, 3, pp. 205-224. Selected Papers from Dycops 7 (2004), Cambridge, Massachusetts.

Kitamori, Y. 1979. Process for producing foamable polyethylene resin. *4168353* U.S., Feb 1979. Patent.

Kitamori, Y. 1976. Process for Producing Polyethylene Resin Particles and Foamable Polyethylene Resin Particles . *3959189* U.S., 1976. Patent.

Kleijnen, J. P. C. 2009. Kriging Metamodeling in Simulation: A Review. *Eur. J. Oper. Res.* 2009, Vol. 192, pp. 707-716.

Klempner, D. and Frisch, K. C. 1994. *Advances in Interpenetrating Polymer Networks.* s.l. : Technomic Publishing AG, Lancaster, 1994.

Kobayashi, S. and Nakamura, M. 1985. *Process for preparing modified polyolefin particles and foamed article made from the particles. 4525486* U.S., Jun 1985. Patent.

Krallis, A., Pladis, P. and Kiparissides, C. 2007. Prediction of the bivariate molecular weight-long chain branching distribution in high-pressure low-density polyethylene *Autoclaves.* 2007, Vol. 16, 6, pp. 593-609.

Krige, D. 1951. *A statistical approach to some mine valuations and allied problems at the Witwatersrand.* Master's thesis. the Univ. Witwatersrand. 1951.

Kruse, T. M., et al. 2002. Mechanistic modeling of polymer degradation: a comprehensive study of polystyrene. *Macromolecules.* 2002, Vol. 35(20), pp. 7830-7844.

Kuhn, W. 1930. On the kinetics of reduction of high molecular weight chains. *Chemische Berichte.* 1930, Vol. 63, p. 1502.

Kumar, S. and Ramkrishna, D. 1996. On the solution of population balance equations by discretization ─ I. A fixed pivot technique. Chem. Eng. Sci. 1996, Vol. 51(8), pp.1311-1332.

Laird, C. D. and Biegler, L. T. 2008. Large-scale nonlinear programming for multi-scenario optimization. [book auth.] H. G. Bock, E. Kostina and H-X Phu. *Modeling, Simulation and Optimization of Complex Processes.* s.l. : Springer, 2008, pp. 323-336.

Lee, S., Yoon, J. and Park, D. 2002. Catalytic degradation of mixture of polyethylene and polystyrene. *J. Ind. Eng. Chem.* 2002, Vol. 8, 2, pp. 143-149.

Lenzi, M., et al. 2005. Modeling of semibatch styrene suspension polymerization processes. *J. Appl. Polym. Sci.* 2005, Vol. 96, pp. 1950-1967.

Li, R. 2003. *Dynamic Modeling and Parameter Estimation for An Ethylene-Propylene-Diene Polymerization Process* . Louisiana State University. Baton Rouge,LA USA : s.n., 2003.

Likozar, B. and Krajnc, M. 2009. Simulation of chemical kinetics of elastomer crosslinking by organic peroxides. *Polym. Eng. Sci.* 2009, Vol. 49, 1, pp. 60-72.

Lin, C. and More, J. J. 1999. Newton's method for large bound-constrained optimization problems. *SIAM J. Optim.* 1999, Vol. 9, pp. 1100-1127.

Liu, S. and Amundson, N. R. 1961. Analysis of polymerization kinetics and the use of a digital computer. *Rubber Chem. Technol.* 1961, Vol. 34, p. 995.

Lootsma, F. A. and Ragsdell, K. M. 1987. State-of-the-art in parallel nonlinear optimization. *Parallel Comput.* 1987, Vol. 6, pp. 133-155.

Lophaven, S. N., Nielsen, H. B. and Sondergaard, J. 2002a. DACE: A Matlab Kriging toolbox, version 2.0. . *IMM Technical University of Denmark, Lyngby.* 2002.

Lophaven, N.S., Nielsen, H. B. and Sondergaard, J. 2002b. Aspects of the Matlab toolbox DACE. 2002b.

Lund, B. and Foss, B. 2008. Parameter ranking by orthogonalization-applied to nonlinear mechanistic models. *Automatica.* 2008, Vol. 44, 1, pp. 278-281.

Marten, F. L. and Hamielec, A. E. 1979. High conversion diffusion-controlled polymerization. *ACS Symp. Ser.* 1979, Vol. 104, pp. 43-70.

Martin, J. D. and Simpson, T. W. 2004. On the use of Kriging models to approximate determinstic computer models. *ASME 2004 International Design Engineering Technical Conferences and Computers and Information in Engineering Conference.* 2004.

Maschio, G and Scali, C. 1999. Analysis of the molecular weight distribution in free radical polymerization: modelling of the MWD from the analysis of experimental GPC curves. 1999, Vol. 200, pp. 1708-1721.

Matsumura, H. and Matsugashita, T. 2007. Styrene-modified particle of linear low-density polyethylene resin, expandable styrene-modified particle of linear low-density polyethylene resin, processes for producing these, pre-expanded particle, and molded foam. *1803752* EP, Jul 2007. Patent.

Matsumura, H. and Yasutaka, T. 2006. Expandable resin beads of styrene-modified straight-chain and low-density polyethylene, process for production thereof, pre-expand beads, and foams. *20060058406* U.S., Mar 2006. Patent.

Matyjaszewski, K., Gnanou, Y. and Leibler, L. 2007. *Macromolecular Engineering: Precise Synthesis, Materials Properties, Applications.* s.l. : Wiley-VCH, 2007.

Mccaffery, W. C., et al. 1996. Thermolysis of polyethylene/polystyrene mixtures. *J. Appl. Polym. Sci.* 1996, Vol. 60, pp. 2133-2140.

McCoy, B. J. and Madras, G. 2001. Discrete and continuous models for polymerization and depolymerization. *Chem. Eng. Sci.* 2001, Vol. 56, 8, pp. 2831-2836.

McKenna, T. F. and Soares, J. B. 2001. Single particle modeling for olefin polymerization on supported catalysts: a review and prodosals for future development. *Chem. Eng. Sci.* 2001, Vol. 56, pp. 3931-3949.

Meyer, T. and Keurentjes, J. 2005. *Chapter 1. Polymer reaction engineering, an Integrated Approach.* Second. s.l. : Wiley-VCH, 2005.

Migdalas, A, Toraldo, G and Kumar, V. 2003. Nonlinear optimization and parallel computing. *Parallel Comput.* 2003, Vol. 29, pp. 375-391.

Millar, J. R. 1960. Interpenetrating polymer networks. styrene–divinylbenzene copolymers with two and three interpenetrating networks, and their sulphonates. *J. Chem. Soc.* 1960, pp. 1311-1317.

Miller, D. R. and Sarmoria, C. 1998. "In-out" recursive probability modeling of branched step-growth polymerizations. *J. Polym. Sci.* 1998, Vol. 38, 4.

Mills, P. 1986. Determination of polymer chain length distributions by numerical inversion of z-transforms. *Comput. Chem. Eng.* 1986, Vol. 10, pp. 399-420.

Montgomery, D. C., Peck, E. A. and Vining, G. G. 2001. *Introduction to Linear Regression Analysis.* Third. s.l. : John Wiley & Sons, Inc.,Hoboken, New Jersey, 2001.

Muske, K. R. and Georgakis, C. 2003. Optimal measurement system design for chemical processes. *AICHE J.* 2003, Vol. 49, 6, pp. 1488-1494.

Myung, D., et al. 2008. Progress in the development of interpenetrating polymer network hydrogels. *Polym. Adv. Technol.* 2008, Vol. 19, pp. 647-657.

Nagasubramanian, K. and Graessley, W. W. 1970. Continuous reactors in free radical polymerization with branching - theoretical aspects and preliminary considerations. *Chem. Eng. Sci.* 1970, Vol. 25, p. 1549.

Nordhus, H., Moen, O. and Singstad, P. 1997. Prediction of molecular weight distribution and long-chain branching distribution of low-density polyethylene from a kinetic model. *J. Macromol. Sci. A.* 1997, Vol. 34, 6, pp. 1017-1043.

Odian, George. 1981. *Principles of polymerization.* Second. s.l. : John Wiley & Sons, Inc.,New York, 1981.

Orlova, T. M., Pavlova, S. A. and Dubrovina, L. V. 1979. Statistical approach to the molecular weight distribution of condensation polymers. *J. Polym. Sc. Pol. Chem.* 1979, Vol. 17, 7, pp. 2209-2221.

Papavasiliou, G, Birol, I and Teymour, F. 2002. Calculation of molecular weight distributions in non-linear free-radical polymerization using the numerical fractionation technique. *Macromol. Theor. Simul.* 2002, Vol. 11, p. 533.

Papoulis, A. 1956. A new method of inversion of the laplace yransform. *Quart. Apply. Math.* 1956, pp. 405-414.

Pedernera, N. M., et al. 1999. An improved kinetic model for the peroxide initiated modification of polyethylene. *Polym. Eng. Sci.* 1999, Vol. 39(10), pp. 2085-2095.

Peter, J. and Marcelet, M. 2008. Comparison of surrogate models for turbomachinery design. *Wseas Trans. Flu. Mech.* 2008, Vol. 3, 1, pp. 10-17.

Pirnay, H., López-Negrete de la Fuente, R. and Biegler, L. T. 2011. Optimal sensitivity based on IPOPT. 2011.

Plessis, C., et al. 2001. Modeling of seeded semibatch emulsion polymerization of n-BA. *Ind. Eng. Chem. Res.* 2001, Vol. 40, p. 3883.

Qin, J., Guo, W. and Zhang, Z. 2002. Modeling of the bulk free radical polymerization up to high conversion—three stage polymerization model I. Model examination and apparent reaction rate constants. *Polymer.* 2002, Vol. 43, 4, pp. 1163-1170.

Ray, A. B., Saraf, D. N. and Gupta, S. K. 1995. Free radical polymerizations associated with Trommsdorff effect under semibatch reactor conditions, I. Modeling. *Polym. Eng. Sci.* 1995, Vol. 35, 6, pp. 1290-1299.

Ray, W. H. 1971. Molecular weight distributions in copolymer systems. I. Living coplymers. 1971, Vol. 4, pp. 161-165.

Ray, W. H. 1972. On the methmatical modeling of polymerization reactors. *Polymer Reviews.* 1972, Vol. 8, 1, pp. 1-56.

Reilly, P. M. and Patino-Leal, H. 1981. A Bayesian study of the error-in-variables model. *Technometrics.* 1981, Vol. 23, 3, p. 221.

Renaut, R. A., Hnětynková, I. and Mead, J. 2010. Regularization parameter estimation for large-scale Tikhonov regularization using a priori information. *Comput. Stat. Data An.* 2010, Vol. 54, 12, pp. 3430-3445.

Renfree, R. W., et al. 1999. *Dual Phase, Co-Continuous Morphology from Mixtures of Dual Phase, Co-Continuous Morphology from Mixtures of.* s.l. : the New Jersey Commission for Science and Technology, the Virginia Center for Innovative Technology., 1999.

Richards, J. R. and Congalidis, J. P. 2006. Measurement and control of polymerization reactors. *Comput. Chem. Eng.* 30, 2006, pp. 1447-1463.

Robertson, D. G., Russell, S. A. and Lee, J. H. 1995. Modeling and control of a batch condensation polymerization reactor. *Processings of the American Control Conference.* 1995, pp. 1746-1750.

Rod, V. and Hancil, V. 1980. Iterative estimation of model parameters when measurements for all variables are subject to error. *Comput. Chem. Eng.* 1980, Vol. 4, pp. 33-38.

Rothschild, B. J., et al. 1997. Estimating growth and mortality in state-structured populations. *J. Plankton Res.* 1997, Vol. 19, pp. 1913-1928.

Russell, G. T., Gilbert, R. G. and Napper, D. H. 1992. Chain-length-dependent termination rate processes in free-radical polymerizations. I. Theory. *Macromolecules.* 1992, Vol. 25, pp. 2459-2469.

Saito, O. 1958. Effects of high energy radiation on polymers II. end-linking and gel fraction. *J. Phy. Soc. Jpn.* 1958, Vol. 13, pp. 1451-1464.

Sakata, S., Ashida, F. and Zako, M. 2003. Structural optimization using Kriging approximation. *Comput. Meth. Appl. Mech. Eng.* 2003, Vol. 192, pp. 923-939.

Salamone, J. C. 1996. *Polymeric materials encyclopedia.* 1st. s.l. : CRC Press, US, 1996. Vol. 4.

Samsatli, N. J., Papageorgiou, L. G. and Shah, N. 1998. Robustness metrics for dynamic optimization models under parameter uncertainty. *AICHE J.* 1998, Vol. 44, 9, pp. 1547-5905.

Sandink, C. A., McAuley, K. B. and McLellan, P. J. 2001. Selection of parameters for updating in on-line models. *Ind. Eng. Chem. Res.* 2001, Vol. 40, pp. 3936–3950.

Sandland, N. W. and Sebborn, M. J. 1987. *CAD/CAM in the Polymer Industry.* Oxford : Pergamon Press, 1987.

Santner, T. J., Williams, B. J. and Notz, W. I. 2002. *The Design and Analysis of Computer Experiments .* New York, NY : Springer-Verlag, 2002.

Sen, A. K., et al. 1991. Studies on crosslinking of EPDM-PE blends by thermoanalytical techniques . 1991, Vol. 37, pp. 19-38.

Shyichuk, A. V. 1996. A way to gel-point determination. *Eur. Polym. J.* 1996, Vol. 32, 9, pp. 1167-1168.

Simon, D. 2006. *Optimal State Estimation: Kalman, H-infinity, and Nonlinear Approaches.* 1st. s.l. : John Wiley & Sons, 2006.

Simpson, T. W., et al. 1998. Comparison of response surface and Kriging models for multidisciplinary design optimization. *Technical Report. AIAA-98-4755*

Simpson, T. W. et al. 2001. Metamodels for computer-based engineering: survey and recommendation . *Eng. Comput.* 2001, Vol. 17, pp. 129-150.

Sivalingam, G. and Madras, G. 2004. Thermal degradation of poly(vinyl acetate) and poly(ϵ-caprolactone) and their mixtures in solution. *Ind. Eng. Chem. Res.* 2004, Vol. 43, pp. 1561-1567.

Soares, J. B. and Hamielec, A. E. 1995. Deconvolution of chain-length distributions of linear polymers made by multiple-site-type catalysts. 1995, Vol. 36, pp. 2257-2263.

Sobol, I. M. 1967. The Distribution of points in a cube and the accurate evaluation of integrals (in Russian). 1967, Vol. 7, pp. 784-802.

Sperling, L. H. 1981. *Interpenetrating Polymer Networks and Related Materials.* s.l. : Plenum Press, New York, 1981.

Sperling, L. H. 1994. *Interpenetrating Polymer Networks.* s.l. : American Chemical Society, Washington DC. 1994.

Sperling, L. H. 2004. Interpenetrating polymer networks. *Encyclopedia Of Polymer Science and Technology*. 2004, Vol. 10, pp. 272-311.

Srinivas, T., et al. 1996. Free radical polymerization associated with the Trommsdroff effect under semibatch reactor conditions, II: Experimental responses to step changes in temperature. *Polym. Eng. Sci.* 1996, Vol. 36, 3, pp. 311-312.

Staudinger, H. 1920. Über Polymerisation. *Ber. Deut. Chem. Ges.* 1920, Vol. 53, p. 1073.

Sterling, W. J., Kim, Y. C. and McCoy, J. B. 2001. Peroxide enhancement of poly(α - methylstyrene) thermal degradation. *Ind. Eng. Chem. Res.* 2001, Vol. 40, pp. 1811-1821.

Stevens, M. P. 1998. *Polymer Chemistry.* Third. s.l. : Oxford University Press, 1998.

Stubbs, J., Karlsson, O. and Jonsson, J. 1999. Non-equilibrium particle morphology development in seeded emulsion polymerization. 1: penetration of monomer and radicals as a function of monomer feed rate during second stage polymerization. *Colloid. Surfaces A.* 1999, Vol. 153, pp. 255-270.

Suwanda, D. and Balke, S. T. 1993. The reactive modification of polyethylene. II: Mathematical modeling. *Polym. Eng. Sci.* 1993, Vol. 33, 24, pp. 1592-1605.

Tai, H. J. 1999. Molecular structure evolution in peroxide-initiated crosslinking of an ethylene vinyl acetate copolymer and a metallocene polyolefin elastomer. *Polym. Eng. Sci.* 1999, Vol. 39, 9, pp. 1577-1583.

Tang, B. 1994. A theorem for selecting OA-based Latin Hypercubes using a distance criterion. *Commun. Stat-Thero. M.* 1994, Vol. 23, 7, pp. 2047-2058.

Tang, B. 1993. Orthogonal array-based Latin Hypercubes. *J. Amer. Statistical Assoc.* 1993, Vol. 88, 424, pp. 1392-1397.

Tefera, N., Weickert, G. and Westerterp, K. 1997. Modeling of free radical polymerization up to high conversion. I. a method for the selection of models by simultaneous parameter estimation. *J. Appl. Polym. Sci.* 1997, Vol. 63, pp. 1649--1661.

Teymour, F. and Campbell, J. D. 1994. Analysis of the dynamics of gelation in polymerization reactors using the "numerical fractionation" technique. *Macromolecules.* 1994, Vol. 27(9), pp. 2460-2469.

Tirrell, M. V., et al. 1975. Analysis of caprolactom polymerization. *Polym. Eng. Sci.* 1975, Vol. 15, p. 386.

Tjoa, I. B. and Biegler, L. T. 1991. Simultaneous strategies for data reconciliation and gross error detection of nonlinear systems. *Comput. Chem. Eng.* 1991, Vol. 15, 10, pp. 679-690.

Tjoa, I. B. and Biegler L. T. 1991. Simultaneous solution and optimization strategies for parameter estimation of differential-algebraic equation systems. *Ind. Eng. Chem. Res.* 1991, Vol. 30, 2, pp. 376-385.

Tjoa, I. B. and Biegler, L. T. 1992. Reduced successive quadratic programming strategy for errors-in-variables estimation. 1992, Vol. 16, 6, pp. 523-533.

Tobita, H. 1994. Kinetics of long-chain branching in emulsion polymerization: 2. vinyl acetate polymerization. *Macromolecules.* 1994, Vol. 35, pp. 3032-3038.

Tobita, H. 1995. Molecular weight distribution in random crosslinking of polymer chains. *J. Appl. Polm. B.* 1995, Vol. 33, 8, pp. 1191-1202.

Tobita, H., Takada, Y. and Nomura, M. 1995. Simulation model for the molecular weight distribution in emulsion polymerization. *J. Polym. Sci. A.* 1995, Vol. 33, 6, pp. 441-453.

Tobita, H. and Hamielec, A. E. 1989. Crosslinking Kinetics in free radical copolymerization. [book auth.] K. H. Reichert and W. Geiseler. *Polymer Reaction Engineering.* New York : s.n., 1989.

Tulig, T. J. and Tirrell, M. 1982. On the Onset of the Trommsdorff Effect. *Macromolecules.* 1982, Vol. 15, 2, pp. 459-463.

Vajda, S., et al. 1989. Qualitative and quantitative identifiability analysis of non-linear chemical kinetic models. *Chem. Eng. Commun..* 1989, Vol. 82, pp. 191--219.

van der Hoff, B. M. E. 1958. The gel effect at low conversion in emulsion polymerization. *J. Polym. Sci.* 1958, Vol. 33, 126, pp. 487-490.

Van, W. and Kleijnen, J. 2004. Kriging interpolation in simulation: a survey. *Proceedings of the 2004 Winter Simulation Conference.* 2004.

Velez-Reyes, M., and Verghese, G. C. 1995. Subset selection in identification, and application to speed and parameter estimation for induction machines. *Proceedings of the 4th IEEE Conference on Control Applications. Albany, NY.* 1995, pp. 991-997.

Verros, G. D. 2003. Calculation of molecular weight distribution in non-linear free radical copolymerization. *Polymer.* 2003, Vol. 44, 22, pp. 7021-7032.

Verros, G. D., Latsos, T. and Achilias, D. S. 2005. Development of a unified framework for calculating molecular weight distribution in diffusion controlled free radical bulk homo-polymerization. *Polymer.* 2005, Vol. 46, pp. 539-552.

Villa, C. M. 2007. Reactor modeling for polymerization process. *Ind. Eng. Chem. Res.* 46, 2007, pp. 5815-5823.

Vivaldo-Lima, E., Wood, P. E. and Hamielec, A. E. 1997. An updated review on suspension polymerization. *Ind. Eng. Chem. Res.* 36, 1997, Vol. 4, pp. 939-965.

Wächter, A. 2002. *An Interior Point Algorithm for Large-Scale Nonlinear Optimization with Applications in Process Engineering.* Carnegie Mellon University. Pittsburgh, PA USA : s.n., 2002.

Wächter, A. and Biegler, L. T. 2006. On the implementation of an interior-point filter line-search algorithm for large-scale nonlinear programming. *Math. Prog.* 2006, Vol. 106, pp. 25--57.

Weisberg, S. 2005. *Applied Linear Regression.* Third. s.l. : John Wiley & Sons, Inc.,Hoboken, New Jersey, 2005.

Wen, M., Scriven, L. E. and McCormick, A. V. 2003a. Kinetic gelation modeling: kinetics of cross-linking polymerization. *Macromolecules.* 2003a, Vol. 36, 11, pp. 4141-4159.

Wen, M., Scriven, L. E. and McCormick, A. V. 2003b. Kinetic gelation modeling: structural inhomogeneity during cross-linking polymerization. *Macromolecules.* 2003b, Vol. 36, 11, pp. 4140-4150.

Wulkow, M. 2008. Computer aided modeling of polymer reaction engineering - the status of Predici, 1 - Simulation. *Macro. React. Eng.* 2008, Vol. 2, 6, pp. 461-494.

Wulkow, M. 1996. The simulation of molecular weight distribution in polyreaction kinetics by discrete Galerkin Methods. *Macromol. Theory. Simul.* 1996, Vol. 5, p. 393.

Xie, T and Hamielec, A. E. 1993. Modelling free-radical copolymerization kinetics - evaluation of the pseudo-kinetic rate constant method, 2. Molecular weight calculations for copolymers with long chain branching. 1993, Vol. 2(3), pp. 455-483.

Xie, T. Y., et al. 1991. Experimental investigation of vinly chloride polymerization at high conversion: semi-batch reactor modeling. *Polymer.* 1991, Vol. 32, 1, pp. 2087-2095.

Xie, T., et al. 1994. Gas phase ethylene polymerization: production processes, polymer properties, and reactor modeling. *Ind. Eng. Chem. Res.* 1994, Vol. 33, pp. 449-479.

Yao, K., et al. 2003. Modeling ethylene/butene copolymerization with multi-site catalysts: parameter estimability and experimental design. *Polym. React. Eng.* 2003, Vol. 11, pp. 563--588.

Yoon, W. J., et al. 2004. Recent advances in polymer reaction engineering: modeling and control of polymer properties. *Korean J. Chem. Eng.* 2004, Vol. 21, 1, pp. 147-167.

Zavala, V. 2008. Computational strategies for the optimal operation of large-scale chemical processes. *Ph.D. Dissertation, Carnegie Mellon University, Pittsburgh, PA.* 2008.

Zavala, V. M., Laird, C. D. and Biegler, L. T. 2008. Interior-point decomposition approaches for parallel solution of large-scale nonlinear parameter estimation problems. *Chem. Eng. Sci.* 2008, Vol. 63, pp. 4834-4845.

Zhang, S., and Ray, W. 1997. Modeling and experimental studies of aqueous suspension polymerization processes. 3. mass-transfer and monomer solubility effects. *Ind. Eng. Chem. Res.* 1997, Vol. 36, 4, pp. 1310-1321.

Zhang, Z. and Saetre, R. 2007. Characterization of styrene copolymers using size-exclusion chromatography with on-line FT-IR viscometer detectors. *Macromol. Symp.* 2007, Vol. 12(3), pp. 185-201.

Zhang, Z. 2009. Use of FT-IR Spectrometry for On-Line Detection in Temperature Rising Elution Fractionation. *Macromol. Symp.* 2009, Vol. 282, p. 111.

Zheng, Z, et al. 2011. Steady-state and dynamic modeling of the Basell multireactor olefin polymerization process. *Ind. Eng. Chem. Res.* 2011, Vol. 50, 1, pp. 322-331.

Zhu, C., Byrd, R. H. and Nocedal, J. 1997. L-BFGS-B: Algorithm 778: L-BFGS-B, FORTRAN routines for large scale bound constrained optimization. *ACM Transactions on Mathematical Software.* 1997, Vol. 23, 4, pp. 550-560.

Zhu, S. 1996. Molecular weight distribution in free radical polymer modification with crosslinking: effect of chain-length dependent termination. *Macromolecules.* 1996, Vol. 29, 1, pp. 456-461.

Zhu, S. and Hamielec, A. E. 1989. Chain-length-dependent termination for free radical polymerization. *Macromolecules.* 1989, Vol. 22, pp. 3093-3098.

Zhu, Y., An, L. and Jiang, W. 2003. Monte Carlo simulation of the grafting of maleic anhydride onto polypropylene at higher temperature . *Macromolecules.* 2003, Vol. 36, 10, pp. 3714-3720.